THE INFLUENCE OF NOZZLE DESIGN ON THE FLIGHT PERFORMANCE OF ROCKET VEHICLES, WITH AN ANALYSIS OF THE RESULTS OF JET SEPARATION

Thesis by

Walter C. Swan

In partial fulfillment of the requirements

for the degree of

Mechanical Engineer

California Institute of Technology

Pasadena, California

1948

ACKNOWLEDGMENTS

The author wishes to express his sincere gratitude to Dr. Martin Summerfield, who suggested this investigation, for his patient guidance and numerous suggestions during the completion of this study, and to Mr. W. D. Rannie and Mr. N. Van de Verg for their numerous suggestions and comments on this paper. Special thanks are extended to Mr. Charles R. Foster for the use of his experimental data in correlating the results obtained from this theoretical analysis.

TABLE OF CONTENTS

SUMMARY

The object of this study was to investigate those parameters which affect the overall performance of a sounding rocket. The index of performance is the maximum summit altitude attained when neglecting separation in a nozzle operated under overexpanded conditions. Secondly, a theoretical analysis was made of the affect of jet separation on nozzle performance.

A nozzle built with a variable area ratio, such that the optimum may be obtained for each altitude, has been chosen as the standard by which maximum performance may be calculated. The ratio of the summit altitude reached by a conventional nozzle of fixed area ratio to that attained by an ideal nozzle is symbolized as the ratio R. The following conclusions have been reached:

a. Increasing the initial acceleration or the chamber pressure increases the magnitude of R.

b. Increasing the loading factor, the specific impulse, or the initial velocity, decreases the magnitude of R.

c. Incorporation of a two-step nozzle increases the performance R by 7 to 8 percent in low-performance vehicles, and to an even greater percentage in high-performance vehicles. A significant increase in performance would not be realized by using more than two steps.

During that portion of the vehicle flight when the jet is overexpanded, the exhaust gases do not cling to the nozzle walls, but separate as a result of simple oblique weak shock wave. This separation occurs at an area ratio of about 3 to 4 larger than the optimum for a given altitude. The following nozzle-performance characteristics can be deduced from this separation theory:

a. The loss in performance of a nozzle in the overexpanded region of operation is not so severe as computations neglecting jet separation indicate.

b. The point of separation varies linearly with chamber pressure and increases with decreasing γ. Increasing the cone angle decreases the area ratio at which jet separation occurs. Experiment has shown that at a cone angle of 15 degrees the detachment or wedge angle equals the cone angle. Thus for a cone angle of 15 degrees, the gas path at the boundary of the detached jet is parallel to the nozzle centerline. Since for a given nozzle the same detachment angle exists regardless of the pressure ratio across the nozzle, and since temperature has no effect on the separation pattern, the wedge angle is a function of the cone angle alone.

c. By controlling the point of separation with some device which would select the optimum separation point for a given set of rocket and flight parameters, the available thrust of the vehicle can be increased.

GENERAL INTRODUCTION

It was decided to divide this analysis into two separate sections, to approach the problem of performance neglecting the affects of separation in the overexpanded nozzle, and then to study separation theory, and determine how this affects the results obtained neglecting separation.

In section 1, an analysis of the effects of the rocket parameters on performance is made, noting what possible design techniques might be incorporated to improve performance. In section 11, a theoretical analysis is made to show the effect of separation in overexpanded nozzles. These results may then be qualitatively applied to the results of section 1, to serve as a correction factor on performance evaluation.

NOMENCLATURE

Symbol	Definition	Units
a_c	Velocity of sound in chamber	ft./sec.
a_1	Velocity of sound before shock	ft./sec.
a_o	Initial acceleration	ft./sec.^{2}
β	Oblique shock angle	degree
C_F	Thrust coefficient	
C_{Fo}	Thrust coefficient at sea-level	
F	Thrust	lbs.
F_o	Thrust at sea-level	lbs.
f_t	nozzle throat area	in.^{2}
f_{xs}	Detachment nozzle area	in.^{2}
f_x	Nozzle area at any location	in.^{2}
ϵ	Area ratio, ratio of exit area to throat area	
ϵ_s	Separation area ratio	
h	Altitude in vacuum at any time, t	ft.
h_p	Burnout altitude	ft.
h_s	Summit altitude	ft.
I_{spo}	Sea-level specific impulse	$\frac{\text{lbs thrust}}{\text{lb. fuel/sec.}}$
I_{AV}, I	Average specific impulse over flight (fixed area ratio)	same
I_{VAR}	Average specific impulse over flight (variable area ratio)	same
M_1	Mach number before shock	
M_p	Initial propellant mass	lbs. mass
M_o	Dead mass of missile	lbs. mass

Nomenclature - continued

Symbol	Definition	Units
P_c	Chamber pressure	psi
P_1	Pressure before shock	psi
P_2	Pressure after shock	psi
P_o	Ambient atmospheric pressure	psi
R	Ratio h_{s_F}/h_{s_v}	
ρ_1	Density before shock	slugs/cu.ft.
ρ_2	Density after shock	same
t	Time	Secs.
t_p	Burnout time	Secs.
u_1	Velocity in nozzle before shock	ft./sec.
u_2	Velocity after shock, parallel to u_1	ft./sec.
v_o	Initial missile velocity	ft./sec.
v_p	Burnout missile velocity	ft./sec.
W	Weight of propellant	lbs.
γ	Ratio of specific heats	
θ	Detachment angle (wedge angle)	deg.
α	1/2 cone angle	deg.
Υ	Loading factor $\frac{M_p}{M'_o}$	
λ	Divergence factor $(1/2 + 1/2 \cos \alpha)$	
η_o	Nozzle efficiency	

SECTION I

THE EFFECT OF NOZZLE DESIGN ON THE VERTICAL FLIGHT PERFORMANCE OF ROCKET VEHICLES.

1. Introduction.

The purpose of Section I is to analyze the relative performance of many types of sounding rockets. In this study a comparison is made between a nozzle having a conventional fixed area ratio and an ideal one having a variable area ratio. All other relevant parameters are held constant.

An attempt is also made to study this ideal nozzle by use of a multi-stage one built in two or more separate sections, each of which has an area ratio fixed at some optimum for a certain portion of the flight.

In this analysis it was decided to use the summit altitude in drag-free flight as the basis of comparing relative performance. Since this study is made over a wide variety of vehicles, it can be used as an index for future design, if very high altitudes are desired.

Throughout the analysis of Section I, no account has been made of the effect of jet separation in an overexpanded nozzle except for the multi-stage type. Obviously, the purpose of such a nozzle is to force jet separation at any desired altitude, and thus to minimize the thrust deficiency when operating under overexpanded conditions.

In order to accomplish this study, it was necessary to develop the flight equation, and under certain assumptions, to evaluate it over a wide range of parametric conditions. A discussion of this equation is presented.

2. Derivation of the Flight Equation.

As a vehicle is launched vertically in still air, it is affected by a combined action of gravity, air resistance, and upward rocket thrust. Obviously, the weight of the rocket decreases as fuel is consumed, during its vertical ascent. After the propellant has been consumed, the vehicle continues to ascent because of inertia until the summit is reached. During the latter portion of the flight only air resistance and gravity are effective. For this analysis it will be assumed that the effect of gravity is constant and that the weight of the fuel expelled is a linear function of time.

In the derivation of the drag-free flight equation the thrust and weight of the missile at any time, t, is denoted by F and W; the initial gross weight by W_o; and the ratio of the initial propellant weight to the total initial weight by γ .

From Newtonian Mechanics, it is known that:

$$\left[\frac{F - D}{W} - 1\right] g = \frac{dv}{dt}$$

in which the drag D is a function of the flight velocity and has the form:

$$D = \frac{1}{2} \rho_o A \sigma C_D V^2$$

in which:

ρ_o = density of the air at sea-level

σ = air density ratio

A = largest cross-section of the missile

C_D = drag coefficient

Since the greatest portion of the flight will occur at low drag, and since the vehicles with values of $u = W_o/A$ (gross weight per unit cross-

sectional area) that equal or exceed 1000 lb/ft., they will be studied, it is justifiable[1] to neglect the effect of air resistance in this analysis. Thus the equation of motion reduces to:

$$\frac{dv}{dt} = \frac{d^2h}{dt^2} = \left[\frac{F - W}{W}\right]g$$

Now the thrust at any time t is given by $F = F_o \frac{C_F}{C_{Fo}}$, where F_o is the thrust obtained at sea-level and C_F and C_{Fo} are the respective thrust coefficients. Also from Newtonian mechanics we have:

$$F_o = M_o' (a_o + g) \quad \text{where } M_o' = M_o + M_p$$

Since a constant rate of fuel consumption has been assumed, the weight of the missile W at any instant can be expressed as:

$$W = W_o \left[1 - \gamma \frac{t}{t_p}\right] \quad \text{for values of } t \leq t_p$$

Therefore, the drag free flight equation becomes:

$$\frac{d^2h}{dt^2} = \frac{M_o'(a_o + g)\ \frac{C_F}{C_{Fo}} - M_o' g \left[1 - \gamma \frac{t}{t_p}\right]}{M_o' \left[1 - \gamma \frac{t}{t_p}\right]}$$

or

$$\frac{d^2h}{dt^2} = \left[\frac{\frac{a_o + g}{g}\ \frac{C_F}{C_{Fo}}}{1 - \gamma \frac{t}{t_p}} - 1\right] g \qquad \text{----------(1)}$$

The specific impulse (thrust per unit mass flow rate) is:

$$I_{sp} = F/mg \quad \text{in which} \quad m = dm/dt$$

The equation for specific impulse at sea-level is written as:

$$I_{sp_o} = \frac{M_o' (a_o + g)\ t_p}{M_p\ g}$$

where M_p is the initial mass of propellant, t_p is the total burning time, and I_{sp_o} is the sea-level specific impulse. Injecting this expression into Equation (1), we obtain:

$$\frac{d^2h}{dt^2} = \left[\frac{\frac{I_{sp_o} \gamma}{t_p} \frac{C_F}{C_{F_o}}}{1 - \gamma \frac{t}{t_p}} - 1 \right] g \qquad \text{- - - - - - - - - - (2)}$$

3. Selection of Parameters.

Considering this flight equation, it is seen that the parameters affecting the flight of a rocket are: the specific impulse, I_{sp}, the total burning time, t_p, the loading factor, Υ, and the variation in thrust coefficient C_F with altitude.

For any rocket the factors which influence these flight parameters will be discussed. The thrust coefficient, neglecting the nozzle efficiency and divergence factor, is defined as:[2]

$$C_F = \Gamma' \sqrt{\frac{2}{\gamma - 1}\left[1 - \frac{P_e}{P_c}^{\gamma-1/\gamma}\right]} + \frac{P_e - P_o}{P_c} \epsilon$$

in which:

$$\Gamma' = \gamma\left[\frac{2}{\gamma + 1}\right]^{\frac{\gamma + 1}{2(\gamma - 1)}}$$

γ = ratio of specific heats

P_c = chamber pressure

P_e = exhaust pressure

P_o = ambient pressure

ϵ = ratio of throat area to exit area

Therefore the thrust coefficient varies with γ, P_c, ϵ, P_o, and P_e, which is an isentropic function of P_c and ϵ. The parameter t_p is a function of the initial acceleration, a_o, and the loading factor, Υ, as shown on page 3 of this thesis. As the flight equation (2) is written I_{sp_o} is the constant value for sea-level operation, but it must be noted that the actual specific impulse I_{sp} at any instant during flight may be quite different from the sea-level value. Obviously, $I_{sp} = I_{sp_o} C_F/C_{F_o}$, and hence the choice is purely arbitrary as to whether I_{sp} or C_F is assumed to be the

variable.

Thus the flight equation may be evaluated for any given rocket design, when specific values of the parameters γ , P_c, ϵ , I_{sp}, a_o, $\forall$, and v_o, are given. It is desired to determine how each of these parameters affect the summit altitude reached by a rocket. The ratio γ was assigned a constant value of 1.2 for all flights, and the area ratio, ϵ , was chosen as the optimum value for each trajectory. An attempt at an analytical solution for determining the optimum area ratio is shown on page 51 of Appendix 1, but was abandoned as considerable questionable approximation is required to carry out each solution. This optimum area ratio, that which will allow the maximum summit altitude to be reached, was finally determined by graphical analysis using a trial and error method.

It should be noted that for fixed optimum area ratios, it has been assumed that no separation occurs in the exhaust nozzle during any portion of the flight. Ordinarily those area ratios required to satisfy rocket performance, which are greater than 3 or 4, would result in overexpanded performance of the nozzle at sea-level. Tests[3] have shown that separation will occur at sea-level when area-ratios greater than 8 are used. When this jet detachment occurs, the loss in net thrust due to over-expansion is reduced. Conversely, those nozzles with low area ratios would become highly underexpanded at high altitudes, but this resulting loss in thrust can be calculated exactly, since the flow process is well defined. Hence it is seen that the optimum area ratio is a continuously changing value, which depends on the local ambient pressure during flight.

It is seen immediately that the maximum total impulse, i.e., the product of thrust and time, can be obtained if the nozzle could expand or contract to satisfy local conditions during flight. This hypothetical

nozzle shall be referred to hereafter as the ideal variable nozzle. Thus, the ratio of the relative performance of a particular nozzle having a fixed area ratio, to that of an ideal variable nozzle, the values of other parameters being the same, would serve to indicate the effectiveness of the nozzle in producing the optimum thrust over the whole flight trajectory. Obviously the ideal variable nozzle is somewhat fictitious, as it would require an infinite area ratio when extremely high altitudes are reached. For this reason an attempt was made to see what relative performance would be, assuming that an ϵ of 50 is the maximum ratio attainable.

As an approach to this perfect nozzle, a step-nozzle was considered. The functions of this step-nozzle can be summarized as follows (see sketch below):

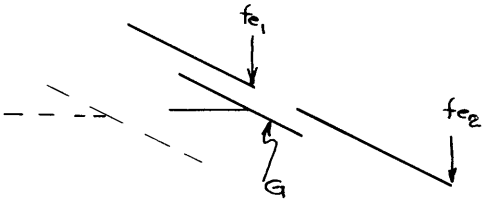

a. During the low altitude operation of the nozzle, the area ratio may be considered as $\epsilon_1 = fe_1/f_t$. As altitude is increased, a point is reached where ϵ_1 becomes optimum. Beyond this point the nozzle would be operating under underexpanded conditions, and the gas jet would leave tangential to the exit area fe_1. Since the exit pressure P_e is greater than the ambient pressure P_o, complete conversion of the issuing jet energy into effective thrust is not accomplished.

b. At some predetermined time, the ring valve, G, is mechanically closed so that fe_1 is no longer the exit area. This added extension (see

sketch) would result in fe_2 becoming the new exit area. The gases would then conform to this new nozzle, and the thrust available would increase. As the vehicle continues its powered flight, a new optimum altitude is reached for this new area ratio ϵ_2. Conceivably, an infinite number of these extensions or steps could be incorporated, and hence, the ideal variable nozzle would be approximated.

A few trajectory solutions are considered using this type of nozzle, to determine what increase in performance is provided by such a two-step nozzle (see page 63 Appendix 1). Also an attempt is made to determine the optimum number of such extensions. (see page 63 Appendix 1).

In an effort to solve the flight equation, the following three methods were attempted:

i. numerical integration

ii. analytical integration

iii. total-impulse method

The first two methods are described in detail on pages 54 and 56 in Appendix, and in both cases considerable questionable approximations would be necessary to facilitate a solution. The conventional total-impulse method, which is presented below, proved to be the most satisfactory solution. A set of sample computations is included on page 60 of Appendix 1.

4. Total-Impulse Method

Conventional Nozzle Solution.

Since all of the methods that were applied to a direct solution of the flight equation appeared to require necessary assumptions which would result eventually in errors of the same magnitude as the desired accuracy of the results, it was decided to use a conventional method based on the variation of specific impulse with altitude. Essentially, the steps involved are as follows: (see Page 60 Appendix 1)

a. A set of standard trajectories was defined, one for each value of I_{sp_o}, a_o, γ , t_p, v_o, P_c, and γ .

b. By use of the drag-free flight equations (3) and (4), (see page 56, Appendix 1), h_∞ is plotted as a function of time, using the I_{sp_o} sea-level value throughout.

c. For each set of parameters, various values of ϵ are used, and a plot of C_F-versus-time is made, up to t_p. Concurrently, a plot of C_F(max.)-versus-time is made, as though the nozzle were expanding to an optimum ϵ at each altitude.

d. The value of $\int C_F \cdot dt$ is obtained by graphical methods for each ϵ selected, as well as for the condition of variable ϵ .

e. The ratio of the $\int C_F \cdot dt$ for a given area ratio to the $(C_{F_o} \cdot t_p)$ is calculated. This shows how the average specific impulse over the total powered flight differs from that of the initially assumed average, i.e. I_{sp_o}.

f. The average specific impulse, $I = \frac{\int C_F \, dt}{C_{F_o} t_p} I_{sp_o}$, is computed for

each set of defining parameters, and the optimum area ratio may then be obtained as that which gives the maximum average $\underline{I}$. Similarly the value of $\underline{I}$ for the variable nozzle is computed.

g. A new corrected trajectory may be calculated by inserting the new average $\underline{I}$ into equations (3) and (4). Actually, all that is desired is the burnout altitude and velocity, and hence equations (5) and (6), on page 57 , Appendix 1, are used. By use of h_p and v_p, the summit altitude is computed, for the two conditions; (i) the optimum fixed area ratio for the flight, and (ii) the ideal variable nozzle.

h. The ratio of h_s to h_s' (summit altitudes under (i) and (ii) above) is then evaluated. The quantity $\underline{1-R}$ shows the remaining altitude that could be obtained if a perfect variable area ratio nozzle could be developed.

The errors in this method may be examined in the following manner: At first, it is noticed that the so-called average specific impulse, $\underline{I}$, computed by graphical integration of the C_F-versus-time curve, assumes a constant value with respect to altitude. Actually, since the vehicle is at a high altitude for the greater duration of the flight, an excess weight has been assigned to the I_{sp} at the low end of the plotted trajectory. The problem should be attacked by several step-wise computations, and the average $\underline{I}$ should be determined over each step. Thus the problem would resolve itself into several solutions of the flight equation, each of which serves as an added effect on the next step.

In an attempt to determine the magnitude of the error in determining the average specific impulse, a two-step approximation is made (see page 64, Appendix 1). Two values of the average specific impulse were determined, one for the low end of the flight trajectory, and the other for the high

end. The summit altitude reached on considerations of both values was determined and was compared with that attained using the weighted average of these two values. From this study it was found that the integrated average $\underline{I}$ gives a value of summit altitude about 6 percent less than a two-step approximation. Although it is admitted that this percentage is a sizeable error, it is also of the same order of magnitude as would be obtained by the initially attempted numerical integration method (see page 54 Appendix 1), which is a far more tedious solution. Furthermore, this 6 percent error always occurs in the same direction, and offers a conservative quantitative result, in contrast with the numerical integration method. However, since a comparison of the relative performance of two rockets is the object, and since this approximation error is introduced for each fixed area ratio, as well as for the ideal variable nozzle, this discrepancy is neglected.

A second error is introduced by the fact that the C_F-versus-time plot is taken from an altitude-versus-time curve that is based on the sea-level value of specific impulse. Actually, by use of the newly obtained $\underline{I}$ in the flight eaution, a second trajectory should be determined. From this curve a second C_F-versus-time curve should be plotted. Obviously, this procedure would result in many such computations; but since this error is in the opposite direction to that described above, it serves as a compensating error. Likewise, this discrepancy is neglected in as much as relative performance is the objective.

Step-Nozzle Solution.

In the selection of two or more ratios to be included in this new nozzle, it was decided to obtain area ratios which are within practical

limits of nozzle size. Yet these areas should be such as to give a near maximum total impulse, and hence a maximum summit altitude. A unique and desirable feature of the total-impulse methods of analysis used in the initial, fixed area-ratio study, is that the method offers an excellent picture of which area ratios should be selected for this second portion of the problem. By inspection of the C_F-versus-time plots (see page 71 of Appendix 1), it is seen immediately that it is desirable to use an area ratio as low as possible during the early stages of flight, and one as high as is mechanically possible during the upper portions of the flight. By merely integrating along several such combinations of plots this conclusion becomes evident (see Table 2, Appendix 1). Of course this method of selection presupposes that the gases detach from the nozzle section with low area ratio and adjust to the nozzle section with larger area ratio at the point of intersection of the C_F-versus-time curves. This assumption is not unreasonable, as it seems possible to control the separation mechanically within the rocket itself by incorporating slots in the nozzle which can be closed at will. Since it is believed that the estimated upper limit to this step problem is reached at about an area ratio of 50, no ratios above this figure are considered. Also, inspection of the C_F-versus-time curve shows that ratios greater than about 35 result in a gain in total impulse that is rapidly diminishing. Consequently, an upper limit of 35 was selected.

Thus the two-step solution resolves itself into exactly the same procedure as for the fixed area-ratio nozzle, with the exceptions as described above.

5. Analysis of Results

Fixed Area-Ratio Nozzles.

In discussing the results obtained from these methods it is first desired to note the effect of varying certain nozzle and rocket parameters on the performance of any nozzle. The basis of comparison was chosen as the ratio R, which is the ratio of the summit altitude for a nozzle having a fixed optimum area-ratio to the summit altitude for an ideal variable nozzle. Reference is made throughout this analysis to the curves in Appendix 1 to be used in conjunction with the table of results and graphs included at the end of this section.

a. Loading Factor. It is noted in Table 5-1 for the case of $I_{sp_o} = 200$, $v_o = 0$, $a_o = 1g$, that as the loading factor, γ, increases from 0.60 to 0.90, the ratio R decreases from 0.992 to 0.819. This decrease implies that although a higher summit altitude will be reached with an improved loading factor, the summit altitude with the ideal nozzle will increase at a greater rate. This result is evident by inspection of curve sheet no. 2. As γ is assigned a greater value, the burning time increases and the total impulse for the variable nozzle continues to increase at a greater rate, whereas the total impulse of the fixed area-ratio nozzle increases only at a constant rate.

b. Initial Velocity. As the initial velocity, v_o, is increased from 0 to 800 ft./sec., the ratio R decreases even though it still increases with a decreasing loading factor. The reason for the rather sharp decrease in relative performance with higher initial velocities is that, although the total impulse is increased, the impulse for the variable nozzle increases

at a greater rate. It is also of interest to note that the optimum fixed area-ratio increased only 3 units with an increase in initial velocity, from 0 to 800 ft./sec., other parameters remaining constant. In both flight programs the variation in specific impulse with ϵ is quite flat (see curve sheets no. 2 and no. 3), and it appears that little loss in performance would result if the nozzle designed for an initial velocity of 0 ft./sec., were used rather than one of 800 ft./sec.

Referring to graph 5-1, it is noted that as higher values of γ are used, the effect of initial velocity on R becomes of decreasing importance. This conclusion is based on the fact that at higher γ and hence at longer burning times, the effect of initial distortion on the total impulse curve becomes of less importance.

c. Specific Impulse. When the specific impulse is increased from 200 to 350 seconds, a decided drop in R occurs. For the case in which $a_o = 1g$, $v_o = 0$, $\gamma = 0.60$, and $P_c = 300$, the value of R dropped from 0.992 to 0.784. Likewise all other values of I_{sp_o} resulted in a similar decrease, between $I_{sp_o} = 200$ to 350 seconds, (see graph 5-1). This sharp drop in R should not be associated with any drastic loss in performance, since the average specific impulse values are of the same relative magnitude as those obtained at $I_{sp_o} = 200$ seconds. The major factor involved here is that an increase in I_{sp_o} increases the burning time. For a γ of 0.60, the burning time is increased from 60 to 105 seconds. It is in this upper range of the flight trajectory that the ineffectiveness of the fixed area-ratio is observed, and hence for longer burning times the ratio R will diminish.

Thus, it is seen that when either the loading factor, γ, or the

specific impulse, I_{sp_o}, is increased, the fixed area-ratio nozzle approaches the ideal still less. The main factor in causing this deficiency is the longer burning time at higher altitudes. It is also of interest to note that for motors of very high impulse (I_{sp_o} = 350 secs.) the initial velocity has a neglible effect on the relative performance, although the total impulse will obviously increase with increasing values of v_o. The reason for this apparent constancy of R with increasing v_o is that a large change in the lower portion of the trajectory has little or no effect when the burning time is of very large magnitude.

It is also noted that when I_{sp_o} = 350 secs., relatively large changes in the initial velocity shifts the optimum area ratio not more than about 3 to 4 units, so that not too great a decrease in performance would result if the same nozzle were used for flights with different values of v_o.

d. Chamber Pressure. Referring to graph 5-2, it is seen that as the chamber pressure is increased from 300 to 1500 psia, the value of R rises linearly from 0.872 to 0.911, when all other parameters are fixed. The effect of chamber pressure is quite interesting in that changes in it do not increase the burning time, but rather increase the net thrust and exhaust velocity. Thus, as was expected, the average impulse for the optimum area ratio nozzle increased from 222 to 245 seconds. Even when the area ratio is held constant at optimum value for P_c = 300 psia., the average impulse will increase (see curve sheets no. 2, 3 and 5). Actually the optimum area ratio increases rapidly with P_c, but the selection of the optimum is quite arbitrary, since the same performance can be expected over a wide range of ϵ . The increase of R with P_c is caused essentially by the fact that the total impulse for the optimum area ratio increases at a

a greater rate than the total impulse with the variable nozzle. This fact can be seen by comparing curve sheets no. 2, 3, and no. 6. Since the burning time is short, the difference between the total impulse obtained by the ideal variable and the fixed area-ratio nozzles is minimized.

e. Initial Acceleration. The effect of changing the initial acceleration can be seen in graph 5-2, and in curve sheets no. 2, 7, and no. 8. The more rapid is the acceleration, the shorter is the burning time. This effect should give a lower value of R with an increased a_o for reasons explained previously. However, the increased acceleration improves the performance in that the net thrust and the thrust coefficient increase greatly. This increased performance tends to balance out the loss in total impulse because of the shorter burning time, so that the average specific impulse is only slightly less. This fact is born out for the cases of a_o = 1g, I = 222; for a_o = 2g, I = 218; and for a_o = 3g, I = 216. However, the ideal variable nozzle loses more impulse than the fixed area ratio type because of burning time. Hence, over the same range of initial accelerations, the average impulse varies from 224 to 234. The net result gives a ratio R that increases from 0.872 at a_o = 1g, to 0.928 at a_o = 3g. It is also interesting to note that the choice of a_o has little effect on the optimum area ratio.

Two-Step Nozzle.

Referring to Table 5-1, it can be seen that the performance improves decidedly when a two-step instead of a fixed-area-ratio nozzle is used. Three sets of parameter values, previously used in the calculations for the fixed area-ratio performance, are used in making this comparison. For these three sets of values a combination of an area ratio of 6 and 35 is

is found to be the most effective, and that no significant improvement will result if more than two steps are considered. This conclusion can be borne out by inspection of the several curve sheets in Appendix 1. For the case of $I_{sp_o} = 200$, $a_o = 1g$, $v_o = 800$, $\gamma = 0.60$, and $P_c = 200$, the value of R increases from 0.964 to 0.937. For the case of $I_{sp_o} = 200$, $a_o = 1g$, $v_o = 0$, $\gamma = 0.85$, and $P_c = 300$, the value of R increases from 0.835 to 0.913. For the case of $I_{sp_o} = 200$, $a_o = 1g$, $v_o = 0$, $\gamma = 0.85$, and $P_c = 300$, the value of R increases from 0.725 to 0.81. It is to be expected that the value of R increases by the greatest amount for the latter case, since the additional burning time allows the maximum available increase in performance. More striking is the fact that such a great improvement is available even for short-duration rocket motors. Thus, it is quite desirable to devise some method such as that previously described, which will allow the exit gases to adjust to a new and larger area ratio when altitudes are reached at which the low area ratio is no longer very effective.

An attempt was made to see how close to unity this ratio R could approximate. For the last case mentioned, i.e. $I_{sp_o} = 350$, it was assumed that a mechanical maximum ϵ of 50 be chosen as the upper limit. Also the nozzle was allowed to expand as a variable nozzle until this of 50 was reached. Following this "practical" ideal nozzle trajectory, it was found that the average impulse would increase only from 428 to 430 seconds. Hence, the assumption of fixed-area-ratios of 6 and 35 for a two-step nozzle gives the maximum attainable R.

Table 5-1

Table of Results

I_{sp_o}	a_o	v_o	ν	P_c	$\epsilon_{opt.}$	$I_{av.}$	$I_{var.}$	t_p	R
200	1g	0	.60	300	6.5	215	222	60	.922
200	1g	0	.75	300	7.0	222	234	75	.872
200	1g	0	.85	300	7.5	223	240	85	.835
200	1g	0	.90	300	8.0	223	243	90	.819
200	1g	800	.60	300	9.5	226	239	60	.864
200	1g	800	.75	300	10.0	230	242	75	.844
200	1g	800	.85	300	10.5	232	246	85	.825
350	1g	0	.60	300	9.0	392	431	90	.784
350	1g	0	.75	300	10.5	398	452	131	.740
350	1g	0	.85	300	11.0	403	467	149	.725
350	1g	0	.90	300	11.5	407	467	157	.716
350	1g	800	.75	300	15.0	415	474	131	.743
350	1g	800	.85	300	16.00	418	483	149	.726
200	1g	0	.75	600	11.0	231	243	75	.884
200	1g	0	.75	1500	23.0	245	255	75	.911
200	2g	0	.75	300	6.0	218	228	50	.905
200	3g	0	.75	300	6.0	216	224	37.5	.928
200	1g	800	.60	300	6-35	233	239	60	.937
200	1g	0	.85	300	6-35	232	240	85	.913
350	1g	0	.85	300	6-35	428	467	149	.81

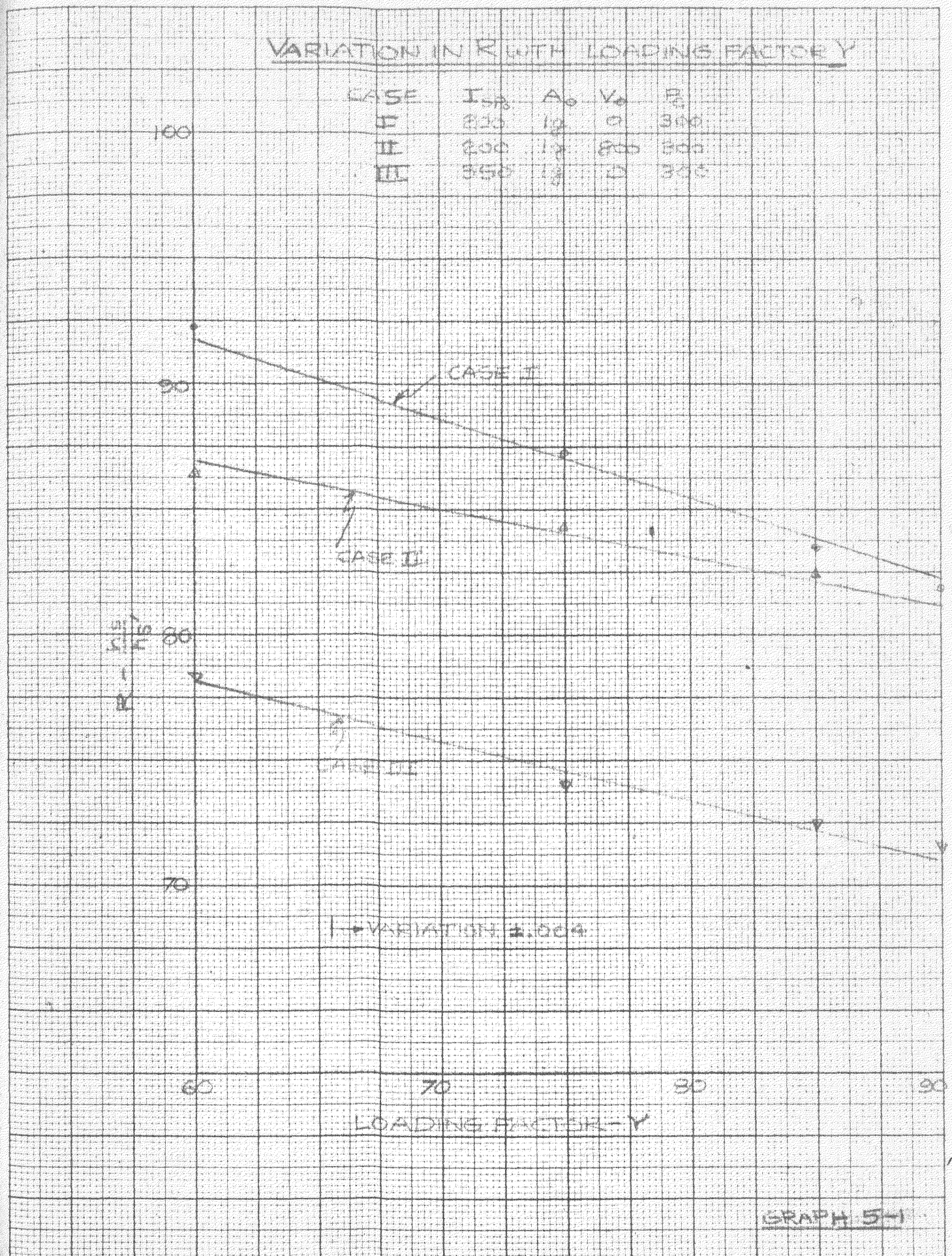
VARIATION IN R WITH LOADING FACTOR Y
CASE I_sp A_o V_o R_c
I 810 1g 0 300
II 600 1g 800 600
III 550 1g 0 300
100
90
80
70
CASE I
CASE II
CASE III
I
II
III
I → VARIATION ±.5 cm
60
70
80
90
LOADING PARAMETER - Y
GRAPH 5-1

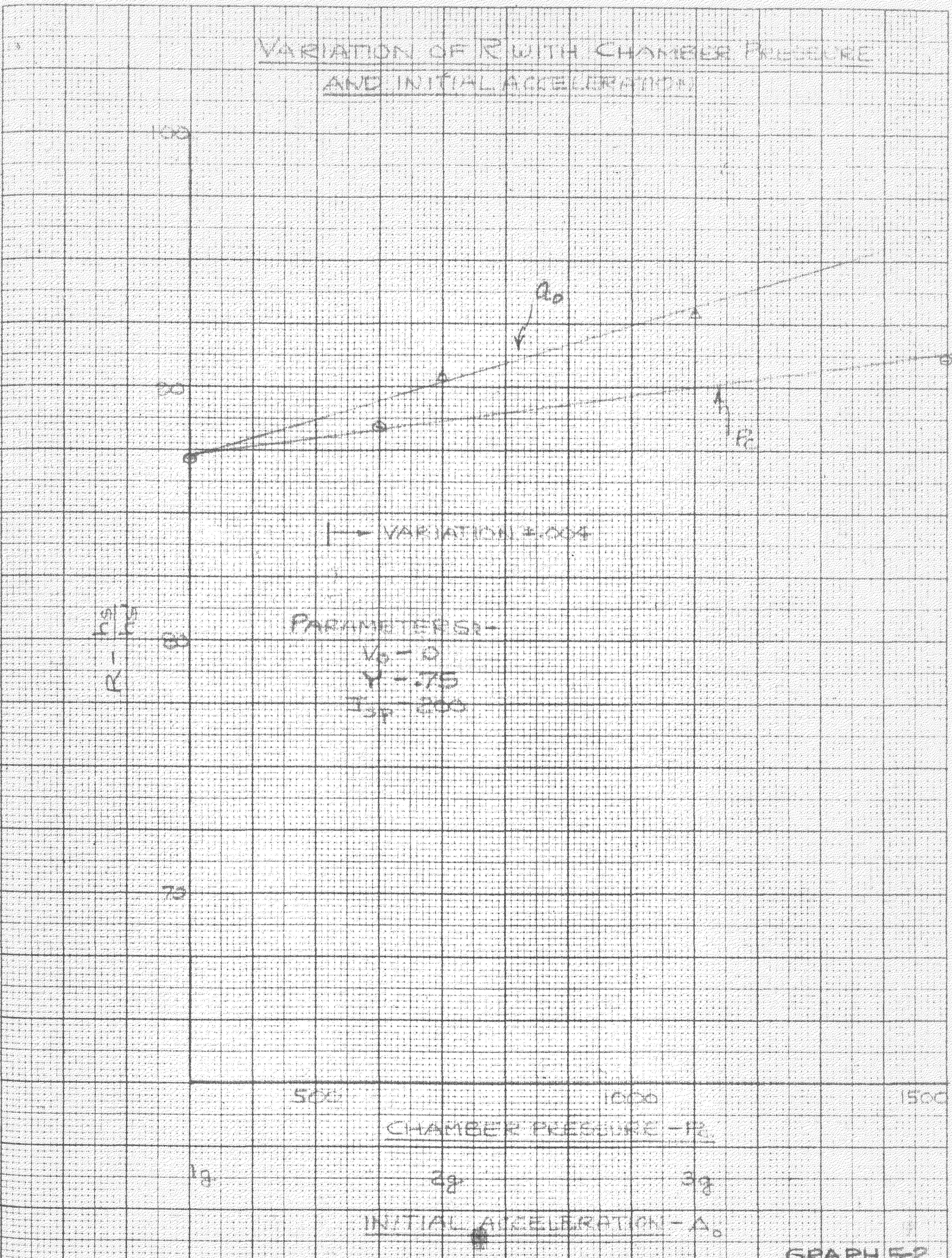
VARIATION OF R WITH CHAMBER PRESSURE
AND INITIAL ACCELERATION
100
90
80
70
a_0
P_c
VARIATION ±.004
PARAMETERS:-
V_0 - 0
Y - .75
I_{sp} - 200
$R - \frac{h_s}{h_c}$
500
1000
1500
CHAMBER PRESSURE - P_c
1g
2g
3g
INITIAL ACCELERATION - A_0

GRAPH 5-2

6. Conclusions.

The results of this study can be classified into two catagories. It is possible to predict how each rocket parameter will aid or hinder the maximum attainable performance from a given rocket, for which summit altitude is the index of performance. By expressing this summit altitude as a function of that attained by a perfect nozzle, the following are the effects of the various rocket parameters on this ratio R:

a. Increasing the loading factor decreases the value of R.

b. Increasing the specific impulse I_{sp_o} lowers the value of R.

c. Increasing the initial acceleration a_o increases the value of R.

d. Increasing the initial velocity v_o decreases the value of R.

e. Increasing the chamber pressure P_c increases the value of R.

By considering for the parameters many more sets of values than are presented in this study, it would be possible to make many crossplots. From these plots it should be possible to note how the parametric values should be adjusted so as to achieve a maximum value of R when certain parameters are frozen by design.

Also, by this analysis, it is shown that the development of a step-nozzle should be undertaken. Its application will not be limited to vehicles of extremely high performance, because increases of 7 to 8 percent in relative performance are available for rocket vehicles of the type in production today, i.e., vehicles operating with specific impulses of the order of I_{sp_o} = 200 seconds. Vehicles operating with larger values of specific impulse than the above would have an even greater increase in performance if a step-nozzle were used.

SECTION II

AN ANALYSIS OF FLOW SEPARATION IN ROCKET NOZZLES AND THE EFFECT ON NOZZLE THRUST.

7. Introduction.

In Section 1 of this presentation no account has been taken as to the effect on performance of separation in the overexpanded nozzle of a sounding rocket, except for the two-step nozzle. In a two-step nozzle, artificial detachment occurs which increases the flight performance. The object of Section II is to determine the effects of spontaneous detachment or separation on the performance of conventional nozzles.

When considering optimum conditions of operation in the preceding performance analysis, it was assumed that at altitudes at which the external pressure exceeded the exit pressure, separation occurs at the exit plane of the nozzle. At higher ambient pressures the nozzle will become proportionally more ineffective in producing thrust than at optimum conditions. The pressure deficiency between the interior and exterior of the nozzle would increase with increasing external pressures, and would thus give a negative thrust component. Hence, a plot of thrust coefficient versus ambient pressure will decrease linearly with increasing ambient pressure. Hence the gases will cling to the walls and hence reduce thrust.

Through an investigation of compression shock-wave theory, it is desired to determine how jet detachment affects both the performance at optimum area ratio and operation at highly overexpanded conditions. It is believed that in the overexpanded operation of a nozzle some point in the nozzle is reached where separation must occur in order to satisfy the laws of motion and thermodynamics. Hence, if this separation does occur, the thrust deficiency will not continue to increase linearly with increasing ambient pressure, but will deviate from this pattern when separation

occurs, and will give somewhat better performance than that previsously estimated.

An attempt is made to determine the effect of separation on the conventional real nozzle by mathematical analysis and to note how this analysis agrees with experimental measurements being conducted as part of a research program at the Jet Propulsion Laboratory.[3]

8. Separation Theory.

Considerable mathematical theory[9] has been developed on the separation of jets from various control surfaces. It has been ascertained that the jet does not detach from the surface when the gas pressure reaches that at the local exit, but clings to the wall until a point is reached at which the inertia effect of the jet is overcome by the demands of the flow contour. At this point, where the gas pressure may be considerably below atmospheric, a shock occurs in the flow as the jet attempts to adjust to the required exit conditions. It is not known definitely whether the separation point occurs at the exact position of this shock wave. Many schlieren photographs[5] show that the separation point and shock location are not identical; the separation occurring at some small distance downstream from the shock, but is apparently caused by the shock. It can be seen readily by inspection of the following picture that this effect of the gases clinging to the nozzle walls is detrimental to the performance of a rocket, since a resulting negative thrust occurs, caused by the pressure deficiency on the nozzle surface:

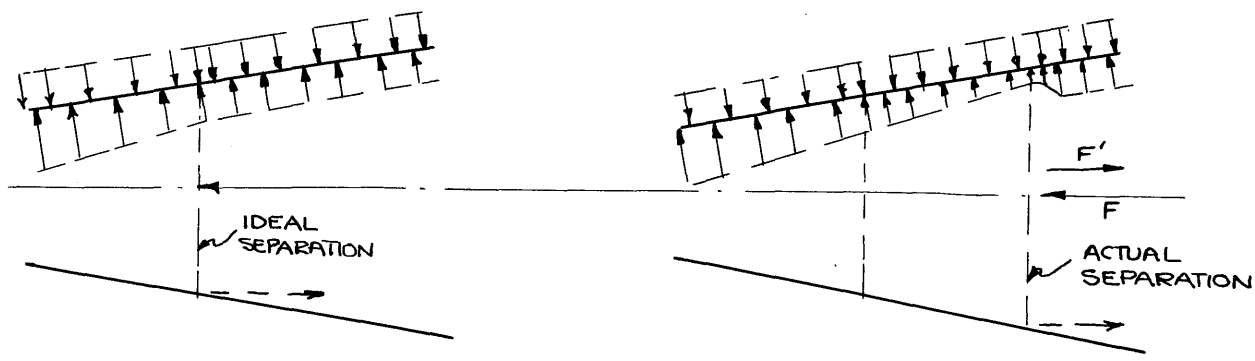

By investigating and determining the point beyond the optimum area ratio

at which actual separation does occur, it will be possible to predict the magnitude of the thrust deficiency caused by the clinging gases. If the magnitude of the negative thrust, F,[1] is large enough, it may be found feasible to install air-bleed holes at various locations, each corresponding to some optimum area ratio, and hence each causing separation to occur at any time desired.

Since it is believed that a shock wave or series of shock waves is the determining factor in locating the point of separation in a nozzle, it was decided to investigate this problem analytically on the assumption that one simple oblique shock wave occurs at the point of separation. Several simplifying assumptions have been made in an effort to keep this analysis clear and concise, without sacrificing the accuracy desired. A one-dimensional analysis has been made throughout, neglecting the effect of curvature in the nozzle. The fact that the study is conducted for a point in the immediate neighborhood of the wall makes the one-dimensional analysis appear reasonable. Since the assumptions will probably lead to a certain amount of error, a more detailed consideration of boundary-layer effects does not appear justified, and hence was neglected. In most rocket nozzles it is known that frozen expansion does not occur, but that the reaction continues beyond the exit of the combustion chamber. Throughout this treatment the flow of gases is assumed to be frozen, and hence remains constant.

When the oblique shock occurs, the jet separates from the wall, and the gas pressure is adjusted through some path to the local ambient pressure. How this adjustment occurs is extremely difficult to ascertain; hence it was decided to consider that the pressure after separation adjusts immediately

to atmospheric. Since the effects of the boundary-layer and three-dimensional flow have already been neglected, and since the flow study is being conducted close to the wall, this assumption appears reasonable.

Since a nozzle contour is divergent and since the gases must adjust to some final flow pattern when separation occurs, the question arises as to how this final pattern appears. There does not appear to be any justification for assuming the flow to be parallel to the nozzle centerline after jet separation occurs. Hence, it was decided to determine the point of separation for various values of wedge angle, θ, and then to superimpose the experimental results for given nozzles, i.e. given cone angles, α, and then to note the relationship between α and θ. Thus for a given nozzle, it would be possible to predict immediately the value of detachment angle.

For any given combustion-chamber-nozzle combination only the rocket parameters, P_c, γ, T_c, P_o, throat area, and mixture ratio are available to aid in the location of the separation point. Therefore, it is necessary to set up the oblique-shock equations for flow in a divergent section of a nozzle, basing the flow pattern on the above assumptions, and to correlate these shock equations with existing rocket-nozzle equations. In the following Section these equations will be considered.

9. Derivation of Oblique Shock Equations[9]

Consider the following flow picture along a control surface form which the flow separation at some detachment angle θ is caused by an oblique shock at some angle, β, from the control surface. The flow conditions in front of a shock are denoted by P_1, u_1, and ρ_1, whereas those after shock occur are P_2, u_2, and ρ_2. From momentum considerations, the stream velocity after a shock will be lower than before, $u_2 < u_1$, but it will still be supersonic at ordinary values of θ. Obviously the pressure P_2, will be larger than P_1 and depending on whether the shock involved is weak or strong, this pressure ratio can be of a reasonably large value.

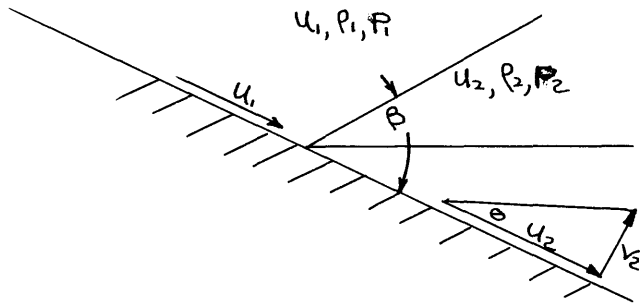

The continuity equation must be satisfied across this shock, hence:

$$\rho_1 u_1 \sin\beta = \rho_2 (u_2 \sin\beta - v_2 \cos\beta)$$

But since

$$v_2 \cos\beta = u_2 \tan\theta \cos\beta$$

$$\rho_1 u_1 \not{\sin\beta} = P_2 (u_2 \sin\beta - u_2 \tan\theta \cos\beta) \text{ and}$$

therefore,

$$\rho_2 = \frac{\rho_1 u_1 \sin\beta}{u_2 \sin\beta - u_2 \tan\theta \cos\beta}$$

Likewise the equation of momentum normal to the shock is

$$P_1 + \rho_1 u_1^2 \sin^2\beta = P_2 + \rho_2 (u_2 \sin\beta - v_2 \cos\beta)^2$$

Consequently,

$$P_1 + \rho_1 u_1^2 \sin^2\beta = P_2 + \rho_2 (u_2 \sin\beta - u_2 \tan\theta \cos\beta)^2 \quad -- (1)$$

The equation of momentum parallel to the shock must also be satisfied

$$\rho_1 u_1^2 \sin\beta \cos\beta = \rho_2 (u_2 \sin\beta - v_2 \cos\beta)(u_2 \cos\beta + v_2 \sin\beta)$$

From the two previous equations

$$\rho_1 u_1^2 \sin\beta \cos\beta = \rho_2 (u_2 \sin\beta - u_2 \tan\theta \cos\beta)(u_2 \cos\beta + u_2 \tan\theta \sin\beta)$$

By dividing the above equation through by (1),

$$u_1 \cos\beta = u_2 \cos\beta + u_2 \tan\theta \sin\beta$$

Rewriting one obtains,

$$u_2 = \frac{u_1 \cos\beta}{\cos\beta + \tan\theta \sin\beta} = \frac{u_1}{1 + \tan\beta \tan\theta} \quad ------ (2)$$

Placing this equation into the continuity equation, there is obtained:

$$\rho_2 = \rho_1 \frac{(1 + \tan\theta \tan\beta)}{(1 - \tan\theta \cot\beta)} \quad ---------- (3)$$

Since $v_2 = u_2 \tan\theta$

Therefore

$$v_2 = \frac{u_1 \tan\theta}{1 + \tan\beta \tan\theta} \quad ---------- (4)$$

The conservation of energy across the shock requires that

$$\frac{1}{2} u_1^2 + \frac{\gamma}{\gamma - 1} \frac{P_1}{\rho_1} = \frac{1}{2} (u_2^2 + v_2^2) + \frac{\gamma}{\gamma - 1} \frac{P_2}{\rho_2}$$

and it follows that

$$\frac{1}{2} u_1^2 + \frac{\gamma}{\gamma - 1} \frac{P_1}{\rho_1} = \frac{u_2^2 \, \mathrm{Sec}^2 \theta}{2} + \frac{\gamma}{\gamma - 1} \frac{P_2}{\rho_2} \qquad \text{- - - - - - - - (5)}$$

The pressure ratio across the shock wave may be obtained by considering the Mach number component normal to the wave; hence, for a normal shock this value has been[4]

$$\frac{P_2}{P_1} = \frac{2\gamma}{\gamma + 1} M_1^2 - \frac{\gamma - 1}{\gamma + 1}$$

and for an oblique shock

$$\frac{P_2}{P_1} = \frac{2}{\gamma + 1} M_1^2 \, \mathrm{Sin}^2 \beta - \frac{\gamma - 1}{\gamma + 1} \qquad \text{- - - - - - - - (6)}$$

By substituting from (2) and (4) into the energy equation (5) one obtains an equation involving only u_1, β, and θ, which is quite useful when the wave angle and deflection angle are known (eq. 4.21 L and P):

$$\frac{1}{M_1^2} = \mathrm{Sin}^2 \beta - \frac{\gamma + 1}{2} \frac{\mathrm{Sin} \beta \; \mathrm{Sin} \theta}{\mathrm{Cos} (\beta - \theta)} \qquad \text{- - - - - - - (7)}$$

Since all of the above equations have been derived from the continuity, momentum, and energy equations associated with the shock wave, it becomes necessary to introduce certain nozzle equations to facilitate the application of an oblique shock solution to a specific type of control surface. For any given nozzle-rocket combination, the following information will be available for determining an analytical solution to the point of jet separation in the nozzle:

1) P_c chamber pressure
2) T_c chamber temperature
3) r mixture ratio
4) γ ratio of specific heats of product gases

5) P_o ambient pressure

6) f_t throat area

7) a_c velocity of sound in the chamber

In order to solve completely the separation problem, a solution based on oblique shock theory requires the determination of the following quantities:

1) P_1 pressure before shock

2) ρ_1 mass density before shock

3) u_1 velocity of initial flow

4) A_s area of nozzle at point of separation

5) u_2 velocity after shock

6) θ wedge angle

7) P_2 pressure after shock

8) β shock angle

9) ρ_2 density after shock

In order to determine the above nine quantities, it is necessary to find nine equations involving them for a complete solution. From the previously derived oblique shock equations one has, in effect, four basic equations (1), (2), (3) and (5). The remaining equations are simply combinations of these and offer convenient methods for their application.

When the above variables are considered, it is possible to reduce this number to seven by making certain simplifying assumptions. Since only one-dimensional flow is considered and also the curvature of the nozzle is assumed large at the point of separation, it seems logical to assume that little or no pressure deficiency occurs beyond the point of shock. It appears reasonable to take the pressure P_2, after shock, to be exactly equal to the ambient pressure, P_o, which is a known quantity.

That this assumption does not lead to too great an inaccuracy will be borne out later in this analysis.

The above assumption is made throughout this analysis in an effort to minimize the number of variables involved, and appears reasonable since all boundary-layer effects have been neglected. Since the wedge angle, θ, will be assigned various values, it becomes necessary to find only seven basic relationships in order to arrive at the desired solution. Since one has four such relationships involving the unknowns, one will investigate the known isentropic nozzle relationships to determine some connection between the known data and the variables.

Isentropic Nozzle Relationships.

From the continuity equation, in conjunction with the condition for isentropic flow through a De Laval nozzle, one obtains the well known relationship between area ratio, ϵ, and the pressure at any point in the flow:(2)

$$\epsilon^2 = \frac{\gamma - 1}{2} \quad \frac{\left[\frac{2}{\gamma + 1}\right]^{\gamma+1/\gamma-1}}{\left[\frac{P}{P_c}\right]^{2/\gamma} \left[1 - \frac{P}{P_c}\right]^{\gamma-1/\gamma}} \qquad \text{- - - - - - - - (8)}$$

From the energy equation for flow in a nozzle:

$$\frac{1}{2} u_1^2 + \frac{1}{\gamma - 1} a_1^2 = \frac{1}{\gamma - 1} a_c^2$$

$$\frac{1}{2} u_1^2 = \frac{1}{\gamma - 1} (a_c^2 - a_1^2) = \frac{1}{\gamma - 1} a_c^2 \left[1 - \frac{a_1^2}{a_c^2}\right]$$

$$u_1 = \left[\frac{2}{\gamma - 1}\right]^{1/2} a_c \left[1 - \frac{a_1^2}{a_c^2}\right]$$

but $a_1^2 = \gamma R T_1$ and $a_c^2 = \gamma R T_c$

therefore

$$u_1 = a_c \left[\frac{2}{\gamma - 1}\right]^{1/2} \left[1 - \frac{T_1}{T_c}\right]^{1/2}$$

Assuming isentropic flow from the chamber to the point of jet separation in the nozzle

$$\frac{T_1}{T_c} = \left[\frac{P_1}{P_c}\right]^{\gamma - 1/\gamma}$$

therefore: -

$$u_1 = a_c \left[\frac{2}{\gamma + 1}\right]^{1/2} \left[1 - \left[\frac{P_1}{P_2}\right]^{\frac{\gamma - 1}{\gamma}}\right]^{1/2} \qquad \text{-------(9)}$$

From the continuity equation

$$\rho_c A_c v_c = \rho_t A_t v_t = \rho_1 A_s v_1$$

$$\rho_1 v_1 \frac{A_s}{A_t} = \rho_t v_t = \rho_t \sqrt{\gamma R T_t}$$

but for an isentropic nozzle

$$\frac{T_t}{T_c} = \frac{2}{\gamma + 1}$$

therefore;

$$\rho_1 v_1 \epsilon_s = \rho_t \sqrt{\gamma R T_c \frac{2}{\gamma + 1}}$$

$$\rho_1 v_1 \epsilon_s = \rho_t \left[\frac{2\gamma}{\gamma + 1} R T_c\right]^{1/2}$$

but

$$\frac{\rho_t}{\rho_c} = \left[\frac{P_t}{P_c}\right]^{1/\gamma} = \left[\frac{2}{\gamma + 1}\right]^{1/\gamma - 1}$$

therefore:-

$$\rho_1 v_1 \epsilon_s = \rho_c \left[\frac{2}{\gamma+1}\right]^{1/\gamma-1} \left[\frac{2\gamma}{\gamma+1} R T_c\right]^{1/2}$$

$$= \rho_c \left[\frac{2}{\gamma+1}\right]^{1/\gamma-1} \left[\left[\frac{2\gamma}{\gamma+1}\right]\frac{P_c}{\rho_c}\right]^{1/2}$$

$$= \left[\frac{2}{\gamma+1}\right]^{1/\gamma-1} \left[\frac{2\gamma}{\gamma+1} \rho_c P_c\right]^{1/2}$$

$$= \left[\frac{2}{\gamma+1}\right]^{1/\gamma-1} \left[\gamma \frac{2}{\gamma+1}\right]^{1/2} \left[P_c \rho_c\right]^{1/2}$$

$$\rho_1 v_1 \epsilon_s = \left[\gamma\left[\frac{2}{\gamma+1}\right]^{\gamma+1/\gamma-1}\right]^{1/2} \left[P_c \rho_c\right]^{1/2} \quad ----(10)$$

Now one has seven basic equations and seven unknowns. The method of combining these equations in conjunction with the known information is discussed on page 79, of Appendix 11, together with the computations involved in carrying out the solution.

10. Experimental Procedure

Since the prime objective of this analysis is to note how closely the analytical results will check with actual performance, it becomes necessary to discuss briefly the method of experimentation being conducted at the Jet Propulsion Laboratory.(3)

In the test setup, a water-cooled, Nitric acid-aniline motor is being operated at various increments of chamber pressure in conjunction with various cone angle nozzles and with varying area ratios. At various locations along the nozzle wall, pressure taps are inserted to record pressures. These pressures are recorded on a mercury manometer bank, and photographic records made after equilibrium has been established. Obviously, at jet separation the pressure will jump along some deficiency curve to approach the local ambient pressure. Hence this pressure gradient curve gives a complete picture (see pages 105 to 114 , Appendix III). This information has been plotted for several conditions of operation, and the point of jet separation is assumed to be the point where the pressure jump commences. Inspection of these curves reveals that it is possible to predict the point of separation within .1 area ratio.

From this experimental arrangement it is also possible to determine the effect of separation on thrust performance. The thrust of a correctly designed nozzle for sea-level is measured, and then a cone section is added. Since the gases cling to the walls beyond this correct design point, a negative thrust component will occur due to the pressure deficiency suffered by the addition of this nozzle extension. This deficiency can be measured, and also calculated from a consideration of the known measured

pressure forces acting on the extended nozzle. A comparison between the thrust deficiency determined by experimentation, and analytical analysis will be considered in the next chapter.

11. Analysis of Results.

General Considerations.

From the oblique shock wave theory, in conjunction with known isentropic nozzle equations, the point of separation was determined in overexpanded nozzles for various chamber pressures and wedge angles. These results, which are based on the assumption that a simple weak oblique-shock wave is associated with the separation, are tabulated on Table 11-1, page 44. These data are also shown graphically in Graph 11-1, page 45. This data is also reduced to a plot of dimensionless parameters on Graph 11-2. This graph can be used to show the area ratio of separation as a function of altitude at constant chamber pressure, as well as a function of chamber pressure at constant altitude.

It will be noted that the point of separation is approximately a linear function of chamber pressure, for a given mixture ratio and wedge angle, assuming frozen flow through the nozzle. This function appears to be entirely within reason, as an increase in chamber pressure should result in increasing the momentum of the gas stream. This added kinetic energy in the flow stream should cause the stream to cling to the divergent exit cone until larger area ratios are reached. As the wedge angle is increased separation occurs at larger area ratios. The effect of changing γ is to shift the point of separation to higher values with decreasing γ. This is easily understood when considering that the exhaust velocity is proportional to $f\left[\sqrt{\frac{T_c}{M}}, \gamma\right]$, M being the molecular weight of the product gases. A plot of exhaust velocity versus γ at constant $\sqrt{\frac{T_c}{M}}$ shows that a decrease in γ results in an increase

in exhaust velocity, and hence momentum of the flow stream. Thus, the increased momentum should cause separtion to occur at higher area ratios. From graph 11-1 it will also be noted that the effect of γ is more pronounced at larger wedge angles, which again can be realized from momentum considerations in the flow stream in conjunction with the physical problem of increasing wedge angle.

From graph 11-1, it will be noted that for θ = 15 degrees, γ = 1.26, the point of separation varies from ϵ_s = 6.0 to 8.1 for P_c = 250 to 350 psia., expanding to an atmospheric pressure of 14.1 psia. Parallel to this is the plot for γ = 1.22, all other conditions being the same. Also on this curve is plotted the experimental results for a nozzle with a cone angle of 15 degrees, and an area-ratio of 10 (see Appendix 111). Inspection of the parallelism of this curve indicates a definite relationship between α and θ. Also from the almost coincidence of the plots, it appears that for a nozzle of α = 15 degrees, that the wedge angle will be θ = 15 degrees, and hence the detachment flow will be parallel to the nozzle centerline. By inspection of the experimental data (see Appendix 111), an explanation is offered for apparent non-linear variation of separation area ratio with chamber pressure. While the experimental point at P_c = 350 psia checks almost exactly with the computed value, the results at lower chamber pressures diverge to a maximum of about 1/2 an area ratio. In the experimental tests, it was found impossible to hold γ constant, but that equilibrium expansion possibly became predominant when operating at lower chamber pressures, resulting in lower values of γ. It will be noted that the lowering of γ in the experimental tests resulted in increasing values of ϵ_s, which is in direct agreement with the computed results. Hence, the comparison of experimental data to theoretical curves

should be viewed by comparing the experimental results in the upper portion of the chamber pressures with those computed for $\gamma = 1.26$, and those for lower chamber pressures with computed values for $\gamma = 1.22$. If this is done, it can be seen that the linearity of P_c versus ϵ_s is upheld remarkably well for a given nozzle.

When a nozzle of cone angle $\alpha = 10$ degrees, was tested experimentally, the variation in ϵ_s with chamber pressure showed a remarkable parallelism to that for $\alpha = 15$ degrees (see Graph 11-1). As in the previous tests, it was impossible to hold γ constant with changing chamber pressures, which accounts for the non linearity on the plot. It is now readily seen that the flow detachment does not occur parallel to the nozzle centerline for all cone angles; only for $\alpha = 15$ degrees does this occur. By inspection of Graph 11-1, it appears that the wedge angle for $\alpha = 10$ degrees is approximately 17 degrees.

From the above comparison of the experimental results with theoretical computations, one very interesting conclusion can be reached. It appears that for a given cone angle, one and only one wedge angle occurs, independent of changes in chamber pressure, mixture ratio, γ, and altitude. On page 88, Appendix 11, it is shown that variations in temperature have no effect on the oblique shock solutions. Hence it can be concluded that the wedge angle is a function of the cone angle alone, and is independent of all other rocket and nozzle parameters. Conversely, for a given nozzle, it is possible to immediately predict the wedge angle.

It is interesting to note how far this oblique shock theory will hold up, as larger wedge angles are considered. Referring to the shock polar diagram (see curve sheet 7, Appendix 11), it will be noted that this theory

can be exptected to offer a correct solution for wedge angles up to about 45 degrees. After this point, either a normal shock or a series of oblique shocks may occur within the nozzle to cause separation; or the gases will issue from the throat as a jet, rather than cling to the diverging portion of the nozzle at all.

Effect on Thrust Coefficient.

In an effort to apply these results to an actual nozzle, noting how this theory affects the methods of predicting rocket performance in use today, a typical nozzle of area-ratio, $\epsilon = 10$, is considered, with a cone angle of 15 degrees. From existing nozzle theory, neglecting the effect of jet separation, a plot of thrust coefficient versus P_o/P_c is made (see Graph 11-3). Obviously, this is a linear relationship. For an area ratio of $\epsilon = 10$, the point of separation was determined by extrapolating Graph 10-2, for $\alpha = \theta = 15$ degrees, $\gamma = 1.26$. This corresponds to point A, on Graph 11-3. Since, as the pressure ratio P_o/P_c is increased, the point of jet separation will move back toward the throat, a family of $\epsilon =$ constant curves must be plotted, to determine how the thrust coefficient varies with P_o/P_c after separation commences. Curve of $\epsilon = 8$, and $\epsilon = 6$, neglecting separation, are dotted in for this purpose. The points of separation for these ratios are then determined, as before, from Graph 11-2. Thus the variation of C_F versus P_o/P_c, considering the effects of separation, is plotted. From the three ϵ_s considered, it appears that C_F is a linear function of P_o/P_c after separation commences. This curve is of interest, in that it shows that a nozzle designed for $\epsilon = 10$, which will be optimum for some definite altitude, will be more effective in producing thrust at sea-level than conventional computations would indicate.

As mentioned previously, this better performance is a result of a lesser degree of pressure deficiency occurring with separation than with complete clinging of the jet to the nozzle.

From the available experimental data on a nozzle with $\alpha = 15$ degrees, and $\epsilon = 10$, this same plot of C_F versus P_o/P_c was determined. Since α and θ are identical for this unique case, a comparison of theory and actual performance can readily be made. From Graph 11-3, it is seen that the results agree very well, although the experimental curve shows values of C_F about .05 below the theoretical curve, for all values of P_o/P_c. Since the theoretical curve is plotted assuming the divergence factor,[2] λ, as unity, and the nozzle efficiency as 100 percent, this is to be expected. For a cone angle $\alpha = 15$ degrees, λ should be .985. Assuming $\eta_D = .99$, the values of C_F (actual) should be about .03 less than the theoretical calculations. Also, in the theoretical calculations, it was assumed that the pressure after shock immediately jumped to atmospheric. Inspection of the actual experimental results (pages 105 to 114, Appendix III) shows a definite pressure deficiency curve over a finite distance along the divergent exit cone, before atmospheric pressure is reached. Consideration of this effect would account for the remaining difference of 0.02 between the theoretical and actual thrust coefficients. This remarkable agreement between theory and actual performance serves as added proof that a simple weak oblique shock wave is sufficient to define the point of separation. From this discussion it is also seen that the initial assumption of neglecting pressure deficiency after shock did not lead to serious error.

Effect on Generalized Thrust Diagram.

To show an even more generalized effect of separation theory on

performance, it becomes desirable to note how these oblique shock solutions affect the studies of previous investigators in nozzle flow. Dr. F. J. Malina[8] did considerable work on nozzle flow, based on the idea that separation does not occur within the nozzle. He was interested primarily in determining where the normal shock location in the flow stream would occur. The results of his study are replotted on Graph 11-4. On this curve Malina plotted F_x/F_t (thrust obtained with the nozzle cut off at any section, to a nozzle cut off at the throat) versus ϵ . He computed this curve and noted the effect of a normal shock occurring, as is shown on the graph. In an effort to see how oblique shock theory alters these curves, the following analysis is made:

a. From curve sheet no. 7, Appendix 11, for $P_o/P_c = .050$, $\gamma = 1.22$, the Mach number M_1, before shock, is $M_1 = 3.1$, for the weak wave solution. By inspection of curve sheets no. 5a and 7, it will be noted that the value of M_1 does not vary appreciably with small changes in γ . Hence, assuming M_1 to be ≈ 3.1, for a γ of 1.20, the area ratio for separation is $\epsilon_s = 7.0$, from curve sheet no. 6.

b. Therefore, for $\epsilon_s = 7.0$, and $P_o/P_c = .050$, point A is plotted in Graph 11-4. Similarly, the remaining points A are determined.

c. For any further increase in nozzle area ratio, the thrust will remain constant, as the gases are completely detached from the walls. Thus F_x/F_t curve becomes a straight line as shown.

Since these oblique shock solutions offer an alternate or strong wave solution, it becomes necessary to note how this would affect the Malina performance curves, if no weak wave occurred. This solution is determined as follows:

a. From curve sheet no. 7, Appendix 11, for $P_o/P_c = .050$, and $\gamma = 1.26$, $M_1 = 4.05$.

b. From curve sheets no. 5 and 5-A, it can be seen that the strong wave Mach number M_1 is not affected very much by small changes in γ (see points B). Thus assuming $M_1 \cong 4.00$, at $\gamma = 1.20$, and using curve sheet no. 6, $\epsilon_s = 29$, is the strong wave solution.

c. For $\epsilon_s = 29$, and $P_o/P_c = .050$, point B on Graph 11-4 is determined. Similarly other points B are determined.

Through the above analysis a very unique qualitative presentation of shock effects on nozzle performance can be realized. Should a weak wave be sufficient to cause separation, the detachment occurs at a relatively small area ratio. Jet separation caused by a strong oblique shock must occur at a very large area ratio. Finally for a single normal shock to cause separation, it must occur at still larger ratios. Of course the latter is impossible, and both experiment and theory have shown that a simple weak wave is sufficient to satisfy the conditions for jet separation for moderate cone angles (up to 20 degrees). These other two solutions, while of academic interests, could not possibly occur within a normal nozzle. Recent experimentshave been made in an attempt to allow both a normal shock and a strong oblique shock occur within the nozzle. Referring to Graph 11-4, it is seen that if a chamber pressure of $P_c = 250$ psia is used in conjunction with a nozzle of area-ratio $\epsilon = 20$, that both of these shocks will occur within the nozzle. The results of these tests fail to show any change in the area-ratio of separation over that obtained with a nozzle of area-ratio $\epsilon = 10$, having the same cone angle. This offers conclusive proof that the simple weak oblique shock alone is associated

with jet separation. Also this fact infers that no matter how long the nozzle is made, the effective thrust will be the constant for the same cone angle, once the area-ratio of separation has been reached.

During the course of experiments, several mixture ratios of the propellants were used to find one appropriate for the tests. Consequently several different chamber temperatures were encountered. It was found that changes in temperatures did not alter the location of the separation area-ratio. This agrees exactly with the analytical computations included in this thesis.

TABLE OF RESULTS

P_c	γ	θ	P_1	ϵ_s	M_1	β	P_2/P_1
250	1.26	15	5.375	6.06	3.07	30.7	2.63
300	1.26	15	5.175	7.1	3.18	29.8	2.73
350	1.26	15	5.00	8.12	3.358	29.0	2.82
250	1.26	20	4.00	7.5	3.06	33.8	3.52
300	1.26	20	3.68	9.05	3.38	33.5	3.83
350	1.26	20	3.50	10.5	3.72	32.7	4.03
250	1.26	10	7.35	4.87	2.89	27.9	1.92
300	1.26	10	7.35	5.51	3.00	26.7	1.92
350	1.26	10	7.27	6.20	3.14	25.7	1.94
250	1.22	15	5.575	6.32	2.97	31.08	2.53
300	1.22	15	5.440	7.40	3.10	29.9	2.59
350	1.22	15	5.275	8.48	3.23	29.5	2.67
250	1.22	20	4.04	8.07	3.13	35.0	3.49
300	1.22	20	3.85	9.55	3.42	34.15	3.66
350	1.22	20	3.70	11.04	3.60	33.5	3.81
250	1.22	10	7.75	5.04	2.61	27.80	1.82
300	1.22	10	7.52	5.80	2.95	27.07	1.87
350	1.22	10	7.50	6.53	3.05	26.15	1.88

Table 11-1

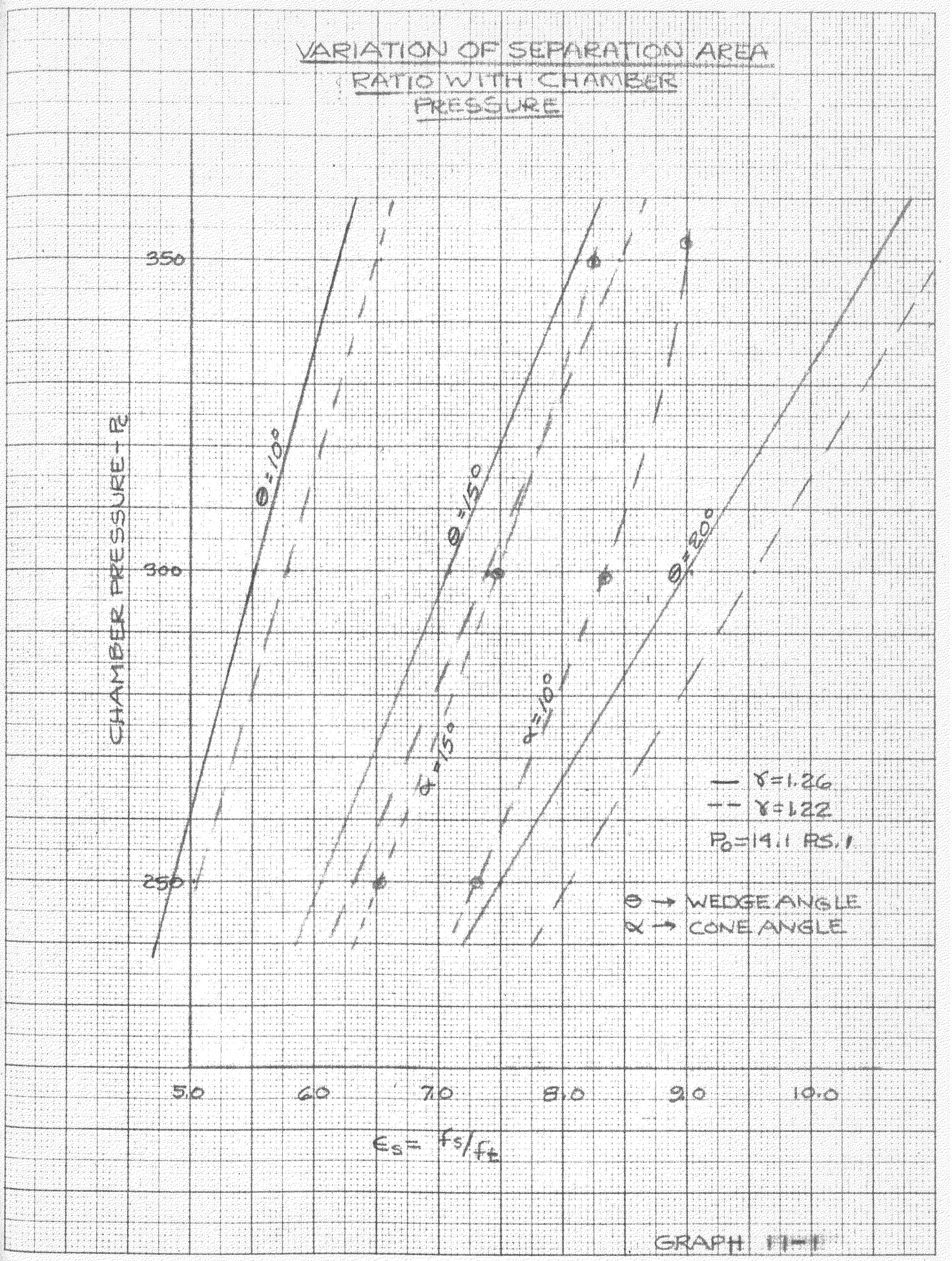
VARIATION OF SEPARATION AREA RATIO WITH CHAMBER PRESSURE
CHAMBER PRESSURE - P2
350
300
250
5.0
6.0
7.0
8.0
9.0
10.0
$\epsilon_s = f_s/f_t$
θ = 10°
θ = 15°
θ = 20°
α = 10°
α = 15°
— γ = 1.26
-- γ = 1.22
P_0 = 14.1 PS.I
θ → WEDGE ANGLE
α → CONE ANGLE

GRAPH III-1

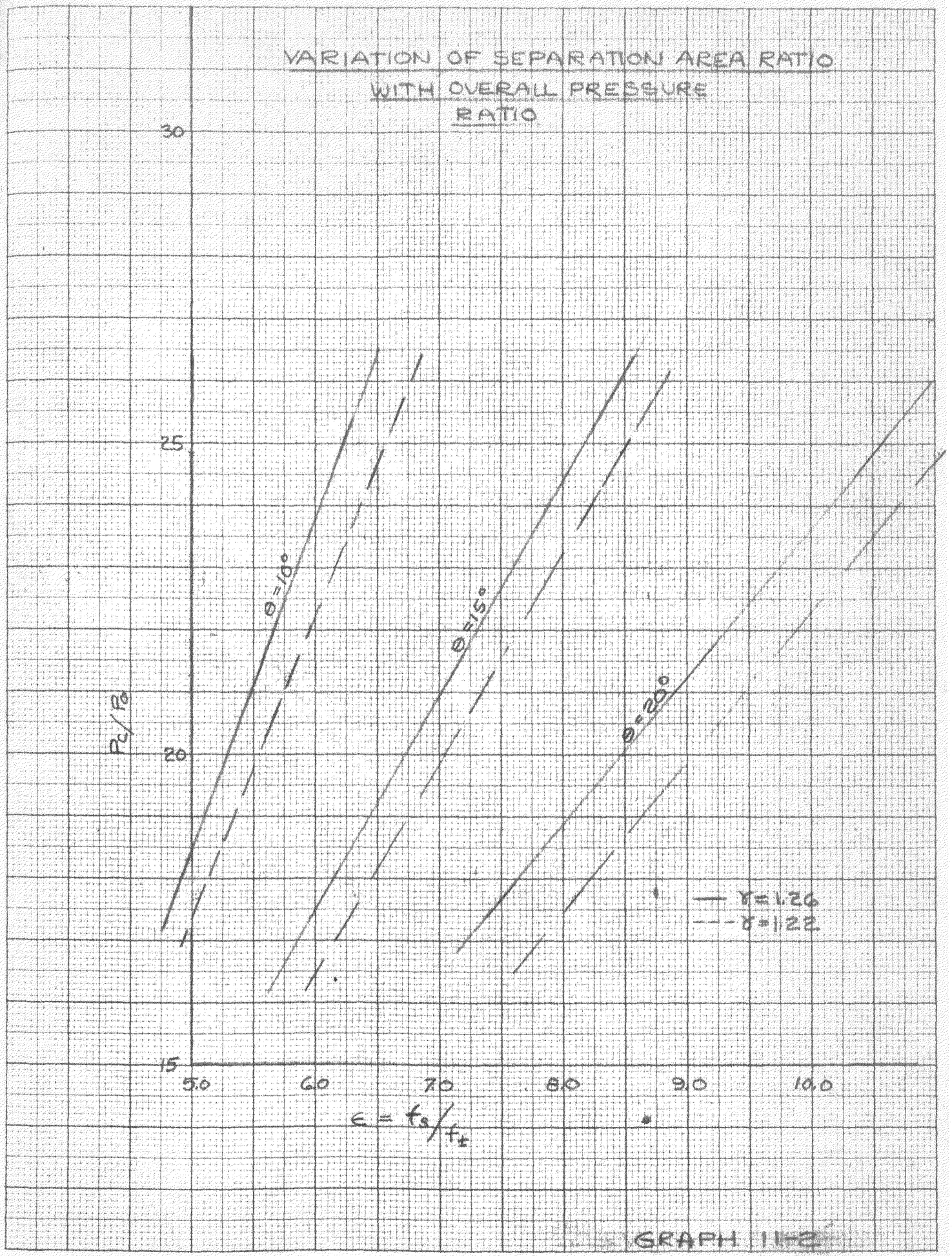
VARIATION OF SEPARATION AREA RATIO
WITH OVERALL PRESSURE
RATIO
30
25
20
15
P_d / P_0
$\theta = 10°$
$\theta = 15°$
$\theta = 20°$
$\gamma = 1.26$
$\gamma = 1.22$
5.0
6.0
7.0
8.0
9.0
10.0
$\epsilon = f_s / f_t$

GRAPH II-2

EFFECT OF SEPARATION ON OVEREXPANDED NOZZLE OF AREA RATIO = 10

DEFINING EQUATION

$$C_F = \Gamma' \left(\frac{2}{\gamma - 1} \left[1 - \frac{P_e}{P_c}^{\frac{\gamma-1}{\gamma}} \right] \right)^{1/2} + \epsilon \frac{P_e - P_0}{P_c}$$

$\gamma = 1.26$
$\lambda = 1.00$
$\eta_0 = 1.00$

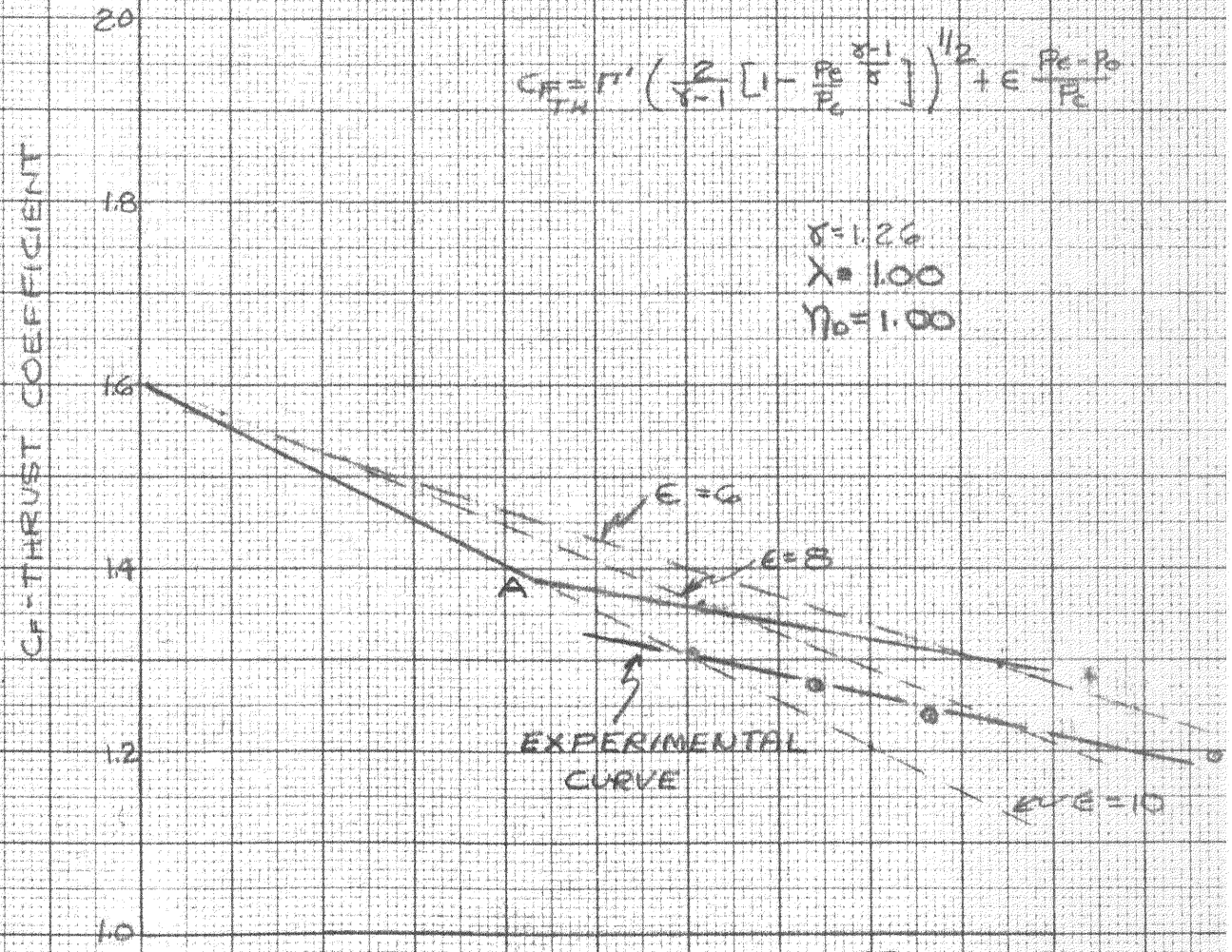

GRAPH II-3

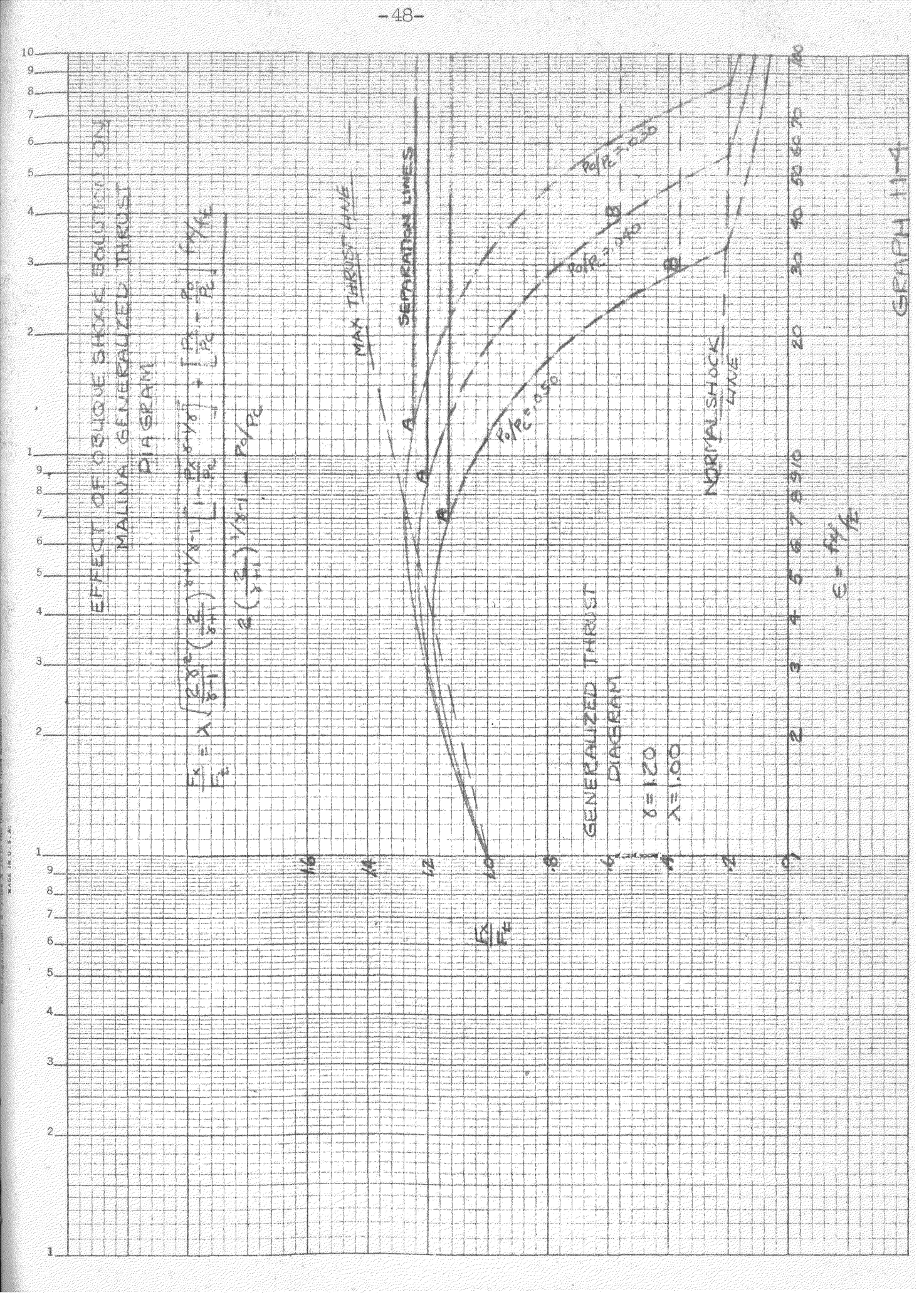
EFFECT OF OBLIQUE SHOCK SOLUTION
MALLINA GENERALIZED THRUST
DIAGRAM
MAX THRUST LINE
SEPARATION LINES
NORMAL SHOCK LINE
GENERALIZED THRUST
DIAGRAM
δ = 12.0
λ = 1.00
GRAPH #1

12. Conclusions.

From the previous analysis of results of this theoretical study, in conjunction with experimental data, the effect of separation on the performance of overexpanded nozzles in sounding rockets may be summarized as follows:

a. The point of separation occurs at an area ratio of about 3 to 4 beyond the optimum area-ratio, for a given set of rocket parameters. The point of separation is independent of mixture ratio and temperature.

b. After separation of the jet occurs, the thrust will remain constant. Should the altitude be changed the thrust will drop off linearly with ambient pressure, for the same chamber pressure, but will not be the sharp drop encountered when separation theory is not used. Hence the performance in highly overexpanded nozzles is much better than previously estimated.

c. The wedge angle is a function of the nozzle cone angle alone, and is relatively unaffected by changes in pressure ratio, gas temperature, adiabatic expansion exponent, and nozzle length.

d. The final pattern of the detached flow is parallel to the nozzle centerline, only when the cone angle is 15 degrees. For smaller cone angles the resultant flow pattern will converge toward the center of the jet.

e. A simple weak oblique shock wave is sufficient to define the location of the jet separation. Only when extreme nozzle lengths are considered, with very low chamber pressures, can a strong shock wave or a normal shock wave occur within the nozzle. Even then if a weak wave

occurs first, the strong wave will have no effect on the point of separation.

f. The point of separation varies linearly with chamber pressure, and increases with decreasing γ .

g. If some device can be constructed which will select, at will, the point of separation at various optimum positions during the course of rocket flight, a definite increase in thrust will be obtained.

h. It is recommended that further study in this subject should be made to determine the relationship between the angle of detachment and the cone angle of the nozzle. Also it might prove of interest to note what effects a three-dimensional analysis would have on the theoretical results. It is known that a simple oblique shock is not sufficient to define the conditions of flow in the center of the jet, and that a normal shock does occur at the center. Only by a rigorous three-dimensional analysis could this be approached. It appears from this study that the neglect of boundary layer influence and of pressure deficiency after the shock are valid assumptions, and could be used in a three-dimensional analysis.

APPENDIX 1

1. Analytical Approach to Finding Optimum Area-Ratio.

Given $$\frac{d^2h}{dt^2} = \left[\frac{\frac{I_{sp_o}\gamma}{t_p} \quad \frac{C_F}{C_{F_o}}}{1 - \frac{\gamma t}{t_p}} - 1 \right] g = \left[\frac{K_1 \quad \frac{C_F}{C_{F_o}}}{1 - K_2 t} - 1 \right] g$$

It is now desired to obtain an equation of h in terms of ϵ, by integrating the above expression twice. From this $\frac{\partial h}{\partial \epsilon}$ could be evaluated, and hence it would be possible to determine ϵ for maximum altitude. It must be borne in mind that the optimum ϵ is that which would give the highest summit altitude, and hence $\frac{\partial hs}{\partial \epsilon}$ must be a maximum. To accomplish the above integration, it is desirable to obtain C_F as a function of ϵ.

$$C_F = C_{F_o} + \frac{\partial C_F}{\partial P} \, dP$$ where the pressure change is that from sea-level to any altitude

A plot of C_F versus pressure results in a straight line relationship for any fixed area ratio, from[2]

$$C_F = C_{F_{MAX}} + \frac{P_e - P}{P_e} \epsilon$$ where P_e is the nozzle exit pressure, which is fixed by P_c, γ, and the nozzle parameters.

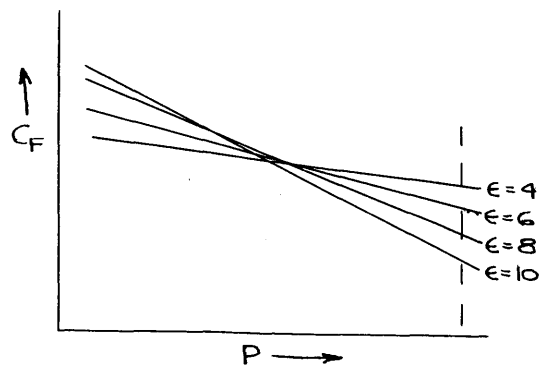

For each assumed value of ϵ, determine the slope of this plot, $\frac{\partial C_F}{\partial P}$, and then a plot is made of $\frac{\partial C_F}{\partial P}$ versus ϵ.

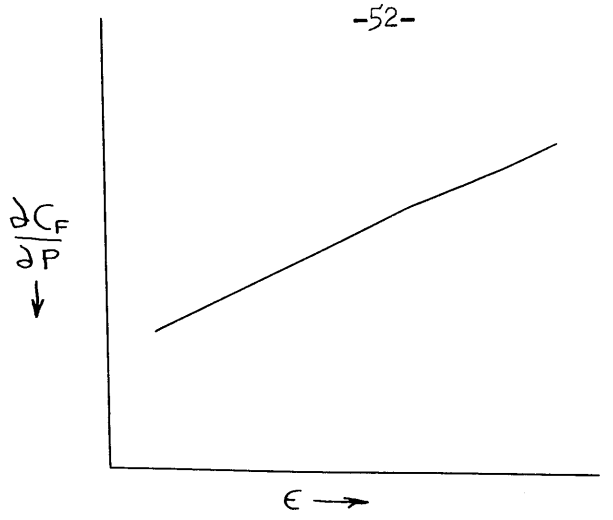

This plot will obviously show a linear relationship, and hence $\frac{\partial C_F}{\partial P} = - K_3 \epsilon$

C_{F_o} can now be expressed as a function of ϵ . Using the desired rocket parameters I_{sp_o}, γ , a_o, v_o, and P_c, in conjunction with existing charts, 1-JD-92,[2] the following plot is made:

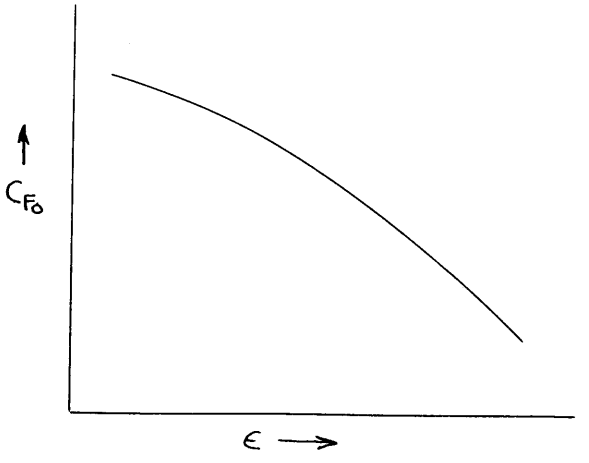

From this plot it was found that a power series equation is the best, as the variation is very nearly linear. Therefore an equation of the form $C_{F_o} = - K_4 \epsilon + K_5 \epsilon^2 - K_6 \epsilon^3 \ldots .$ is evaluated.

Now $C_F = \frac{\partial C_F}{\partial P} \Delta P + C_{F_o}$, therefore an expression for ΔP in terms of the existing parameters is desired. $\Delta P = P - P_o = f(h)$. From standard altitude data, an equation of the form $P = P_o e^{- h}$ represents the

pressure variation with altitude. Substituting the above expressions into the differential equation for drag free flight, the equation reduces to:

$$\frac{d^2h}{dt^2} = \left[\frac{\dfrac{-K_4\epsilon + K_5\epsilon^2 + K_6\epsilon^3 \ldots - K_3\epsilon (P_o\, e^{-\alpha h})}{K_1 \qquad -K_4\epsilon \quad + K_5\epsilon^2 - K_6\epsilon^3 \ldots .}}{1 - K_2 t} - 1 \right] g$$

This reduces to:

$$\frac{d^2h}{dt^2} = \frac{A + B\, e^{-\alpha h}}{1 - K_2 t} - g \qquad (8)$$

This integration can obviously be carried out, though a tedious one, after which the derivative $\frac{\partial h}{\partial \epsilon}$ is evaluated and equated to zero for a maximum. However, as mentioned before, this solution will not necessarily give the maximum v_p, although the maximum h_p will occur. Only a solution of this equation under a given set of parameter values would ascertain this question.[a]

Considering that a new equation (8) to be doubly integrated is required for each set of parameters, it is felt that a trial and error solution by graphical means is the most practical attack. Hence this analytical solution was disregarded, and is included here only for academic interest.

2. Numerical Integration Process.

Given the flight equation $$\frac{d^2h}{dt^2} = \left[\frac{\frac{I_{sp_o} \gamma}{t_p} \frac{C_F}{C_{F_o}}}{1 - \gamma \frac{t}{t_p}} - 1 \right] g$$

it is desired to determine the altitude reached at the end of burning and the vehicle velocity attained at this altitude. To accomplish this aim, the following numerical integration process is used:

a. Determine the total burning time for a given set of rocket parameters.

b. Split up this t_p into several even increments of Δt.

c. Obviously, at $t = 0$, $\frac{d^2h}{dt^2}$ will equal a_o.

d. Taking this value of change in velocity over the initial Δt, add it to v_o and obtain the velocity at the end of the first increment of time.

e. Compute the average velocity over this increment, from which the increase in altitude over h_o is computed.

f. From the new altitude obtained, determine the thrust coefficient under either ideal variable nozzle or fixed area ratio conditions, as desired.

g. With this new C_F evaluate the flight equation again over the second Δt increment, and continue as before.

Thus a table shown below is computed:

t	$\frac{d^2h}{dt^2}$	$\frac{d^2h}{dt^2}\Delta t$	V_{Final}	$\bar{V}_{Av.}$	$\bar{V}_{\Delta t}$	h	P_o	P_c/P_o	C_F

Continuing this procedure until the burnout time is reached, the h_p and v_p were evaluated under both fixed area ratio and variable ideal area ratio conditions. It was noted that because the altitude variation with time is of an exponential nature, that Δh and hence ΔP are larger in the upper range. Hence smaller Δt increments are required for the high altitude considerations. Several attempts were made at determining how small a value of Δt was necessary in order to obtain results within the accuracy of the end results desired. For the case of $I_{sp_o} = 200$, $a_o = 1g$, $\gamma = .75$, $P_c = 300$, and $v_o = 0$, it was found that, with a Δt of 5 seconds throughout the integration process, the burnout altitude for the optimum fixed area ratio condition was higher than for the ideal variable nozzle and that the summit altitude ratio was very close to unity. But when steps of the order of two seconds apart were used the magnitudes of the burnout altitudes were reversed, and the summit altitude ratio reduced to the expected value of .90. Hence, it was concluded that it would be necessary to resort to the impractical value of $\Delta t = 1$ second, if the expected accuracy were to be obtained. Since this would involve tedious calculation, this method was abandoned.

3. Analytical Approach.

A second attempt at solving the drag-free flight equation by analytical methods is now presented. The procedure followed assumes essentially a trajectory in a vacuum, i.e., no change in thrust due to atmospheric changes. By applying a correction term to account for the variation in thrust with altitude, the true trajectory for drag-free flight is approached.

From the flight equation, and assuming a vacuum trajectory:

$$\frac{d^2h}{dt^2} = \frac{d^2h_\infty}{dt^2} = \frac{dv_\infty}{dt} = \left[\frac{\frac{I_{sp_o}\gamma}{t_p}}{1 - \gamma\frac{t}{t_p}} - 1\right] g$$

$$\therefore V_\infty = \int_{t_o}^{t_p} \left[\frac{\frac{I_{sp_o}\gamma}{t_p}}{1 - \gamma\frac{t}{t_p}} - 1\right] g\, dt = \frac{g\, I_{sp_o}\gamma}{tp} \int_{t_o}^{t_p} \left[\frac{1}{1 - \gamma\frac{t}{t_p}} - \frac{t_p}{I_{sp_o}\gamma}\right] dt$$

where I_{sp_o} is assumed to be a constant.

$$\therefore V_\infty = \frac{g\, I_{sp_o}\gamma}{t_p} \left[-\frac{t_p}{\gamma} \ln\left(1 - \gamma\frac{t}{t_p}\right) - \frac{t_p}{I_{sp_o}\gamma}\, t \right]_{t_o}^{t_p}$$

$$V_\infty = -gI_{sp_o} \ln\left(1 - \gamma\frac{t}{t_p}\right) - gt + v_o \qquad (3)$$

$$h_\infty = \int_{t_o}^{t_p} \frac{g\, I_{sp_o}\, t_p}{\gamma} \left[-\frac{\gamma}{t_p} \ln\left(1 - \gamma\frac{t}{t_p}\right)\right] - gt + v_o$$

$$h_{\infty} = \frac{g\, I_{sp_o}\, t_p}{\gamma}\left(1 - \gamma\frac{t}{t_p}\right)\ln\left(1 - \gamma\frac{t}{t_p}\right) + I_{sp_o} g t - \frac{1}{2} g t^2 + V_o t \qquad (4)$$

for the case where $t = t_p$, equations (3) and (4) become:--

$$V_{p_{\infty}} = g\, I_{sp_o} \ln(1-\gamma) - g\, t_p + V_o \qquad (5)$$

$$h_{p_{\infty}} = \frac{I_{sp_o}\, g\, t_p}{\gamma}(1-\gamma)\ln(1-\gamma) + I_{sp_o}\, g\, t_p - \frac{1}{2} g\, t_p^2 + V_o\, t_p \qquad (6)$$

To apply the corrections δh and δv for variation in specific impulse with altitude, a logarithmic series expansion to equation (4) is made and second and higher order terms are dropped. Hence:

$$h_{\infty} = \frac{\gamma}{2t_p} + I_{sp_o}\, g\, t^2 - \frac{1}{2} g\, t^2 + V_o t$$

This simplified form of the altitude variation with time may now be inserted into the altitude correction term, as a first approximation method of determining the magnitude of δh. The magnitude of this altitude correction term, caused by variation of thrust with altitude is determined as follows; Since:

$$\frac{d^2h}{dt^2} = \left[\frac{\dfrac{I_{sp_o}\gamma}{t_p}\dfrac{C_F}{C_{F_o}}}{1-\gamma\dfrac{t}{t_p}} - 1\right] g \qquad (1)$$

$$\therefore \frac{d^2(\delta h)}{dt^2} = \left[\frac{\dfrac{I_{sp_o}\gamma}{t_p}}{1-\gamma\dfrac{t}{t_p}} - 1\right] g - \left[\frac{\dfrac{I_{sp_o}\gamma}{t_p}\dfrac{C_F}{C_{F_o}}}{1-\gamma\dfrac{t}{t_p}} - 1\right] g$$

$$\frac{d^2(\delta h)}{dt^2} = \frac{\frac{I_{sp_o}\gamma}{t_p}\left(1 - \frac{C_F}{C_{F_o}}\right) g}{1 - \gamma\frac{t}{t_p}}$$

Since:(3)

$$C_F = C_{F_{MAX}} - \frac{P_e - P_o}{P_c} \epsilon = C_{F_{MAX}} - \frac{P_e}{P_c}\epsilon + \frac{P_o}{P_c}\epsilon$$

$$C_{F_o} = C_{F_{MAX}} - \frac{P_e - P_{S.L.}}{P_c} \epsilon = C_{F_{MAX}} - \frac{P_e}{P_c}\epsilon + \frac{P_{S.L.}}{P_c}\epsilon$$

but $P_o = P_{S.L.} e^{-\alpha h}$

$$\therefore \quad 1 - \frac{C_F}{C_{F_o}} = \frac{1 - A + Be^{-\alpha h}}{A + B}$$

hence:--

$$\frac{d^2(\delta h)}{dt^2} = \frac{I_{sp_o}\gamma}{t_p} g\left[\frac{B}{A+B} - \frac{B}{A+B} e^{-\alpha h}\right] \frac{1}{1 - \gamma\frac{t}{t_p}}$$

let:--

$$\frac{I_{sp_o}\gamma g}{t_p} \left[\frac{B}{A+B}\right] = M$$

$$\frac{\gamma}{t_p} = K$$

therefore:--

$$\frac{d^2(\delta h)}{dt^2} = M\frac{(1 - e^{-\alpha h})}{1 - Kt}$$

Letting $h = h_\infty$ as a first approximation, this equation becomes:--

$$\frac{d\ (\delta h)}{dt} = M \int_{t_1}^{t_2} \frac{1 - e^{-\alpha\left(\frac{\gamma}{2t_p} I_{sp_o}\ g\ t^2 - \frac{1}{2}\ g\ t^2\right)}}{(1 - Kt)}\ dt$$

letting:--

$$N = \frac{\alpha \gamma\ I_{sp} g}{2\ t_p} - \frac{\alpha g}{2}$$

this equation becomes:--

$$\frac{d(\delta h)}{dt} = \int_{t_1}^{t_2} \frac{(1 - e^{-Nt^2})}{1 - Kt}\ dt \qquad (7)$$

The solution of this equation obviously requires a numerical tabulation method of solution, from which δh and δv can be evaluated. The evaluation of this type of equation has been carried out by Chien,[4] but the values are only approximate as only a first order solution was obtained. Again, this problem requires such small increment Δt for the desired accuracy that this method of solution was abandoned.

4. Sample Computations.

Determination of the Altitude Index Factor by Total-Impulse Method.

a. Parameter Selection

$I_{sp_o} = 350$

$a_o = 1\ g$

$v_o = 0$

$\gamma = .85$

$P_c = 300$

$\delta = 1.2$

b. Determination of t_p

$$t_p = \frac{I_{sp_o} \gamma\, g}{(a_o + g)} = \frac{(350)(.85)}{2} = 149 \text{ secs.}$$

c. Set-up of Vacuum Flight Equation.

$$h_\infty = \frac{I_{sp_o} g t}{\gamma}\left(1 - \gamma \frac{t}{t_p}\right) \ln\left(1 - \gamma \frac{t}{t_p}\right) + I_{sp_o} g t - \frac{1}{2} g t^2 + v_o t$$

$$h_\infty = \frac{(350)g(149)}{.85}\left(1 - \frac{.85t}{149}\right)\ln\left(1 - \frac{.85t}{149}\right) + (350)gt - 16.09^2 + 0$$

$$h_\infty = 1{,}970{,}000 \ln(1 - .0057t) - 11250t \ln(1 - .0057t) + 11280t - 16.09\, t^2 \qquad (1)$$

d. Tabulation of C_F versus t (using vacuum trajectory).

From equation (1) above, Table #1, shown on page **69** is compiled, showing the variation of altitude with time. Use is made of NACA TN.#218[6]

and #1200,[7] for obtaining altitude versus pressure data. The values of C_F for various P_c/P_o ratios at a given ϵ were obtained from charts 1-JD-92,[2] where both λ and N_D were assumed to equal unity, and $\gamma = 1.2$. Those values of C_F, exceeding 1000, were obtained by computing from the standard equation:

$$C_F = \Gamma' \sqrt{\frac{2}{\gamma - 1} \left(1 - P_o/P_c^{\frac{\gamma-1}{\gamma}}\right)}$$

The values of C_F for the ideal variable nozzle were obtained by following the "line of maximum thrust coefficient" on this GALCIT JPL chart 1-JD-92.

e. Determination of Optimum Area Ratio and I_{AV}

Curve sheet #1 shows a plot of thrust coefficient, C_F, versus burning time. From this curve the total impulse is evaluated by obtaining the integral $\int C_F \, dt$, for various selected area ratios, and also for the ideal variable nozzle flight. Then this value of impulse is compared with that obtained with a nozzle correctly designed for sea-level operation, when operated for the same period of time at sea-level.

Thus this ratio $\frac{\int C_F \, dt}{C_{F_o} \, t_p}$ represents the improvement in specific impulse over the I_{sp_o} under sea-level conditions. Since I_{sp_o} was used throughout the previous computation for vacuum flight trajectory, repeating this process using a new $\underline{I}$ (average) would correct for the effect of atmospheric pressure variation on performance.

From curve sheet #1 it is seen that the optimum area ratio is 10, and the $\underline{I}$ (average) corresponding to this fixed area ratio flight is 407.5. Also the $\underline{I}$ (average) for the variable nozzle is 467.

f. Determination of Summit Altitude Ratio - R.

Injecting the two new values for specific impulse into the vacuum flight equations:

$$v = - gI \ln \left(1 - \gamma \frac{t}{t_p}\right) - gt + v_o$$

$$\therefore \quad v_p = - gI \ln (1 - \gamma) - gt_p + v_o$$

$$v_p = - g(407.5) \ln(1-.85) - 149g$$

$$v_p = 20{,}060 \text{ ft./sec.}$$

$$v'_p = -g(467) \ln(1-.85) - 149g$$

$$v'_p = 23{,}710 \text{ ft./sec.}$$

also:

$$h_p = \frac{Igt}{\gamma} (1 - \gamma) \ln(1 - \gamma) + I gt_p - \frac{1}{2} gt_p + v_o t_p$$

$$h_p = \frac{(407.5)g\ (149)(.15) \ln(1-.85)}{.85} + (407.5)\ g\ (149) - 16.09\ (149)$$

$$h_p = 946{,}000 \text{ feet}$$

$$h'_p = \frac{(467)\ g\ (149)\ (.15) \ln(1-.85)}{.85} + (467)\ g\ (149) - 16.09\ (149)$$

$$h'_p = 1{,}133{,}000 \text{ feet}$$

also:

$$h_s = h_p + v_p^2/2g$$

$$h_s = 946{,}000 + (20{,}060)^2/2g = 7{,}166{,}000 \text{ ft. (for } \epsilon = 10)$$

$$h'_s = 1.133{,}000 + (23{,}710)^2/2g = 9{,}873{,}000 \text{ ft. (for variable nozzle)}$$

therefore:

$$R = h_s/h'_s = \underline{\underline{.725}}$$

g. Determination of Step-nozzle Solution.

From curve sheet #1 it can be seen that in order to combine two or more area ratios in one nozzle, it is only necessary to start the integration process following one fixed area ratio until the second desired nozzle shape is crossed (graphically). At this point the integration process should follow the new path. In this manner the average specific impulse, I, for any number of nozzle combinations may be computed. Obviously, this assumes no separation occurring and that the gases instantaneously fans out to follow the larger ratio at this intersection point.

Using this method of integration, various combinations of area ratio were integrated, see Table 2. It was found that using the lowest possible area ratio, i.e. approaching sea-level optimum design, in combination with the highest value of area ratio within mechanical limits, gave the greatest overall total impulse. Although area ratios greater than 50 were not considered, it is readily seen, from curve sheet #1, that larger values would show diminishing increase in effectiveness. Eventually a maximum would be reached which is probably very close to 50.

Since an area ratio of 50 shows no great improvement over that at 35, i.e. $\epsilon = 35$ shows about the greatest rate of increase in performance, it was decided that under the given parameters, a combination of $\epsilon = 6$, and $\epsilon = 35$ would be the most practical.

From table 2 $\int C_F \, dt = 258.64$ secs.

$$\frac{\int C_F \, dt}{C_{F_o} \, t_p} = \frac{(258.64)}{(1.42)\ (149)} = 1.223 \qquad \therefore \text{ I (average)} = 428$$

$$v_p = -g(428)\ \ln(1-.85) - 149g$$

$$v_p = 21{,}210 \text{ ft./sec.}$$

$$h_p = \frac{(428)\ g\ (149)\ (.15)\ (\ln(1-.85)}{.85} + 428\ g(149) - \frac{1}{2}\ g\ (149)^2$$

$$h_p = 1{,}016{,}000 \text{ ft.}$$

$$h_s = h_p + v\ /\ 2g = 1{,}016{,}000 + (21{,}210)^2\ /2g$$

$$h_s = 7{,}996{,}000 \text{ ft.}$$

$$R = h_s/h_s' = 7{,}996{,}000/9{,}873{,}000 = \underline{.81}$$

h. Consideration of Ideal Variable Nozzle Limited to $\epsilon = 50$.

Since all comparisons are based on an ideal nozzle with infinite expansion ratio, it was decided to note how close a two step nozzle approaches the best possible nozzle that could be built. Obviously, an infinite nozzle is out of reason, hence a nozzle was considered that would be ideal until it reached an $\epsilon = 50$, after which it would follow the impulse pattern of a nozzle with a fixed area ratio of 50.

By integrating along the ideal curve until the $\epsilon = 50$ curve deviated from the ideal, it was found that the $\int C_F\ dt$ obtained was 259.40. This resulted in an average I of 430, as compared to 428 obtained in the two-step process. Thus, it is felt that a two-step nozzle is as close to the ideal limit as is possible to obtain, and that more steps are not practical.

i. Determination of Error in $\int C_F\ dt$ Method.

Since there is some argument as to the justification of using the total impulse method of evaluating the average specific impulse over the whole period of flight, it was decided to note what quantitative error is involved.

To approach the actual average impulse, it would be necessary to divide the flight program into several increments and evaluate the I(average) over each increment. From this value the velocity and altitude attained at the end of this increment should be added into the equation for the next increment evaluation. It was decided to approach this problem by a one-step computation, as shown graphically below:

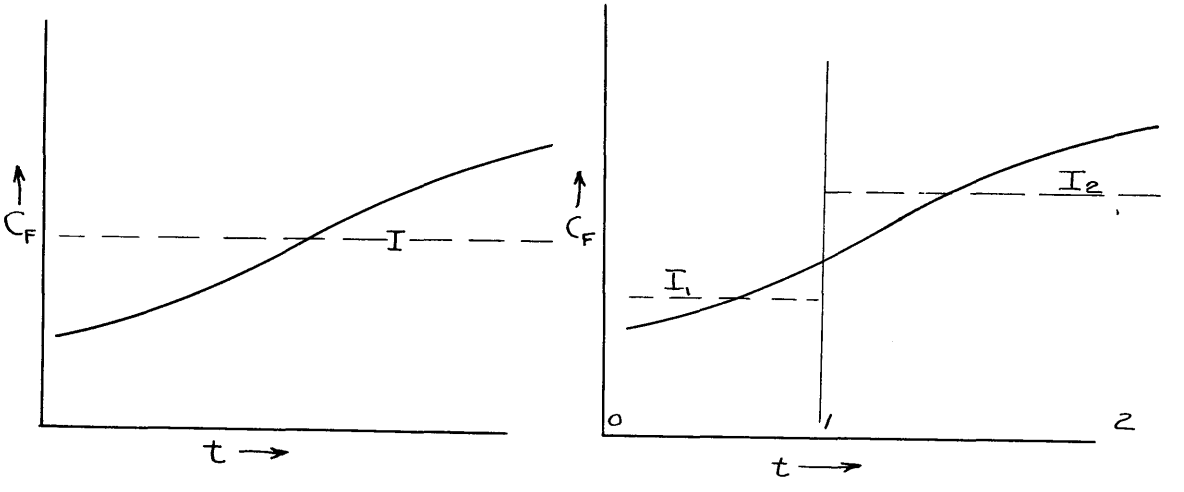

By this one-step approximation method, the upper portion of the flight pattern can be more justifiably weighted as against the poorer performance of the lower portion.

Referring to curve sheet #1, the optimum curve of 10 was used. It was decided to place the step at a burning time of 45 seconds, as the inflection point occurs in this region. By integrating the area 0-1, a mean value of C was obtained, and similarly for the region from 1-2. These values were applied to determine the respective values of specific impulse, I_1 and I_1' .

$$I_1 = I_{sp_o} \frac{\int C_F \, dt}{C_{F_o} \, t_p} = \frac{(350)\ (1.408)(45)}{(1.42)(45)} = 347 \text{ secs.}$$

$$I_1' = I_{sp_o} \frac{\int C_F \, dt}{C_{F_o} \, t_p} = \frac{(350)\ (1.717)(149-45)}{(1.42)\ (149-45)} = 423 \text{ secs.}$$

The average I for the flight, on the basis of this one-step approximation would be:

$$I = \frac{I_1 \, t_{p_1} + I_1' \, t_{p_1'}}{t_p} = \frac{(347)(45) + (423)(149-45)}{149}$$

$$= 401 \cong 407.5 \text{ (obtained by the total impulse method)}$$

Hence, by comparing the summit altitude reached by the one-step method, as against the weighted average of the one-step method, it is possible to realize the magnitude of the error involved.

1) Average of One-Step Method.

$$v_p = - gI \ln(1 - \nu) - gt_p + v_o$$

$$v_p = -g(401) \ln(1-.85) -g(149)$$

$$v_p = 19{,}660 \text{ ft./sec.}$$

$$h_p = \frac{Igt_p}{\nu} (1-\nu) \ln(1 - \nu) + Igt_p - \frac{1}{2} gt_p^2 + v_o t_p$$

$$h_p = \frac{(401)(g)(149)(.15) \ln(10.85)}{.85} + 401g(149) - \frac{1}{2} g(149)^2$$

$$h_p = 921{,}000 \text{ ft.}$$

$$h_s = 921{,}000 + (19{,}660)^2/2g = \underline{6{,}921{,}000} \text{ ft.}$$

2) One-step Method.

Let γ' be the loading factor for the flight commencing at t = 45 secs.

$$\gamma = \frac{M_p}{M_p + M_o}$$ where M_o is the dead weight

at time t = 45 secs., $M_p' = \frac{149-45}{149} M_p$

$$M_p' = .70M_p$$

therefore

$$\frac{.70M_p}{.70M_p + M_o} = \gamma'$$

but

$$\frac{M_p}{M_p + M_o} = .85$$

$\therefore$ $M_p = .85M_p + .85M_o$

$\therefore$ $M_o = \frac{.15M_p}{.85} = .176\ M_p$

$\therefore$ $\gamma' = \frac{.70M_p}{.70M_p + .176M_p} = .80$

a. Flight 1

$$v_{p_1} = -gI_1 \ln(1-\gamma) - gt_{p_1} + v_o$$

$$v_{p_1} = -g(347) \ln(1-.85) - g(45)$$

$$v_{p_1} = 1770 \text{ ft./sec.}$$

$$h_{p_1} = \frac{I_1 gt}{\gamma} (1-\gamma) \ln(1-\gamma) + I_1 gt_{p_1} - \frac{1}{2} gt_{p_1}^2 + v_o t_{p_1}$$

$$h_{p_1} = \frac{(347)g(45)(.15)\ \ln(1-.85)}{.85} + (347)g(45) - 10.09(45)^2$$

$$h_{p_1} = 302{,}400 \text{ ft.}$$

b. Flight 2

$$v_{p_2} = -gI_1' \ln(1-\nu') - gt_{p_1}' + v_o'$$

$$v_{p_2} = -g(423)\ln(1-.80) - g(149-45) + 1770$$

$$v_{p_2} = 20{,}040 \text{ ft./sec.}$$

$$h_{p_2} = \frac{I_1' gt}{\nu'}(1-\nu')\ln(1-\nu') + I_1' gt_{p_1}' - \frac{1}{2} gt_{p_1}' + v_o' t_{p_1}'$$

$$h_{p_2} = \frac{(423)g(104)(.20)(\ln(1-.80)}{.80} + (423)g(104) - 16.09(104)^2 + 1770(104)$$

$$h_{p_2} = 856{,}000 \text{ ft.}$$

therefore:

$$h_p \text{ (total)} = h_{p_1} + h_{p_2}$$

$$= 302{,}400 + 856{,}000 = \underline{1{,}158{,}400 \text{ ft.}}$$

$$h'_s \text{ (summit)} = 1{,}158{,}400 + (20{,}040)^2/2g$$

$$= \underline{7{,}368{,}400 \text{ ft.}}$$

c. Error in (a) versus (b)

$$\% \text{ error} = \frac{h'_s - h_s}{h'_s} = \frac{7{,}368{,}400 - 6{,}921{,}000}{7{,}368{,}400}$$

$$\% \text{ error} = 6.0\%$$

Thus it is seen that the total impulse method gives a quantitative error of 6% lower than a one-step approximation to the actual flight pattern.

TABLE 1

DETERMINATION OF C_F VERSUS TIME CURVE

EQUATION: $H_\infty = 1,970,000\ LN(1-.0057t) - 11250t\ LN(1-.0057t) + 11250t - 16.09t^2$

PARAMETERS:-
$H_{SP_0} = 350$ $\gamma = .85$
$a_0 = 1g$ $\gamma = 1.20$
$P_c = 300$
$V_0 = 0$

(1) TIME (SECS)	(2) 1,970,000 x LN(1-.0057t)	(3) 11250t x LN(1-.0057t)	(4) 11250t	(5) $16.09t^2$	(6) ALTITUDE H_∞	(7) P_0 IN. HG.	(8) P_c/P_0	(9) C_F $\epsilon=6$	(10) C_F $\epsilon=8$	(11) C_F $\epsilon=10$	(12) C_F $\epsilon=15$	(13) C_F $\epsilon=25$	(14) C_F $\epsilon=35$	(15) C_F $\epsilon=50$	(16) C_F ϵ=VARIABLE
0	—	—	—	—	—	29.92	204	1.385	1.33	1.25	1.00				1.42
5	-57,100	1630	56,200	402	300	29.6	20.6								
10	-116,000	6490	112,500	1609	840	28.98	21.1								
15	-175,200	15090	169,000	3620	5200	24.7	24.7	1.410	1.39	1.34	1.12				1.45
20	-238,200	27,300	225,200	6430	7820	22.35	27.3	1.46	1.44	1.38	1.23				1.47
25	-305,000	43,600	281,000	10080	9600	20.9	29.2	1.47	1.45	1.41	1.28				1.482
30	-370,000	63,400	337,000	14500	15900	16.28	37.5	1.51	1.48	1.46	1.38	1.16	.87		1.515
35	-441,000	88,300	394,000	19700	21600	12.85	47.5	1.54	1.54	1.52	1.49	1.30	1.10		1.54
40	-507,000	115,500	450,000	25700	32800	7.86	78.2	1.59	1.60	1.595	1.57	1.48	1.36	1.18	1.60
45	-565,000	145,500	506,000	32600	43900	4.60	133	1.62	1.65	1.66	1.665	1.64	1.58	1.49	1.67
50	-661,000	189,000	562,000	40200	50000	3.43	178	1.635	1.665	1.68	1.69	1.69	1.66	1.60	1.70
55	-740,000	232,000	618,000	48600	61400	1.99	306	1.66	1.69	1.715	1.74	1.75	1.75	1.74	1.76
60	-828,000	283,000	675,000	57800	72200	85.0*	503	1.67	1.705	1.72	1.765	1.79	1.805	1.81	1.81
65	-917,000	340,000	731,000	67900	96100	26.5	1603	1.68	1.715	1.736	1.78	1.82	1.85	1.87	1.89**
70	-989,000	394,000	788,000	78900	114000	11.65	3600								↓
75	-1,105,000	473,000	843,000	90300	121000	8.7	4950								1.955**
80	-1,200,000	549,000	900,000	103000	146000	3.4	12700								↓
85	-1,310,000	635,000	955,000	115900	164000	1.94	22200								↓
90	-1,420,000	731,000	1,015,000	130200	196000	.749	57000								2.055**
95	-1,535,000	834,000	1,070,000	145000	229000	.305	124,000								↓
100	-1,660,000	950,000	1,125,000	160200	254000	.096	459,000								↓
105	-1,790,000	1,050,000	1,182,000	177000	290000	.021	2×10^6								↓
110	-1,940,000	1,220,000	1,238,000	194500	324000	.007	6.7×10^6								↓
115	-2,090,000	1,372,000	1,294,000	213000	363000	.002	17×10^6								2.17**
120	-2,270,000	1,550,000	1,350,000	231000	399000										↓
125	-2,420,000	1,725,000	1,408,000	251000	462000										↓
130	-2,660,000	1,975,000	1,462,000	272000	505000										↓
135	-2,900,000	2,235,000	1,520,000	293000	562000										↓
140	-3,140,000	2,510,000	1,575,000	315000	630000										↓
145	-3,450,000	2,859,000	1,630,000	338000	692000										↓
149	-3,740,000	3,180,000	1,675,000	357000	758000			1.68	1.718	1.745	1.79	1.842	1.875	1.905	2.24**

NOTE:-
* → PRESSURE IN P.S.F
** → COMPUTED FROM

$$C_F = \Gamma\sqrt{\frac{2}{\gamma-1}\left[1-\frac{P_e}{P_c}^{\gamma-1/\gamma}\right]}$$

TABLE 2

DETERMINATION OF OPTIMUM STEP NOZZLE

COMBINATION	INTEGRATED AREA - IN^2	$\int C_F \, dT$
6-50	55.70	260.40
6-45	55.28	259.56
6-35	54.82	258.64
6-25	51.00	250.00
10-50	54.73	258.46
10-45	54.24	257.48
10-35	53.70	256.40
10-25	51.85	252.70
15-50	51.64	252.28
15-45	51.18	251.36
15-35	50.65	250.30
15-25	49.00	247.00

PARAMETERS

$I_{SP_0} = 350$

$q_0 = 19$

$\gamma = .85$

$P_L = 300$

$V_0 = 0$

$\delta = 1.2$

CURVE SHEET #1

PLOT OF C_F VERSUS TIME AT VARIOUS ϵ

$I_0 = 350$
$A_0 = 19$
$R_t = 300$
$\gamma = 1.60 - .90$
$\gamma = 1.2$
$V_0 = 0$

CASE	AREA	$\int C_F dT$	$\int C_F dT$ / $C_{F_0} \Delta T$	I (A.V.)
$\epsilon = 6$	46.05	241.10	1.140	399
$\epsilon = 10$	48.10	245.20	1.161	407
$\epsilon = 15$	46.95	242.30	1150	402.5
$\epsilon = 25$	—	—	—	—
$\epsilon = 35$	—	—	—	—
$\epsilon = 50$	—	—	—	—
ϵ = VARIABLE	60.79	282.58	1.335	467

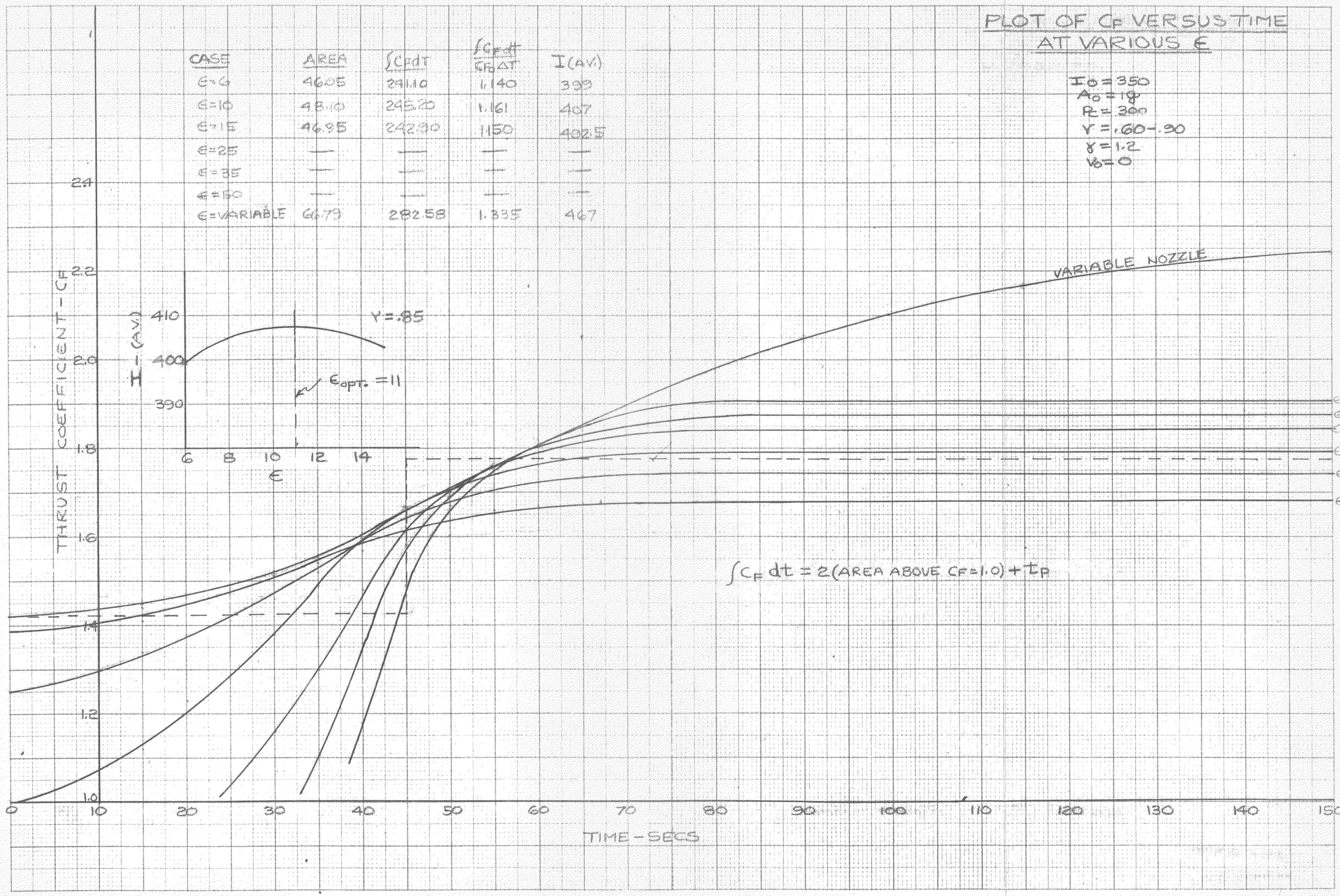

CURVE SHEET #2

PLOT OF C_F VERSUS TIME AT VARIOUS ϵ.

$I_{sp_e} = 200$
$A_p = 19$
$P_c = 300$
$\delta = 1.12$
$V_e = 0$
$\gamma = .60 - .90$

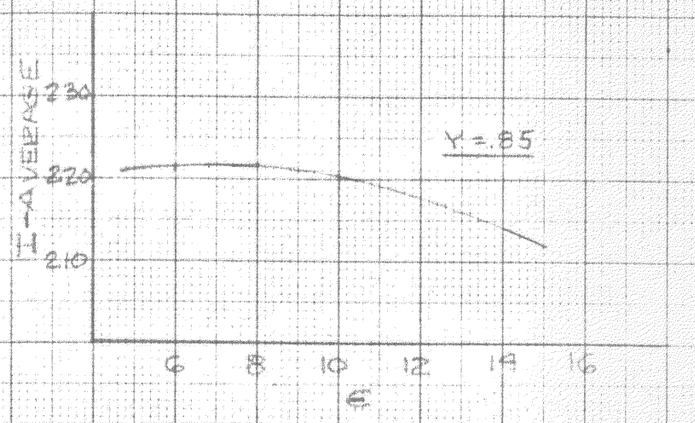

CURVE SHEET #3

PLOT OF C_F VERSUS TIME AT VARIOUS ϵ

$I_0 = 200$
$A_0 = 1\frac{1}{2}$
$P_0 = 300$
$\gamma = .60 - .80$
$\gamma = 1.2$
$V_0 = 800$ FT/SEC

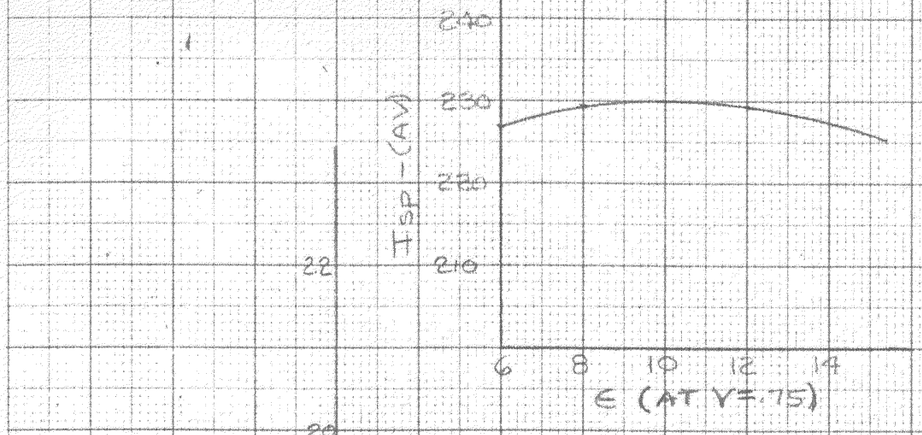

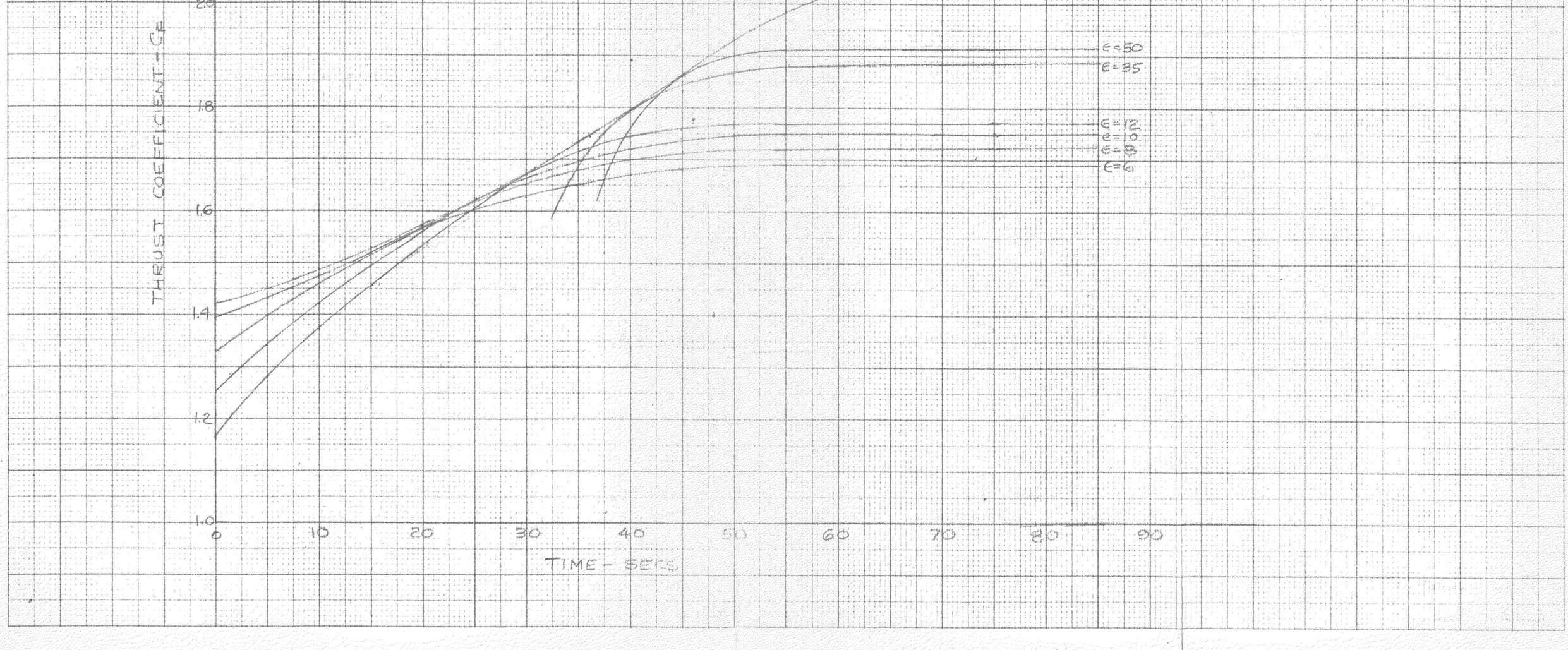

CURVE SHEET #4

PLOT OF C_F VERSUS TIME AT VARIOUS ϵ

$I_{SP_0} = 350$
$a_0 = 1\%$
$V_0 = 850$
$P_c = 300$
$\gamma = .75 - .95$

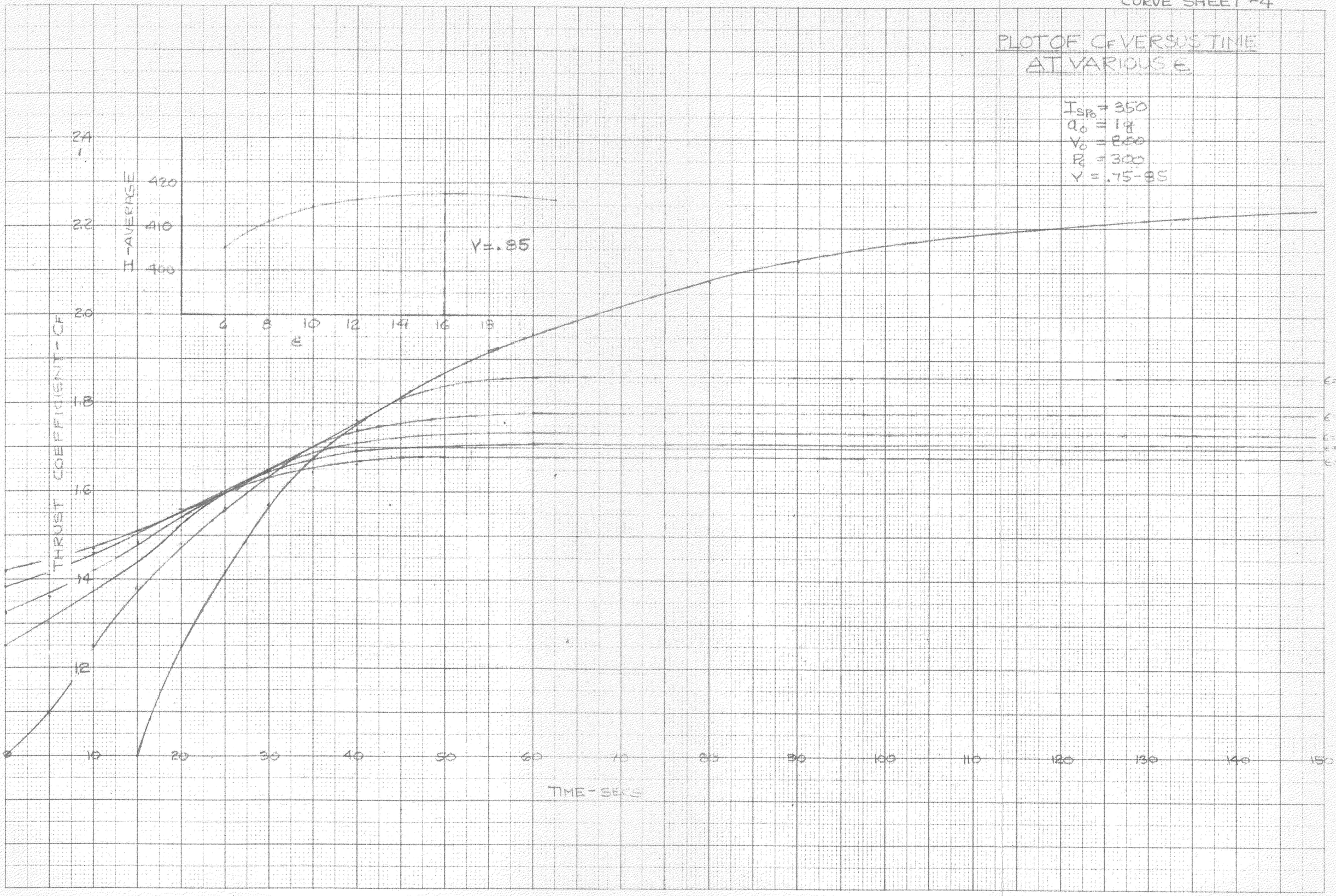

CURVE SHEET #5

PLOT OF C_F VERSUS TIME FOR VARIOUS ϵ

$T_{SP_0} = 200$
$a_0 = 1\,g$
$V_0 = 0$
$R_c = 600$
$\gamma = .75$

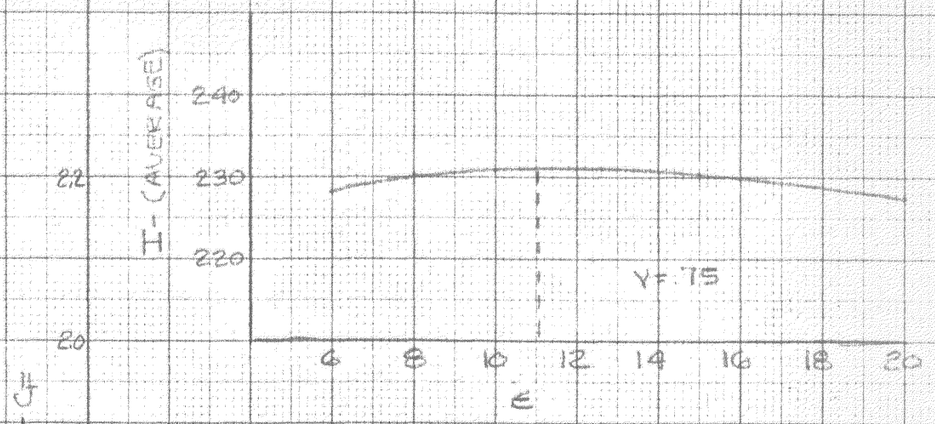

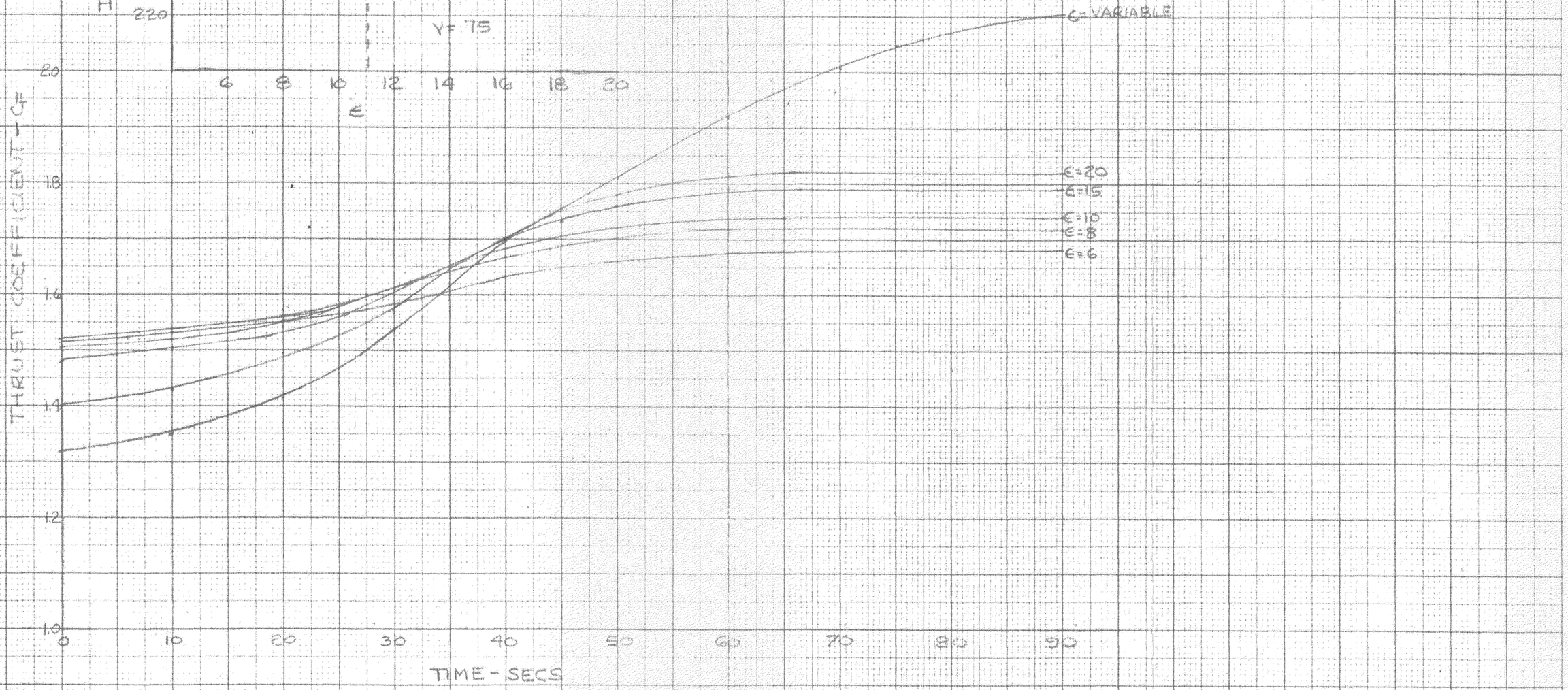

CURVE SHEET #6

PLOT OF C_F VERSUS TIME AT VARIOUS ϵ

I_{SP_0} = 200
a_0 = 1g
V_0 = 0
P_c = 1500
γ = 1.75

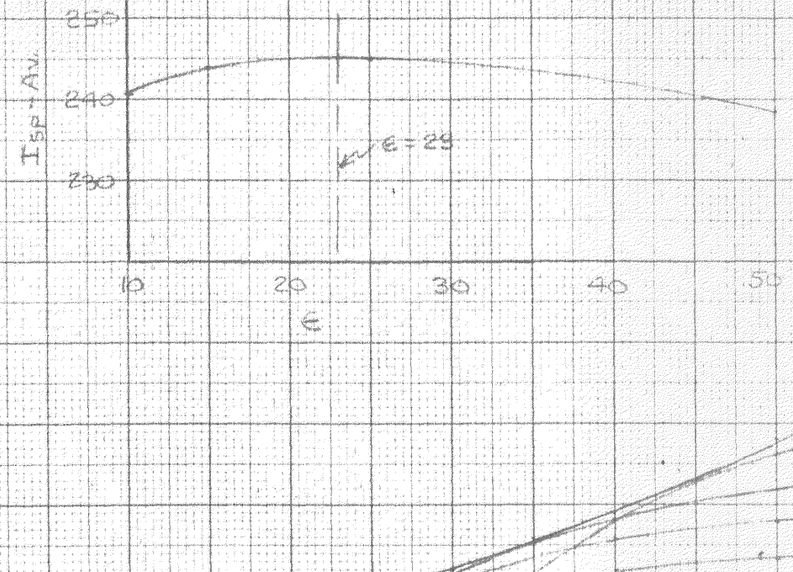

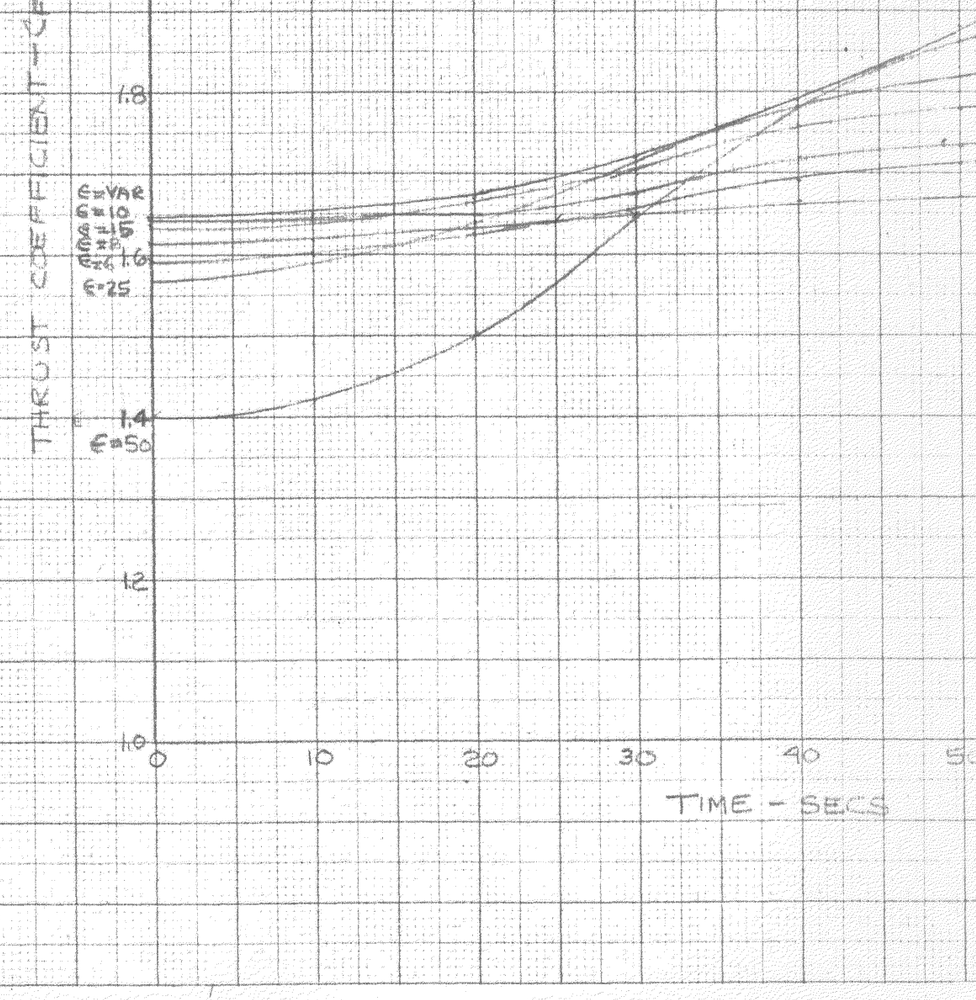

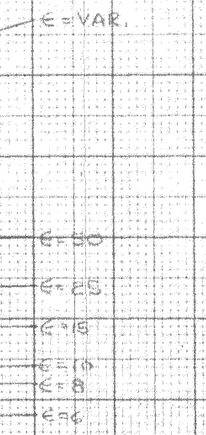

NOTE: BECAUSE OF THE EXTREME VALUE OF P_2 THE CURVES DO NOT REVERSE THEMSELVES AS THEY DO AT LOW P_2

CURVE SHEET #7

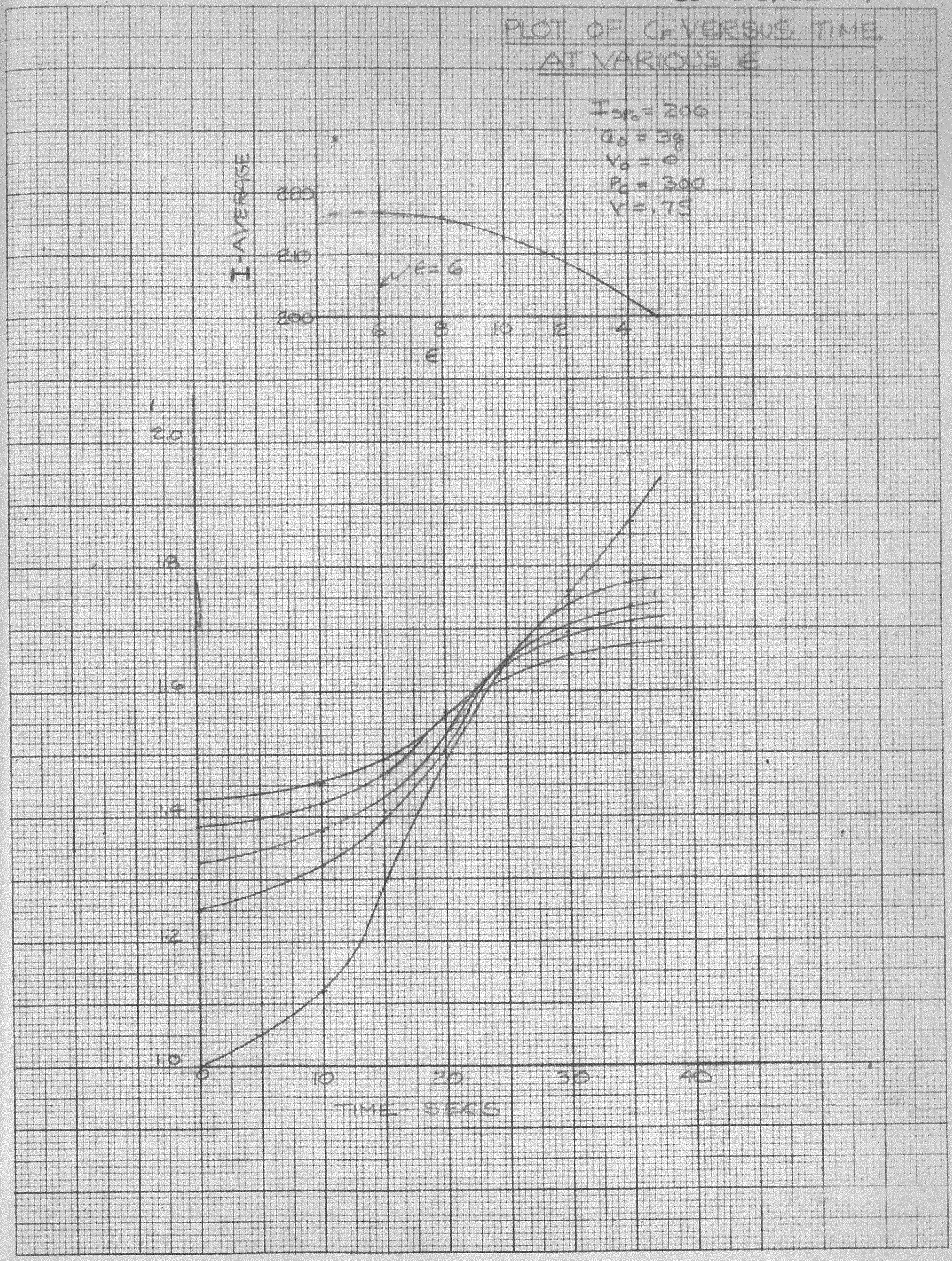

CURVE SHEET #8

PLOT OF C_F VERSUS TIME AT VARIOUS ϵ

$I = 200$
$a_0 = 2g$
$V_0 = 0$
$P_c = 300$
$\gamma = .75$

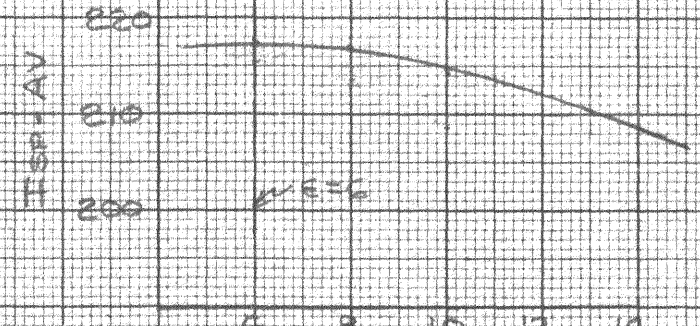

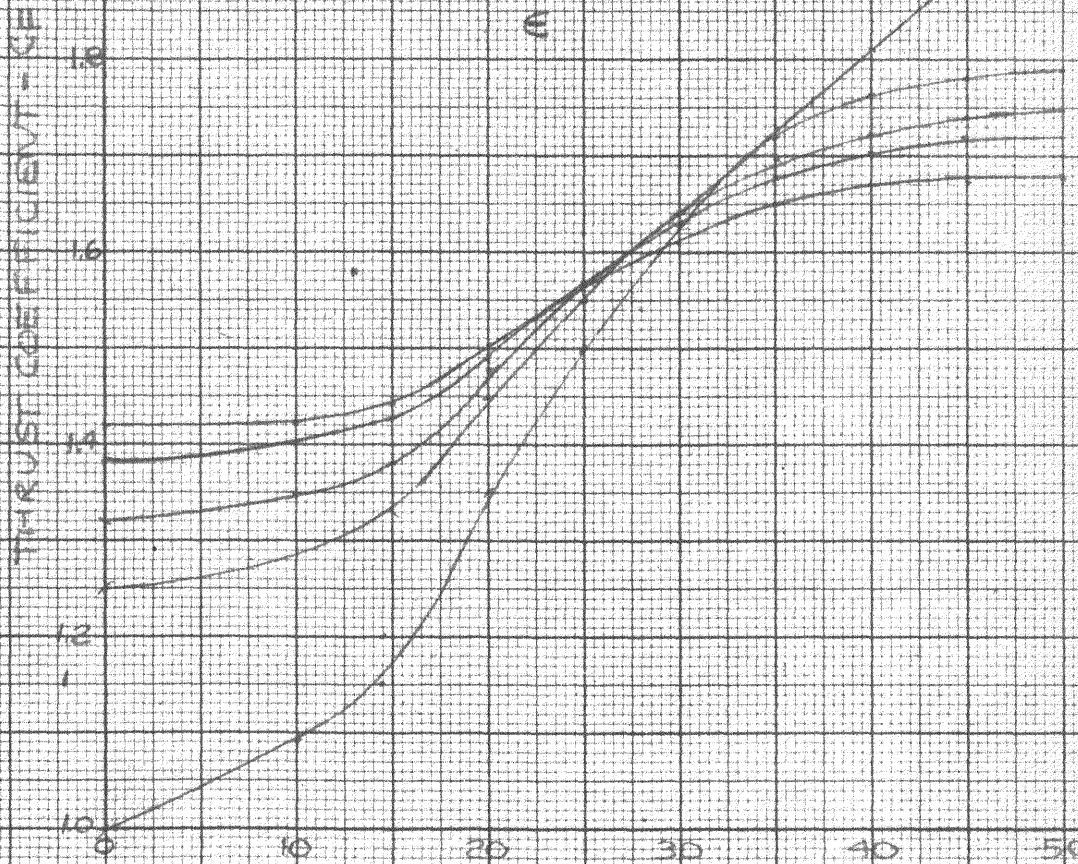

APPENDIX 11

Computations.

A. Graphical Analysis of the Oblique Shock.

The following isentropic nozzle equations, previously derived are given:

$$\epsilon^2 = \frac{\gamma - 1}{2} \quad \frac{\left(\frac{2}{\gamma + 1}\right)^{\gamma+1/\gamma-1}}{\frac{P_1}{P_c}^{2/\gamma}\left[1 - \frac{P_1}{P_c}^{\frac{\gamma-1}{\gamma}}\right]} \tag{8}$$

$$U_1 = a_c\left[\frac{2}{\gamma - 1}\right]^{1/2} \quad \left[1 - \frac{P_1}{P_c}^{\gamma-1/\gamma}\right]^{1/2} \tag{9}$$

$$\rho_1 U_1 \epsilon = \left[\gamma\left(\frac{2}{\gamma + 1}\right)^{\gamma+1/\gamma-1}\right]^{1/2} (\rho_c P_c)^{1/2} \tag{10}$$

To fit with the desired experimental test, using acid-aniline as the propellent combination, and to allow usable mixture ratios of from 1.9 to 3.1, it was decided to perform the analytical computations for values of γ of 1.22 to 1.26. To note the effect of chamber pressure, P_c, on the separation point, values of P_c, of 250, 300, and 350 psia were chosen. Using P_1/P_c as a parameter, curves of ϵ and U_1 can immediately be plotted from the above equations. GALCIT JPL curves 1-JD-170[3] give values of the gas constant, R, and chamber temperature, T_c, for various mixture ratios of acid-aniline combination, and hence "a_c" can be determined. For each choice of ϵ and U_1, ρ_1, may be computed, and hence a plot of ρ_1 versus P_1/P_c for different fixed P_c can be made.

To illustrate the above, consider the case of $\gamma = 1.26$. For this

case equation (8) reduces to:

$$\epsilon^2 = \frac{.455}{\left(\frac{P_1}{P_c}\right)^{1.588}\left[1-\left(\frac{P_1}{P_c}\right)^{.208}\right]}$$

Since $a_c = \sqrt{\gamma RT_c}$ and for $\gamma = 1.26$; R = 72 ft./deg. F; T_c takes successive values of 3785 degrees R, 3810 degrees R, and 3835 degrees R for values of P_c of 250, 300, and 350 psia, respectively. Hence a_c becomes 3340 ft/sec., 3350 ft./sec., and 3360 ft./sec., for increasing values of chamber pressure. Using these values for a_c, equation (9) reduces to;

$$U_1 = 8.8\, a_c \left[1 - \left(\frac{P_1}{P_c}\right)^{.208}\right]^{1/2}$$

Hence <u>three</u> curves of U_1 versus P_1/P_c are plotted (see page 91). The density before shock, ρ_1, becomes:

$$\rho_1 = \frac{.667\sqrt{P_c \rho_c}}{U_1 \epsilon}$$

But, for:

$$P_c = 250 \text{ psia}, \rho_c = \frac{P_c}{R\,T_c} = \frac{(250)(144)}{(72)(3785)(32.2)} = 4.1 \times 10^{-3} \text{ slugs/cu.ft.}$$

$$P_c = 300 \text{ psia}, \rho_c = \frac{(300)(144)}{(72)(3810)(32.2)} = 4.89 \times 10^{-3}$$

$$P_c = 350 \text{ psia}, \rho_c = \frac{(350)(144)}{(72)(3835)(32.2)} = 5.67 \times 10^{-3}$$

therefore:

$$\rho_1 = \frac{(.667)(4.1 \times 10^{-3} \times 250 \times 144)^{1/2}}{U_1 \epsilon} = \frac{8.13}{U_1 \epsilon} \quad \text{for } P_c = 250 \text{ psia}$$

similarly:

$$\rho_1 = \frac{9.77}{U_1 \epsilon} \qquad \text{for } P_c = 300 \text{ psia.}$$

$$\rho_1 = \frac{11.58}{U_1 \epsilon} \qquad \text{for } P_c = 350 \text{ psia.}$$

Since ϵ is a direct function of P_1/P_c, the density, ρ_1, can be plotted as a function of P_1/P_c for different chamber pressures using the appropriate U_1, previously computed.

Using this method, the curve sheet #1 was plotted.

Considering the oblique shock equation (6):

$$\frac{P_2}{P_1} = \sin^2\beta\left(\frac{2\gamma}{\gamma+1}\right) M_1^2 - \frac{\gamma-1}{\gamma+1}$$

Solving in terms of $\sin^2\beta$, and replacing M_1^2 by $U_1^2 \rho_1/\gamma P_1$, we obtain:

$$\sin^2\beta = \frac{\frac{P_2}{P_1} + \frac{\gamma-1}{\gamma+1}}{\frac{2\gamma}{\gamma+1}\left[\frac{U_1^2\rho_1}{\gamma P_1}\right]}$$

For the case when $\gamma = 1.26$, this reduces to:

$$\sin^2\beta = \frac{\frac{P_2}{P_1} + .115}{.885\left[\frac{U_1^2\rho_1}{P_1}\right]}$$

It has been assumed in this study, that when separation does occur, there is no pressure deficiency, but that the gases immediately adjust themselves to ambient atmospheric pressure. For this computation it was decided to use $P_o = P_2 = 14.1$ psia as the standard pressure, as the experimental tests were to be conducted under these conditions.

Hence, it is immediately seen, that for any assumed value of P_1, the values of U_1 and ρ_1 can be obtained from curve sheet #1. Then $\sin^2\beta$ can be computed. To facilitate this solution, P_2/P_1 of U_1 and ρ_1 compatable with a given P_1, for fixed P_c were tabulated. From this tabulation $\sin^2\beta$ could be plotted as a function of P_2/P_1 for fixed P_c. On this same graph, it was found desirable to plot β versus $\sin^2\beta$, and hence for a given P_1, pressure before shock, the angle of shock, β, can be immediately ascertained. This graphical presentation is shown on curve sheet #2.

To evaluate the conditions after the oblique shock has occurred, it becomes desirous to make use of the previously derived momentum equations:

$$\rho_2 = \rho_1 \frac{(1 + \tan\theta \tan\beta)}{(1 - \tan\theta \tan\beta)} \qquad (3)$$

$$U_2 = U_1 \frac{1}{(1 + \tan\beta \tan\theta)} \qquad (2)$$

These equations have been plotted as a function of β, for values of θ equal to 10, 15, and 20 degrees. See curve sheets 3 and 4, pages 95 and 98.

B. Solution of Oblique Shock Equations.

To solve the oblique shock equations, the following steps can be used:

1. Assume a value of P_1; from curve sheet #1, obtain U_1, ρ_1 and ϵ, for the given P_c and γ.

2. From curve sheet #2 obtain β, for the given P_c and γ.

3. With this β and the given θ, obtain the required value of ρ_2 and U_2.

4. With these values of U_1, P_1, ρ_1, θ, U_2, P_2, γ and ρ_2, substitute into the oblique shock energy equation:

$$\frac{U_1^2}{2} + \frac{\gamma}{\gamma - 1}\frac{P_1}{\rho_1} = \frac{U_2^2 \sec^2 \theta}{2} + \frac{\gamma}{\gamma - 1}\frac{P_2}{\rho_2} \qquad (5)$$

and check for compatability.

5. After having found that unique condition which checks the above equation, recheck the result by use of the momentum equation across the shock:

$$P_1 + \rho_1 U_1^2 \sin^2\beta = P_2 + \rho_2 (U_2 \sin\beta - U_2 \tan\theta \cos\beta)^2 \qquad (1)$$

C. Illustrative Example.

To show how this combined graphical-analytical solution works, the case where P_c = 300 psia, γ = 1.22, $P_o = P_2$ = 14.1, and θ = 20 degrees will be considered.

Making successive trials at assumed values of P_1, in conjunction with the enclosed curves, the following table is evaluated:

P_1	P_c/P_1	U_1	$\rho_1 x10^{-4}$	ϵ	P_2/P_1	β	U_2	$\rho_2 x10^{-4}$
3.5	85.8	7820	1.15	10.25	4.03	35.2	6230	2.97
4.5	66.7	7665	1.40	8.50	3.13	32.2	6235	4.15
5.0	60	7605	1.50	7.85	2.82	31.1	6235	4.60
5.5	54.5	7540	1.65	7.30	2.565	30.0	6235	5.37

Inserting these values, for the case of θ=20 degrees, into the energy equation:

$$\frac{U_1^2}{2} + \frac{\gamma}{\gamma - 1}\frac{P_1}{\rho_1} = \frac{U_2^2 \sec^2 \theta}{2} + \frac{\gamma}{\gamma - 1}\frac{P_2}{2}$$

we obtain the following table:

P_1	$U_1^2/2$	$5.54\ P_1/\rho_1$	$.568\ U_2^2$	$11250/\ P_2$
3.5	30.5	24.4	22.1	37.9
4.5	29.4	25.7	22.1	27.1
5.0	28.9	26.7	22.1	24.4
5.5	28.4	26.5	22.1	20.9

Plotting both sides of this equation versus P_1, we find the unique value of $P_1 = \underline{3.85}$, as that which satisfies this equation. Returning to the curve sheets, it is noted that for $P_1 = 3.85$, that $\epsilon_s = 9.55$, $\beta = 34.15$, $\rho_1 = 1.22 \times 10^{-4}$, $U_1 = 7760$, $\rho_2 = 3.30 \times 10^{-4}$, and $U_2 = 6225$.

Inserting these values into the momentum equation across the shock to check for compatability:

$$P_1 + \rho_1 U_1^2 \sin^2\beta = P_2 + \rho_2 (U_2 \sin^2\beta - U_2 \tan\theta \cos\beta)^2$$

$$(3.85)(144) + (1.22 \times 10^{-4})(7760)(.314) = (14.1)(144) + (3.30 \times 10^{-4}) \times \left[(6225)(.560) - (6225)(.364)(.828)\right]^2$$

$$555 + 2310 = 2030 + 842$$

$$2865 = 2872 \ (\underline{\text{close}})$$

Thus, we have determined that $\epsilon_s = 9.55$ is the area ratio at which separation occurs, when operating at $P_c = 300$ psi., with a deflection angle of 20 degrees, and with $\gamma = 1.22$, under sea-level atmospheric condition of $P_o = 14.1$ psia.

Since our oblique shock wave theory shows us that two possible shocks can satisfy these equations, it becomes necessary to consider not only which of these solutions is actually found by the above method, but whether the alternate solution is possible.

D. Determination of Alternate Solution.

The mach number, M_1, corresponding to the solution just obtained for $P_1 = 3.85$, is calculated by:

$$M_1 = U_1/a_1 = U_1 \Big/ \sqrt{\frac{\gamma P_1}{\rho_1}} = \frac{(7760)(1.22 \times 10^{-4})^{1/2}}{(1.22)^{1/2}(3.85 \times 144)^{1/2}} = \underline{3.42}$$

Referring to the oblique shock equations:

$$\frac{1}{M_1^2} = \sin^2\beta - \frac{\gamma + 1}{2} \left[\frac{\sin\beta \sin\theta}{\cos(\beta - \theta)} \right] \qquad (7)$$

$$\frac{P_2}{P_1} = \frac{2\gamma}{\gamma + 1} M_1^2 \sin^2\beta - \frac{\gamma - 1}{\gamma + 1} \qquad (6)$$

By taking successive values of β, and solving for M_1, for $\theta = 20^\circ$, $\gamma = 1.22$, the following table is prepared:

β	$\sin^2\beta$	$\frac{\gamma+1}{2} \sin\theta \sin\beta$	$\cos(\beta - \theta)$	$\frac{1}{M_1^2}$	M_1^2	M_1
25	.177	.160	.996	.016	62.5	7.94
30	.250	.189	.984	.058	17.2	4.16
35	.327	.217	.965	.102	9.8	3.14
45	.499	.268	.906	.203	4.92	2.23
60	.747	.329	.766	.347	2.88	1.70
75	.930	.366	.573	.290	3.45	1.86
80	.962	.373	.500	.216	4.63	2.16
85	.988	.378	.423	.094	10.6	3.28
87	.988	.3788	.390	.024	41.7	6.48

Taking these values of M_1, β, and inserting them into equation (6), we obtain the following set of data:

β	M_1	$\sin^2\beta$	$\frac{2\gamma}{\gamma+1} M_1^2 \sin^2\beta$	P_2/P_1
25	7.94	.177	12.26	12.16
30	4.16	.250	4.77	4.67
35	3.14	.327	3.55	3.45
45	2.23	.499	2.725	2.625
60	1.70	.747	2.38	2.28
75	1.86	.930	3.54	3.44
80	2.16	.967	4.97	4.87
85	3.28	.988	11.70	11.6
87	6.48	.998	46.00	45.90

Plotting M_1 versus P_2/P_1, we obtain curve sheet #5. For isentropic flow through a nozzle we have the defining relation:

$$P_2/P_1 = P_c/P_1 \times P_2/P_c$$

therefore:

$$P_2/P_1 = P_2/P_c \frac{(1 + (\gamma - 1)M_1^2)^{\gamma/\gamma-1}}{2}$$

for this problem, $P_2/P_c = 14.1/300 = .047$

therefore:

$$P_2/P_1 = .047 \frac{(1 + (\gamma - 1)M_1^2)^{\gamma/\gamma-1}}{2}$$

for various values of M we obtain:

M	$(1 + .11M_1^2)$	$(1 + .11M_1^2)^{5.55}$	P_2/P_1
2	1.44	7.58	.356
3	1.99	45.7	2.115
4	2.76	277.0	13.03
5	3.75	1525.	71.60

Plotting these values on the same graph, we find that two solutions satisfy these equations. That solution, marked A, represents the solution previously

determined, analytically, i.e., $M_1 = 3.42$, for $P_1 = 3.85$ (or $P_2/P_1 = 3.78$). This solution corresponds to a weak wave oblique shock, as the pressure rise occurring is reasonably small. However, a second solution, marked B, occurs for a mach number $M_1 = 4.4$, with an accompanying pressure rise P_2/P_1 of 23.5. Obviously, this strong wave solution would require that the gases cling to the nozzle until the pressure was about .6 psia. To determine what area ratio this represents, a plot of ϵ versus M_1 has been incorporated, see curve sheet #6. From this curve it can be seen that for a mach number, $M_1 = 4.4$, an area ratio of approximately 42.5 would be needed before this shock occurred. Hence this strong wave does not appear to have any practical significance at this point.

This point represents the minimum Mach number which can occur in the gas flow, where the gases can be turned through a wedge angle of 20 degrees, by a simple oblique shock wave. Any flow mach number, M_1, less than 1.70 would have to be turned by a normal shock or some combination of waves. Since this point is of definite interest, it was decided to see how this varied with changing θ, and to note what further prediction could be made by such an investigation.

Following a similar procedure to that just described, a complete diagram, curve sheet #7, was constructed, for various θ, at $\gamma = 1.26$. Note that a line connecting all these critical points, line A-A, could be called a "line of maximum deflection angle". If the isentropic nozzle equation is plotted on this diagram, the point where these two lines intersect serves to indicate the maximum deflection angle that could occur, and allow a simple shock to satisfy the resulting flow. On curve sheet #7, are plotted three such nozzle equations (for $P_o/P_c = .040$, .047 and

.056). It appears that for the cases considered in this treatment, that a maximum of $\theta = 45$ degrees might still allow a simple oblique shock solution.

E. Temperature Considerations.

The question arises as to whether varying the temperature of the gases flowing through a nozzle would have any effect on this solution. Throughout the solution it has been assumed that the gases flow in a frozen state, i.e., combustion is completed in the combustion chamber, and hence γ does not vary through the nozzle.

Inspection of the isentropic nozzle equations:

$$\rho_1 = \left[\gamma \left(\frac{2}{\gamma+1}\right)^{\frac{\gamma+1}{\gamma-1}}\right]^{1/2} \frac{\sqrt{P_c \rho_c}}{U_1 \epsilon} \qquad (10)$$

$$U_1 = \left(\frac{2}{\gamma-1}\right)^{1/2} a_c \left[1 - (P_1/P_c)^{\frac{\gamma-1}{\gamma}}\right]^{1/2} \qquad (9)$$

shows that

$$\rho_1 \propto \frac{\sqrt{P_c \rho_c}}{a_c} \propto \frac{\sqrt{P_c \rho_c}}{\sqrt{\gamma RT_c}} \propto \sqrt{\frac{\rho_c^2 T_c}{T_c}}$$

Therefore, the nozzle equations show no temperature sensitivity. Referring to the oblique shock equations, it is seen that

$$P_2/P_1 \propto M_1 \propto U_1 \sqrt{\gamma RT_1} \propto \sqrt{T_c} / \sqrt{T_1}$$

But T_1 is dependent on T_c such that any change in T_c would also result in a change in T_1 in the same direction. Hence it can be concluded that temperature is not of prime importance.

F. Effect on Thrust Coefficient.

In an effort to note how the previously accepted thrust coefficient variation with altitude would be affected by separation, a typical nozzle, of area-ratio $\varepsilon = 10$, was considered. The effect of ambient pressure change on the coefficient, C_F, is determined as follows, neglecting separation:(3)

Since:

$$C_{F_{th}} = C_{F_{MAX}} + \frac{P_e - P_o}{P_c} \epsilon$$

where:

$$C_{F_{MAX}} = \Gamma' \left[\frac{2}{\gamma - 1} \left[1 - \frac{P_e}{P_c}^{\gamma-1/\gamma} \right] \right]^{1/2}$$

and P_e is that unique value of exit pressure which exactly equals the ambient pressure. For a given ϵ this value of P_e is determined by solution of the equation.(3)

$$\epsilon = \frac{\frac{2}{\gamma+1}^{\frac{\gamma+1}{2(\gamma-1)}}}{\left(\frac{P_e}{P_c}\right)^{\frac{1}{\gamma}} \left[\frac{2}{\gamma-1} \left[1 - \frac{P_e}{P_c}^{\frac{\gamma-1}{\gamma}} \right] \right]^{1/2}}$$

From the above equations, it is readily seen that a plot of C_F versus P_o/P_c would be a linear relationship, continually decreasing with increasing P_o. This is obviously the effect of the gases clinging to the nozzle, even though pressures far below the ambient pressure, P_o, exist in the nozzle. This plot is made for $\epsilon = 10$, on Graph 11-3 in the "Results and Conclusions", for $\gamma = 1.26$

Since separation does occur, and for a given divergence angle and γ, the value of separation area-ratio, ϵ_s, has been determined, as a function of P_c/P_o, it is now possible to determine the point at which the C_F versus P_o/P_c curve deviates from the linear relation. Also the variation in C_F versus P_o/P_c after separation commences can be determined.

By referring to Graph 11-2, for an $\epsilon_s = 10$, $P_c/P_o = 31.3$, this represents the point at which separation commences to occur for this nozzle. As atmospheric pressure is further reduced, or P_c/P_o increases, the separation point will move back toward the throat. Hence it becomes necessary to consider other separation locations to note the effect on C_F. Similar area-ratio versus P_o/P_c curves were constructed, by consideration of the above equations, for various values of ϵ. The value of P_c/P_o for successive ϵ_s values was noted from Graph 11-2, and thus Graph 11-3 was constructed.

CURVE SHEET # 1-A

PLOT OF VELOCITY AND DENSITY AND AREA RATIO VERSUS P_2/P_1 FOR ISENTROPIC NOZZLE FLOW

DEFINING EQUATIONS :-

$$U_1 = a_c \left(\frac{2}{\gamma-1}\right)^{1/2} \left[1-\left(\frac{P_1}{P_c}\right)^{\gamma-1/\gamma}\right]^{1/2}$$

$$\rho_1 = \frac{1}{U_1 \epsilon} \left[\gamma \left(\frac{2}{\gamma+1}\right)^{\gamma+1/\gamma-1}\right]^{1/2} \sqrt{P_c \rho_c}$$

$$\epsilon^2 = \frac{\gamma-1}{2} \frac{(\gamma^2+1)^{\gamma+1/\gamma-1}}{\left(\frac{P_1}{P_c}\right)^{2/\gamma}\left[1-\frac{P_1}{P_c}\right]^{\gamma-1/\gamma}}$$

$\gamma = 1.22$

$U_1 (P_2 = 250)$

$U_1 (P_2 = 300)$

$U_1 (P_2 = 350)$

$\rho_1 (P_2 = 350)$

$\rho_1 (P_2 = 300)$

$\rho_1 (P_2 = 250)$

E

$\rho_1 \times 10^4$

U_1 - FT/SEC

E - RATIO

P_2/P_1

CURVE SHEET # 1-B

PLOT OF VELOCITY AND DENSITY AND AREA RATIO VERSUS P_2/P_1 FOR ISENTROPIC NOZZLE FLOW

DEFINING EQUATIONS:-

$$U_1 = a_c \left(\frac{2}{\gamma+1}\right)^{1/2} \left[1-\left(\frac{P_1}{P_c}\right)^{\gamma-1/\gamma}\right]^{1/2}$$

$$\rho_1 = \frac{1}{U_1 \epsilon} \left[\gamma\left(\frac{2}{\gamma+1}\right)^{\gamma+1/\gamma-1}\right]^{1/2} \sqrt{P_c \rho_c}$$

$$\epsilon^2 = \frac{\gamma-1}{2} \frac{(\gamma^2+1)^{\gamma+1/\gamma-1}}{\left(\frac{P_1}{P_c}\right)^{2/\gamma}\left[1-\frac{P_1}{P_c}\right]^{\gamma-1/\gamma}}$$

$\gamma = 1.26$

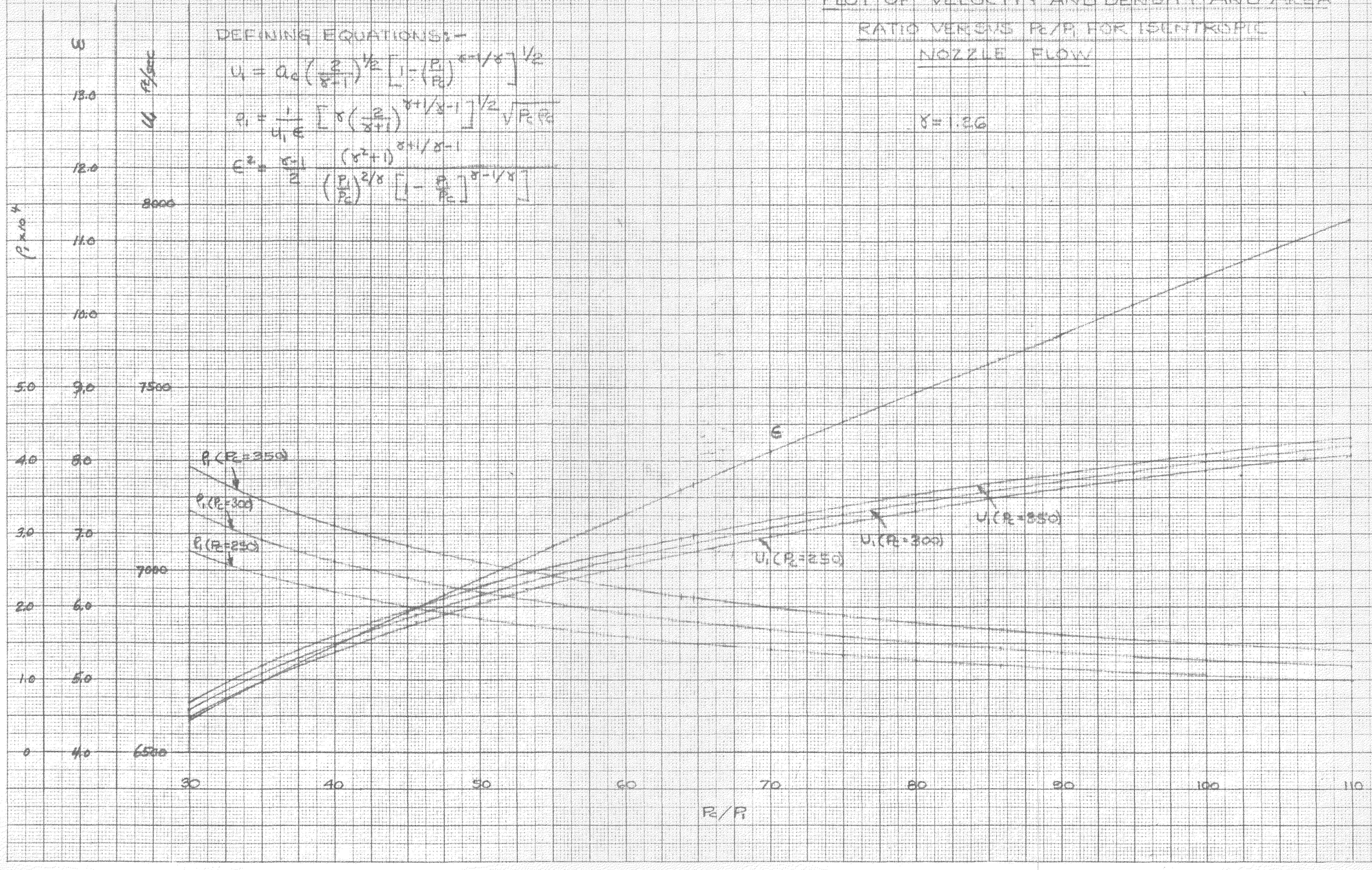

CURVE SHEET # 2-A

GRAPHICAL SOLUTION FOR SHOCK ANGLE, β, KNOWING

P_1, THE PRESSURE BEFORE SHOCK

$\gamma = 1.22$

$P_1 = 14.1$

DEFINING EQUATION:-

$$\frac{P_2}{P_1} = \frac{2\gamma}{\gamma+1} M_1^2 \sin^2\beta - \frac{\gamma-1}{\gamma+1}$$

$\frac{P_2}{P_1}(P_2 = 250)$

$\frac{P_2}{P_1}(P_2 = 350)$

$\frac{P_2}{P_1}(P_2 = 500)$

β

$P_2/P_1 + \frac{\gamma-1}{\gamma+1} = \frac{2\gamma}{\gamma+1}\left(\frac{1}{M_1^2 \sin^2\beta}\right)$

$\sin^2\beta$

0.5, 0.4, 0.3, 0.2, 0.1

20°, 22°, 24°, 26°, 28°, 30°, 32°, 34°, 36°, 38°, 40°, 42°, 44°, 46°, 48°

SHOCK ANGLE = β°

1.0, 2.0, 3.0, 4.0, 5.0, 6.0

P_2/P_1

CURVE SHEET # 2 B

GRAPHICAL SOLUTION FOR SHOCK ANGLE, β, KNOWING P_1, THE PRESSURE BEFORE SHOCK

DEFINING EQUATION:-

$$\frac{P_2}{P_1} = \frac{2\gamma}{\gamma+1} M_1^2 \sin^2\beta - \frac{\gamma-1}{\gamma+1}$$

$\gamma = 1.26$

$P_1 = 14.1$

β

$P_2/P_1 (P_2 = 250)$

$P_2/P_1 (P_2 = 300)$

$P_2/P_1 (P_2 = 350)$

$\frac{P_2/P_1 + \frac{\gamma-1}{\gamma+1}}{\frac{2\gamma}{\gamma+1}\left(\frac{M_1^2 P_1}{\gamma P_2}\right)} = \sin^2\beta$

0.5, 0.4, 0.3, 0.2, 0.1

22°, 24°, 26°, 28°, 30°, 32°, 34°, 36°, 38°, 40°, 42°, 44°, 46°, 48°

SHOCK ANGLE - β

1.0, 2.0, 3.0, 4.0, 5.0, 6.0

P_2/P_1

CURVE SHEET 3-A

$$P_2 = P_1 \frac{(1 + \tan\Theta \tan\beta)}{(1 - \tan\Theta \cot\beta)}$$

$\Theta = 10°$

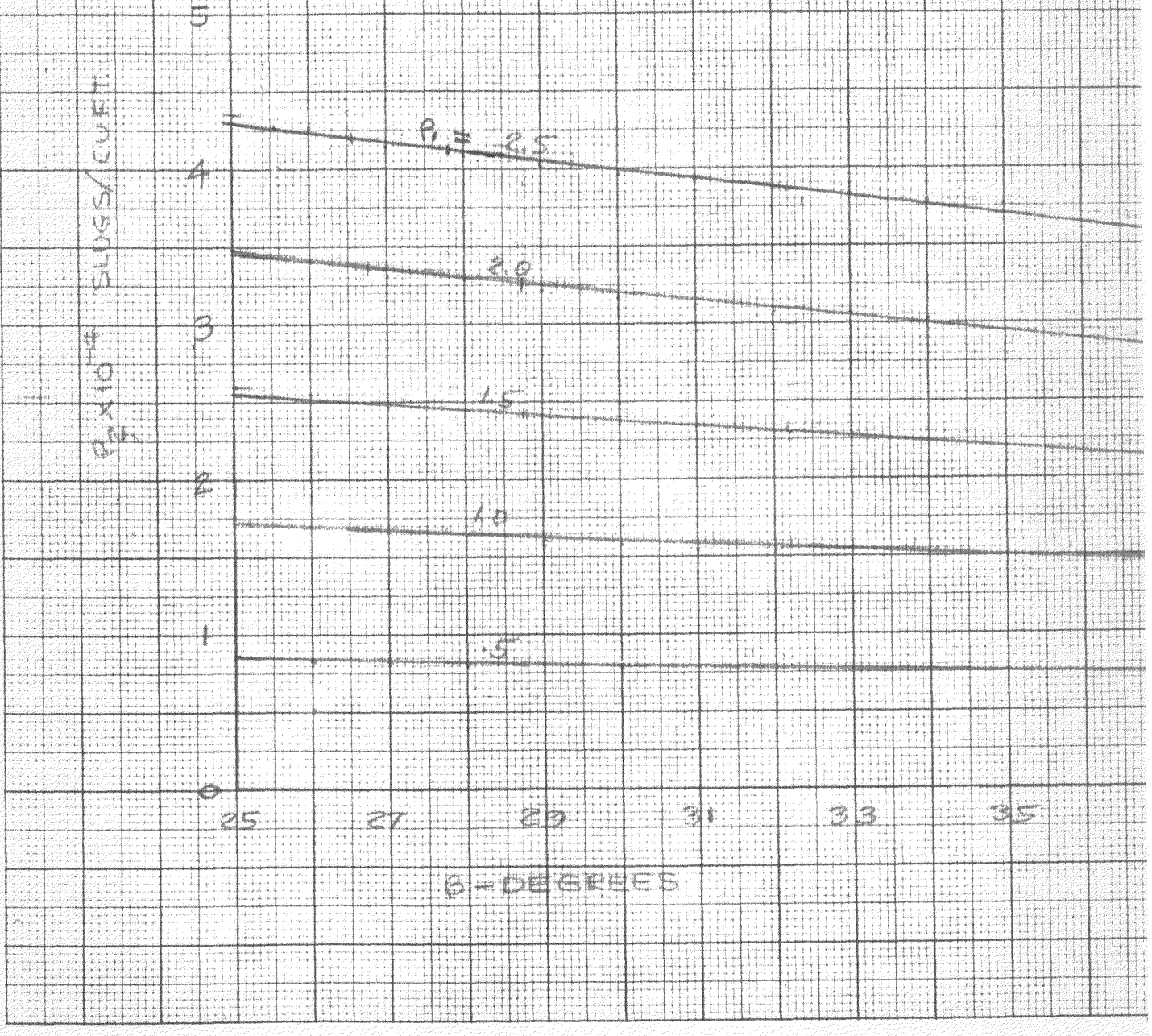

CURVE SHEET 3-8

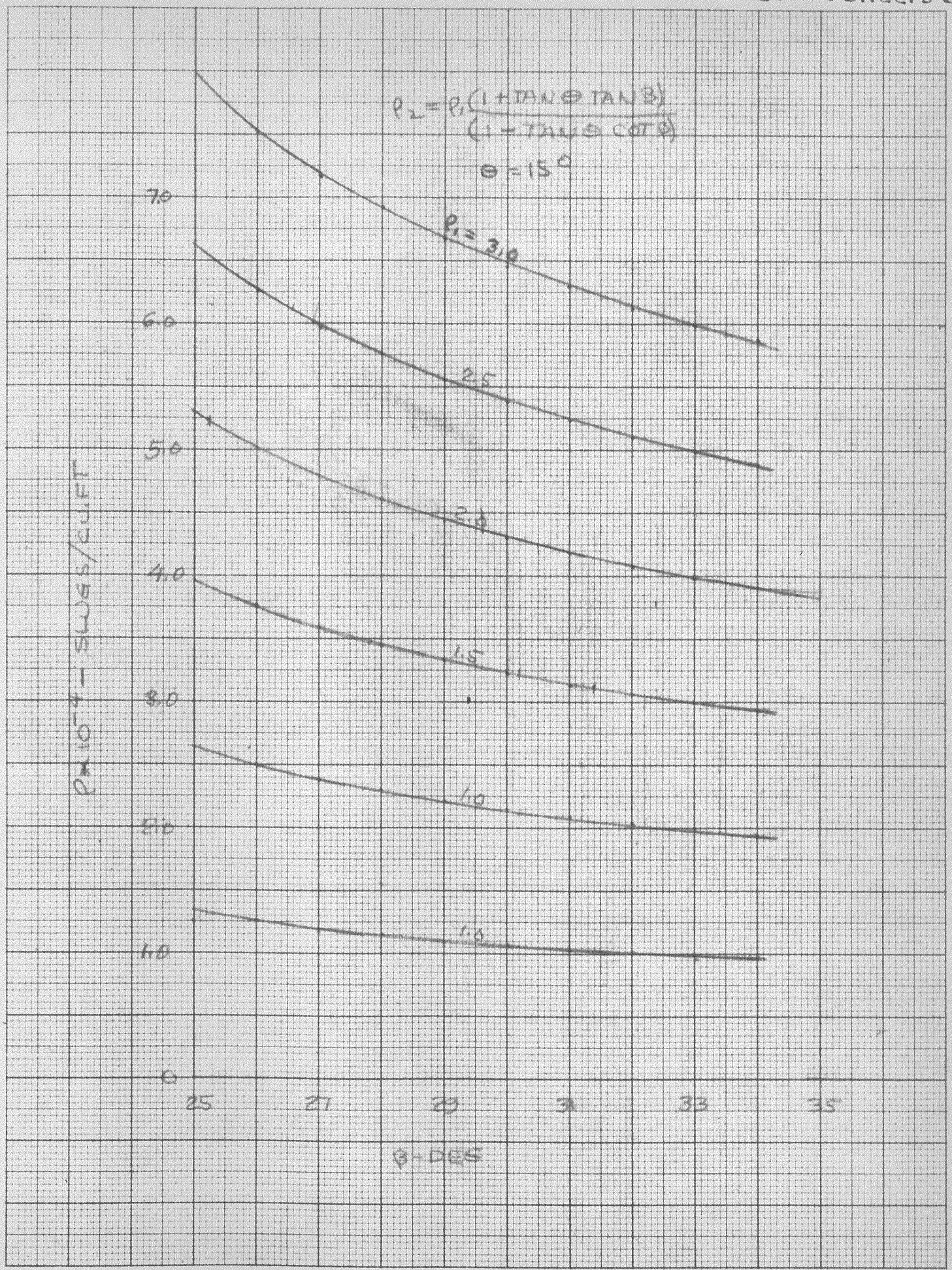

CURVE SHEET 3-C

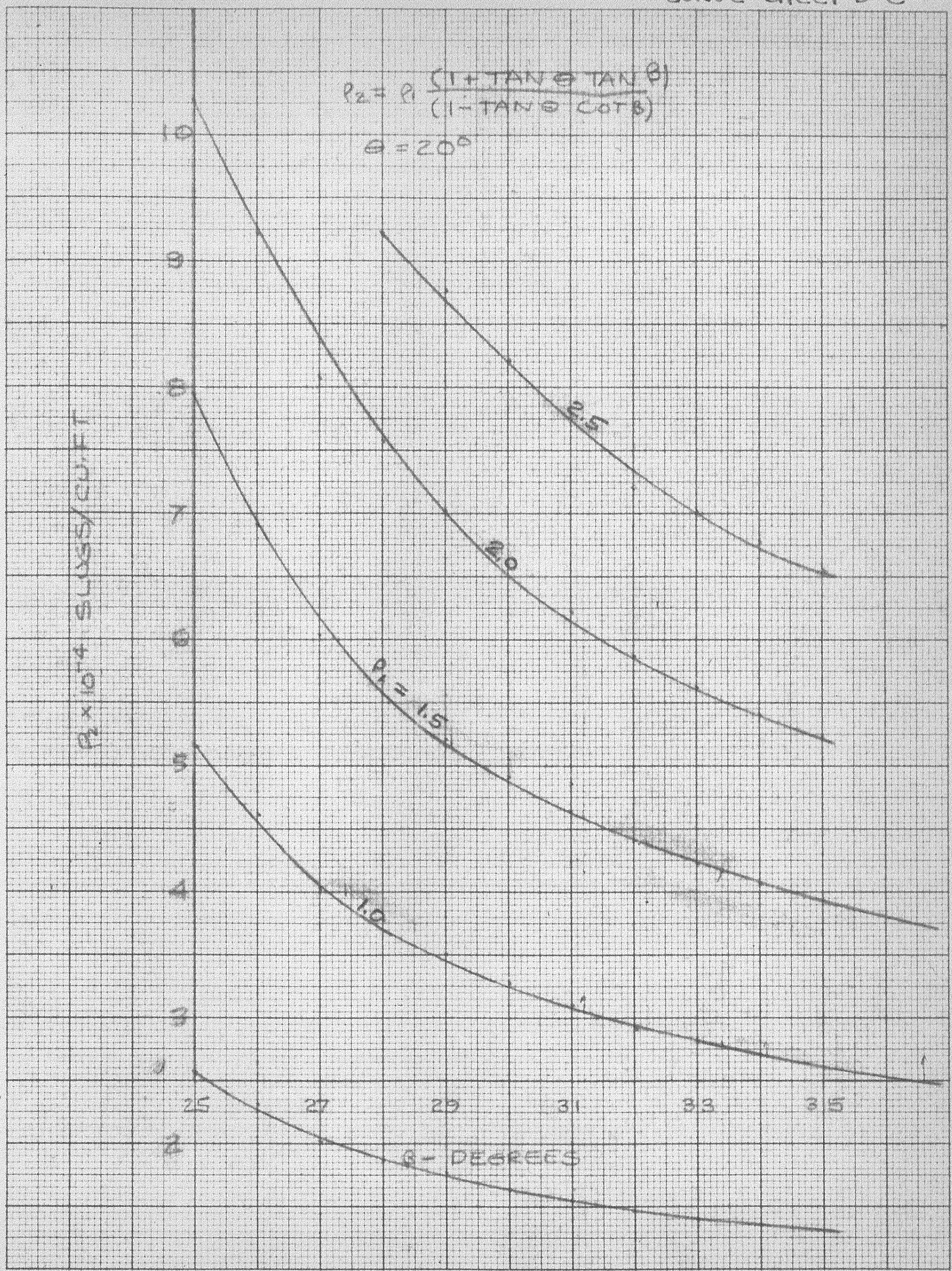

CURVE SHEE 4-A

$$U_2 = \frac{U_1}{1 + \tan\delta \tan\theta}$$

$\theta = 10°$

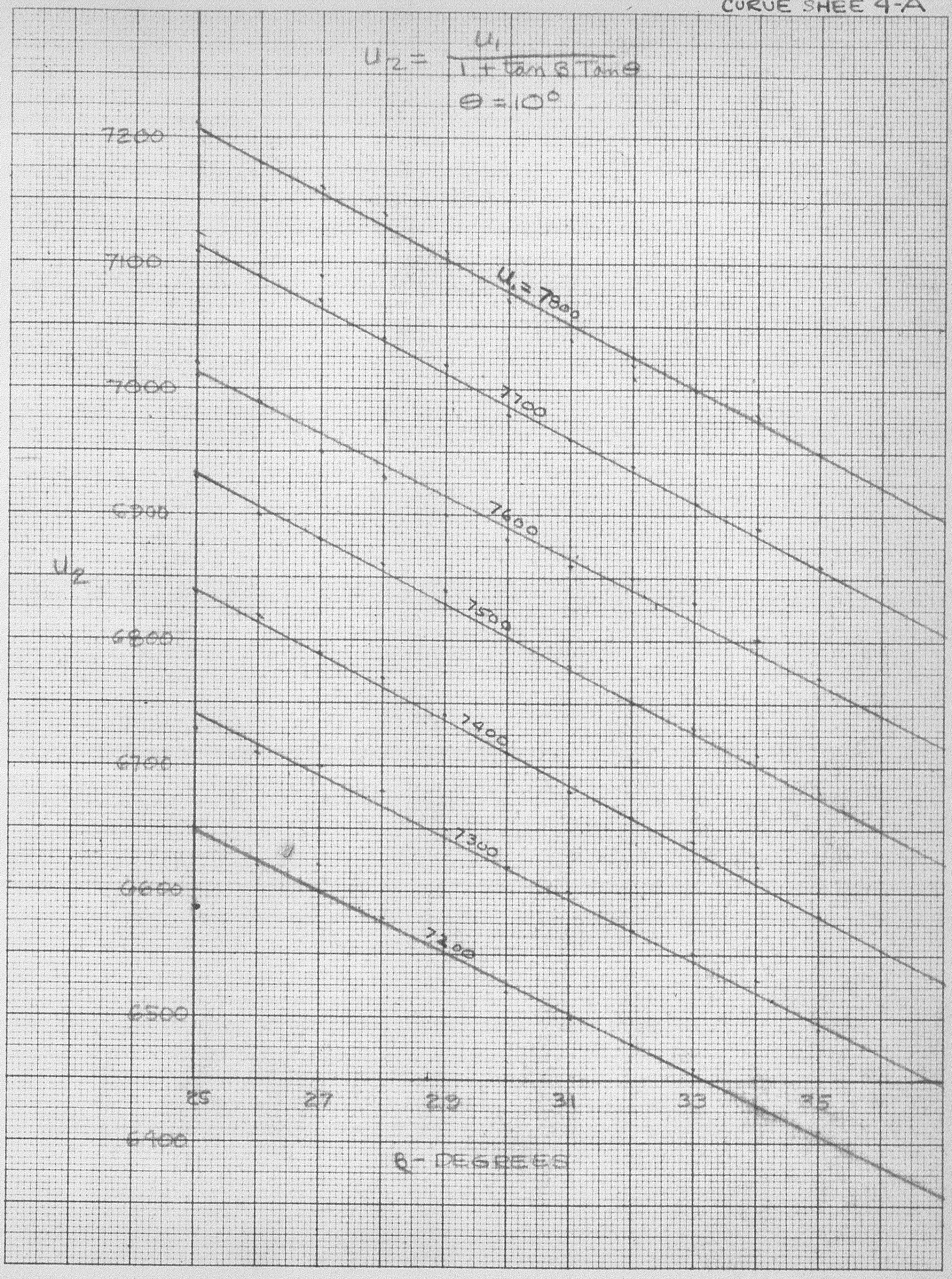

CURVE SHEET 9-B

$$U_2 = \frac{U_1}{1 + TAN\theta\, TAN\beta}$$

$\theta = 15°$

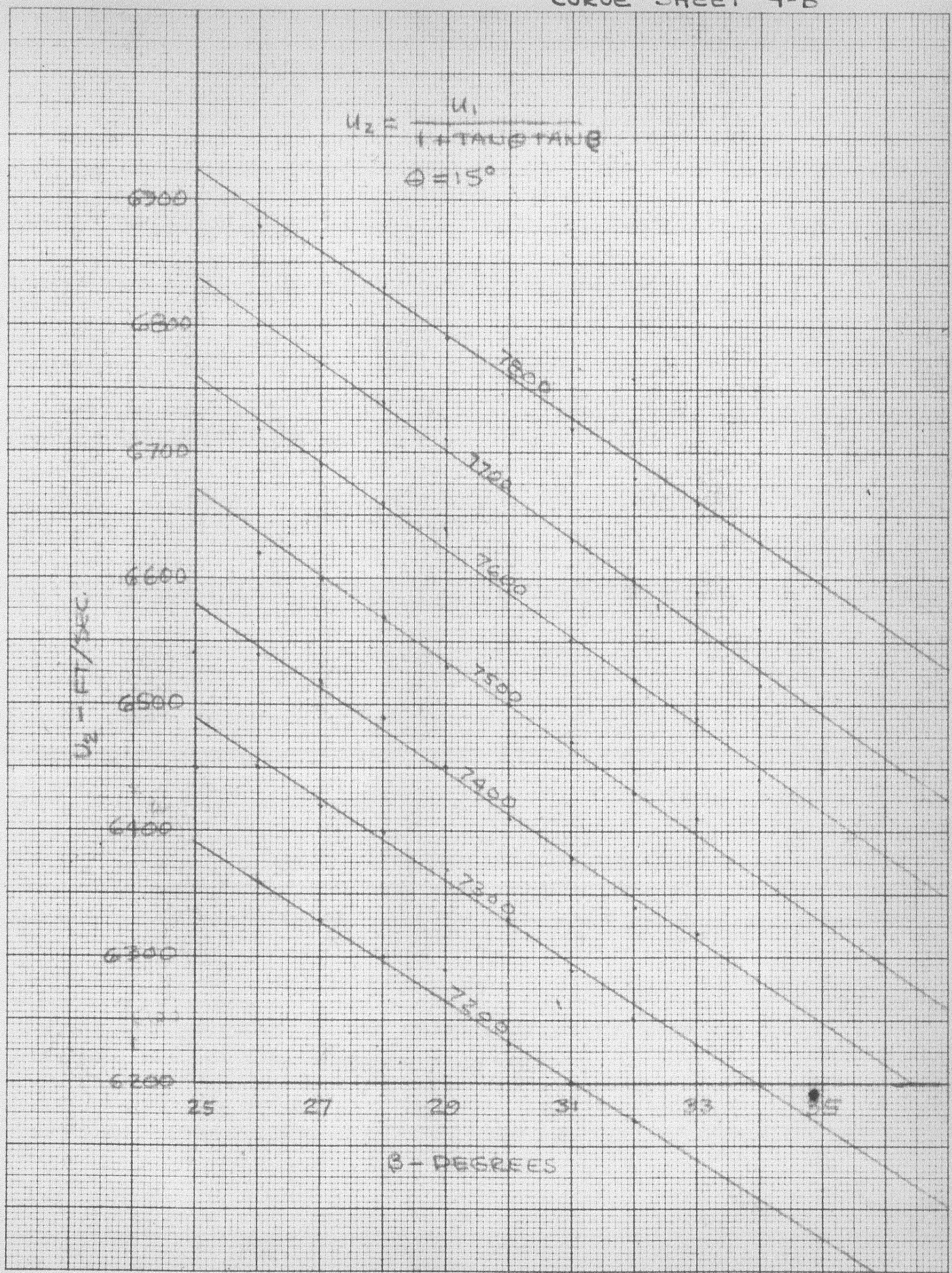

CURVE SHEET 4-C

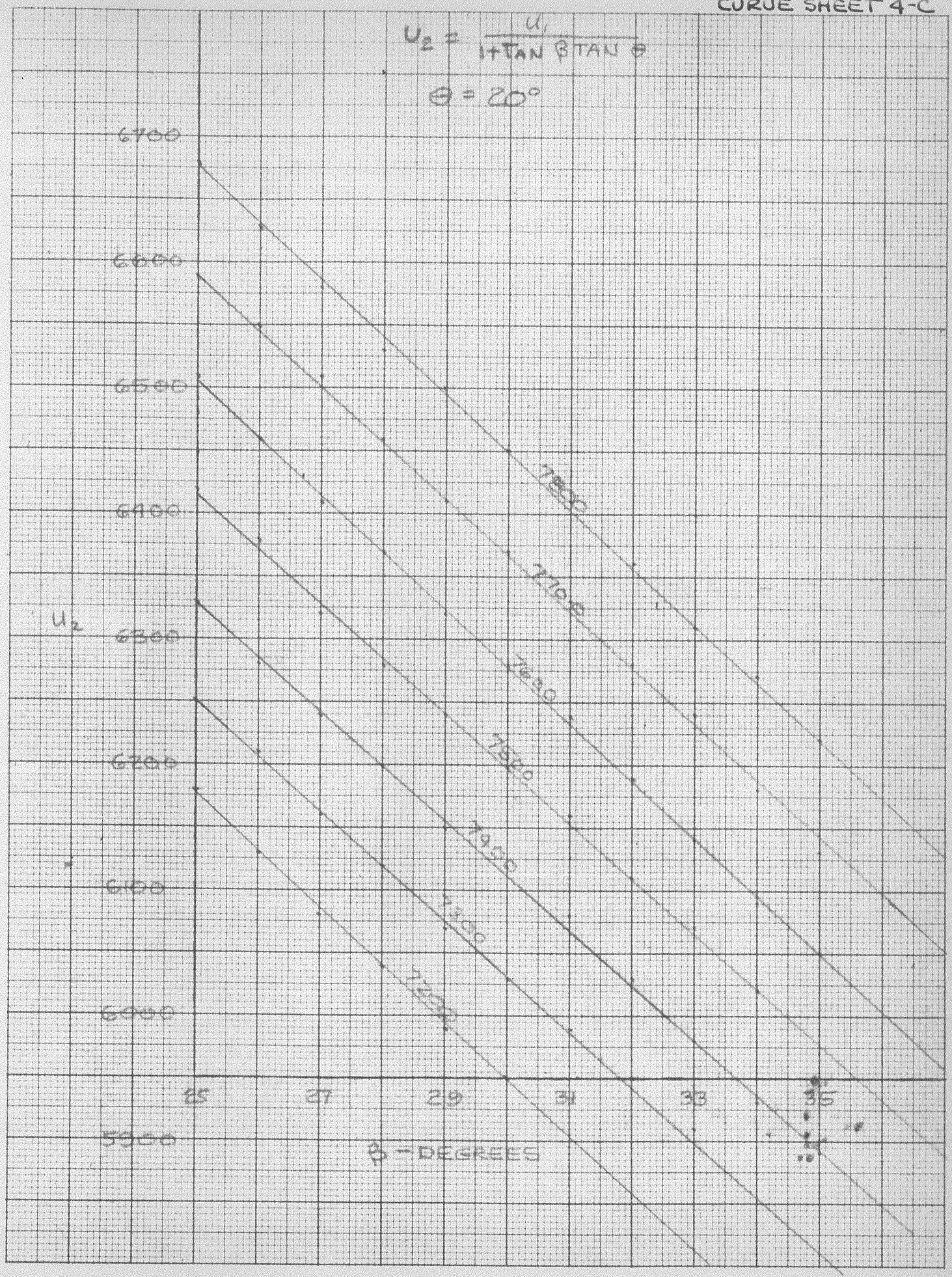

CURVE SHEET 5

DETERMINATION OF STRONG AND WEAK WAVE SEPARATION SOLUTIONS

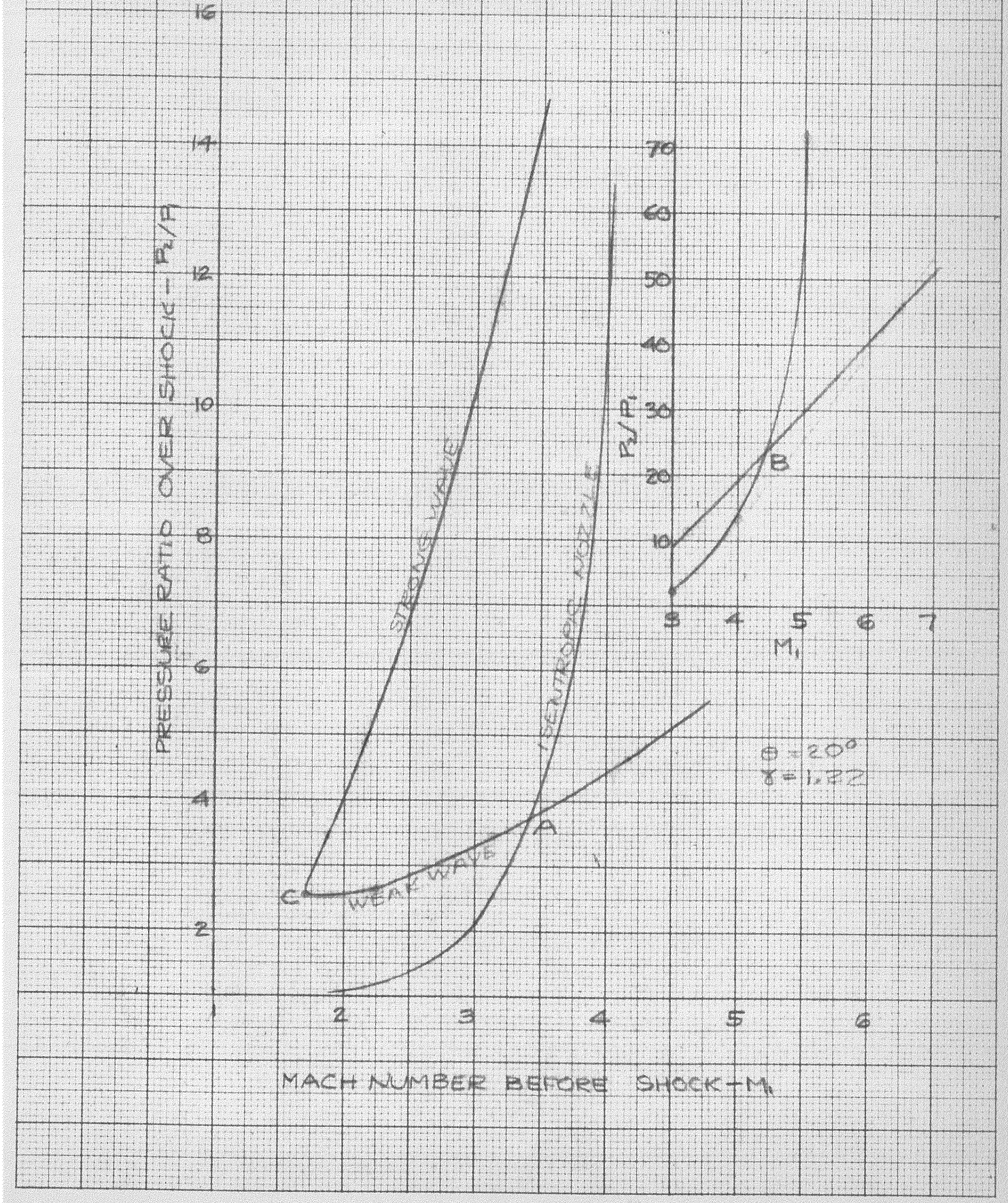

CURVE SHEET 57A

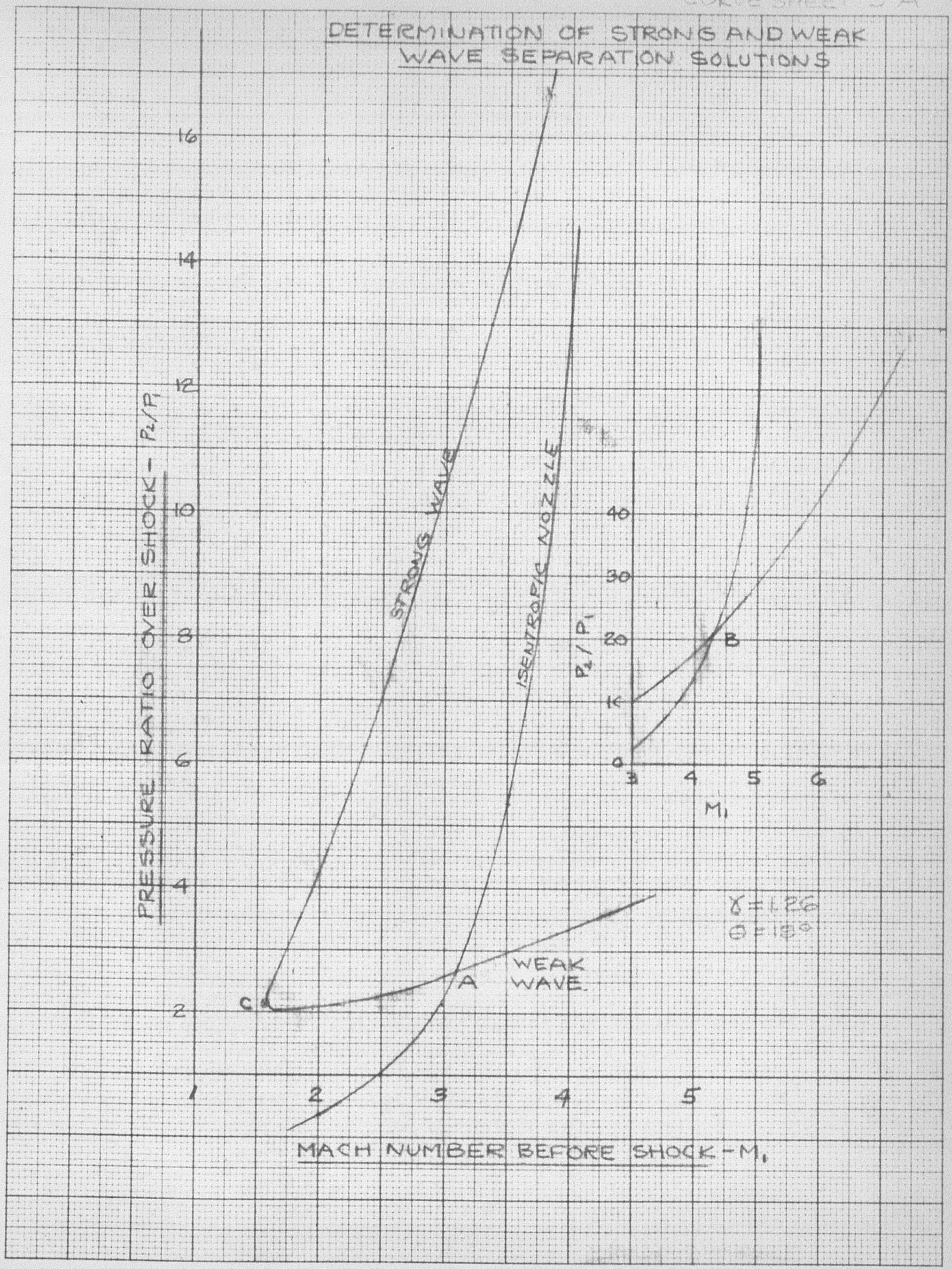

CURVE SHEET 6

MACH NUMBER - AREA RATIO VARIATION

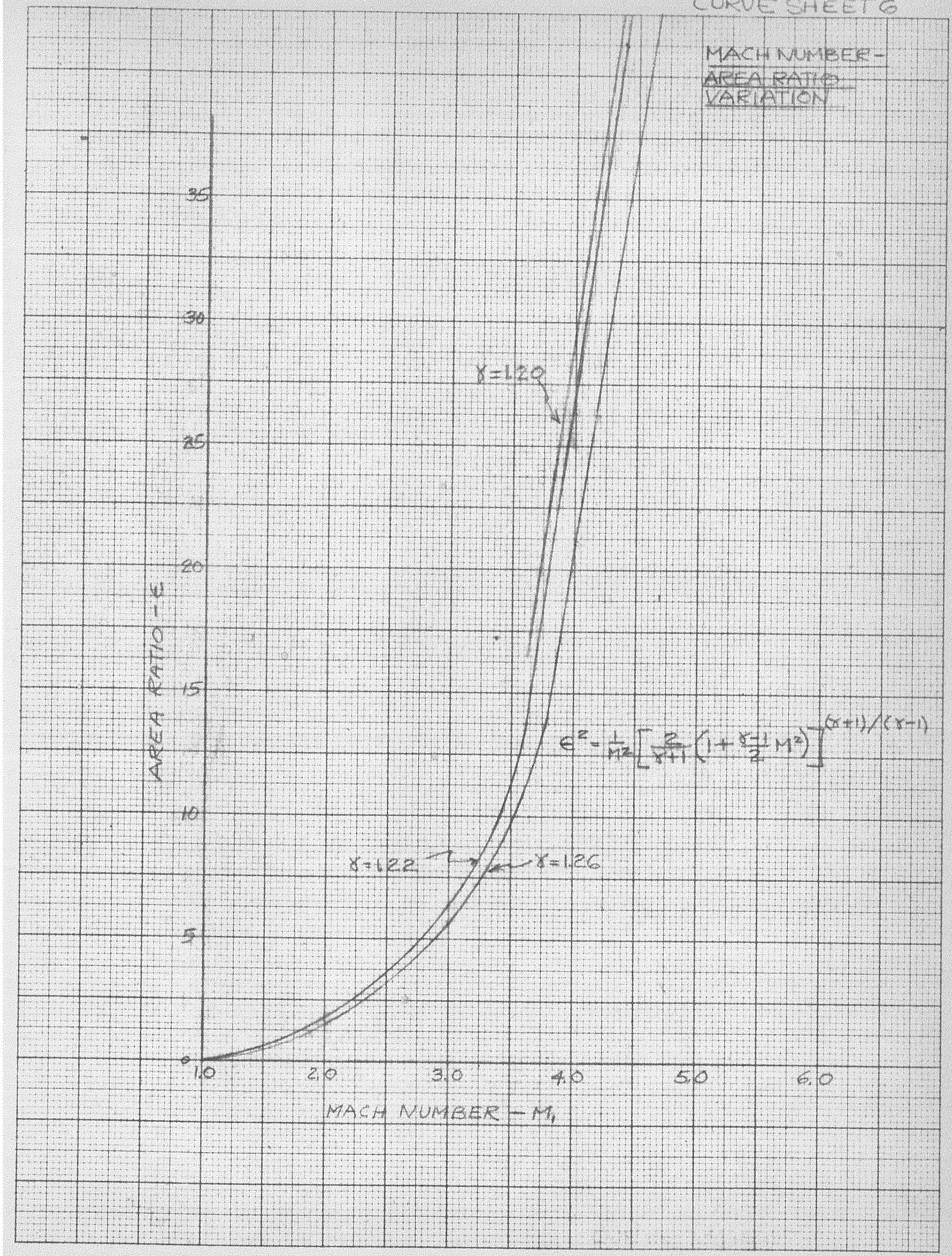

CURVE SHEET # 7

SHOCK POLAR DIAGRAM SHOWING POSSIBLE STRONG AND WEAK WAVE SOLUTIONS

$\gamma = 1.26$

EQUATIONS:- (OBLIQUE SHOCK)

$$\frac{1}{M_1^2} = \sin^2\beta - \frac{\gamma+1}{2}\frac{\sin\beta\sin\theta}{\cos(\beta-\theta)}$$

$$\frac{P_2}{P_1} = \frac{2\gamma}{\gamma+1}M_1^2\sin^2\beta - \frac{\gamma-1}{\gamma+1}$$

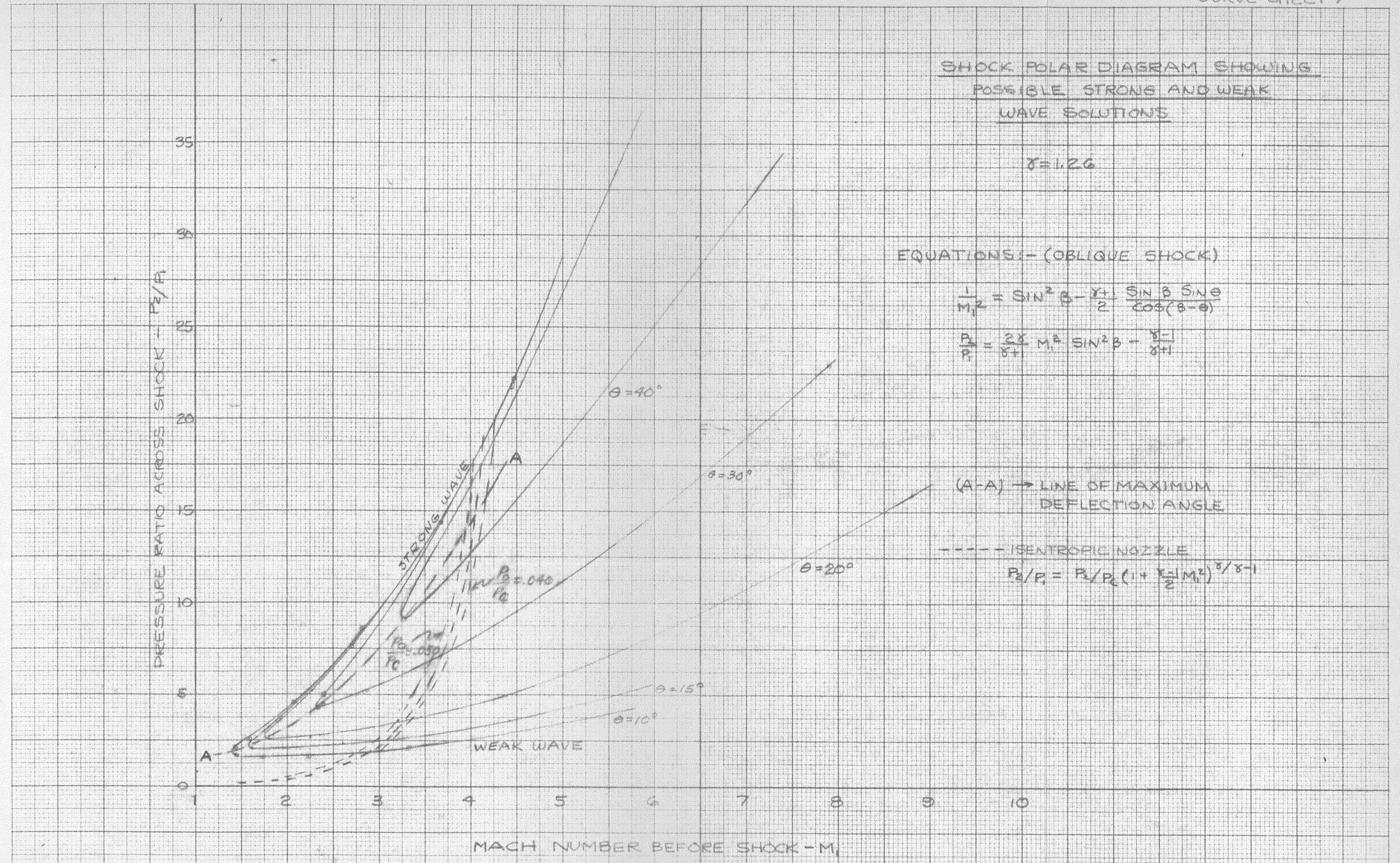

APPENDIX 111

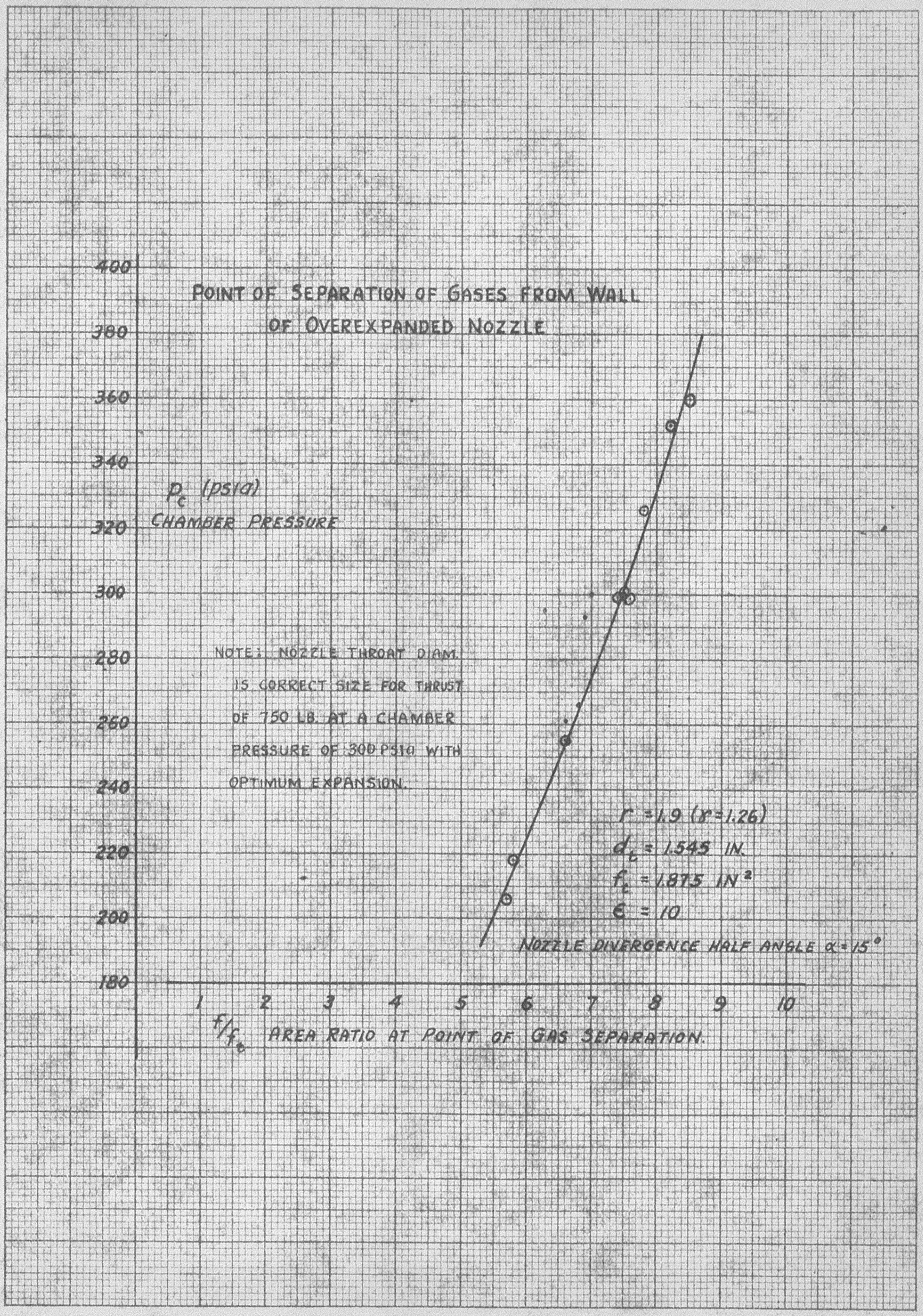
POINT OF SEPARATION OF GASES FROM WALL
OF OVEREXPANDED NOZZLE
400
380
360
340
320
300
280
260
240
220
200
180
P_c (psig)
CHAMBER PRESSURE
NOTE: NOZZLE THROAT DIAM.
IS CORRECT SIZE FOR THRUST
OF 750 LB. AT A CHAMBER
PRESSURE OF 300 PSIG WITH
OPTIMUM EXPANSION.
$\gamma = 1.9$ ($\gamma = 1.26$)
$d_t = 1.545$ IN.
$f_t = 1.875$ IN^2
$\epsilon = 10$
NOZZLE DIVERGENCE HALF ANGLE $\alpha = 15°$
1
2
3
4
5
6
7
8
9
10
f/f_t AREA RATIO AT POINT OF GAS SEPARATION.

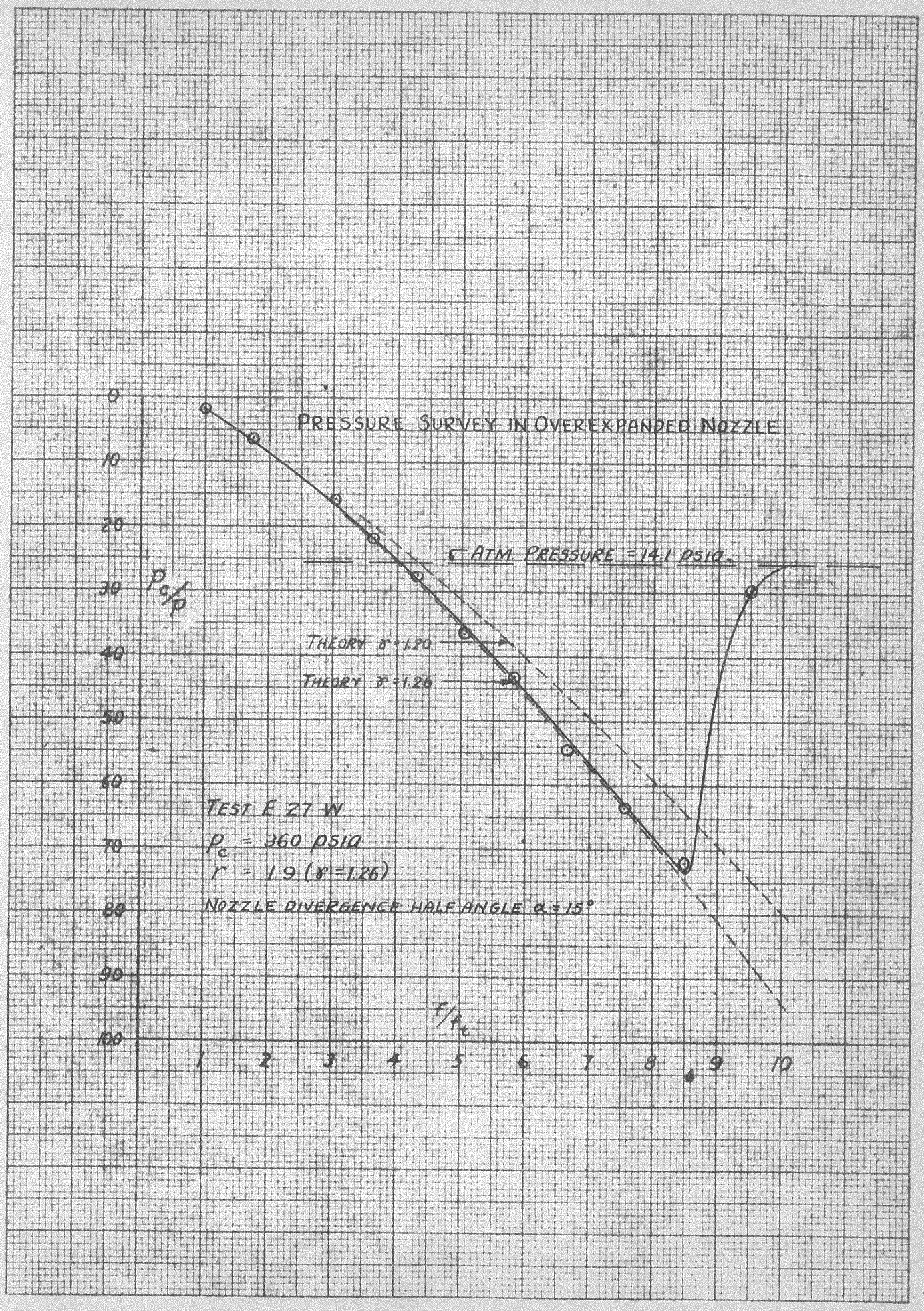
PRESSURE SURVEY IN OVEREXPANDED NOZZLE
ATM. PRESSURE = 14.1 PSIA
THEORY γ = 1.20
THEORY γ = 1.26
TEST E 27 W
P_c = 360 PSIA
r = 1.9 (γ = 1.26)
NOZZLE DIVERGENCE HALF ANGLE α = 15°
P_c/p
r/r_t
9
10
20
30
40
50
60
70
80
90
100
1
2
3
4
5
6
7
8
9
10

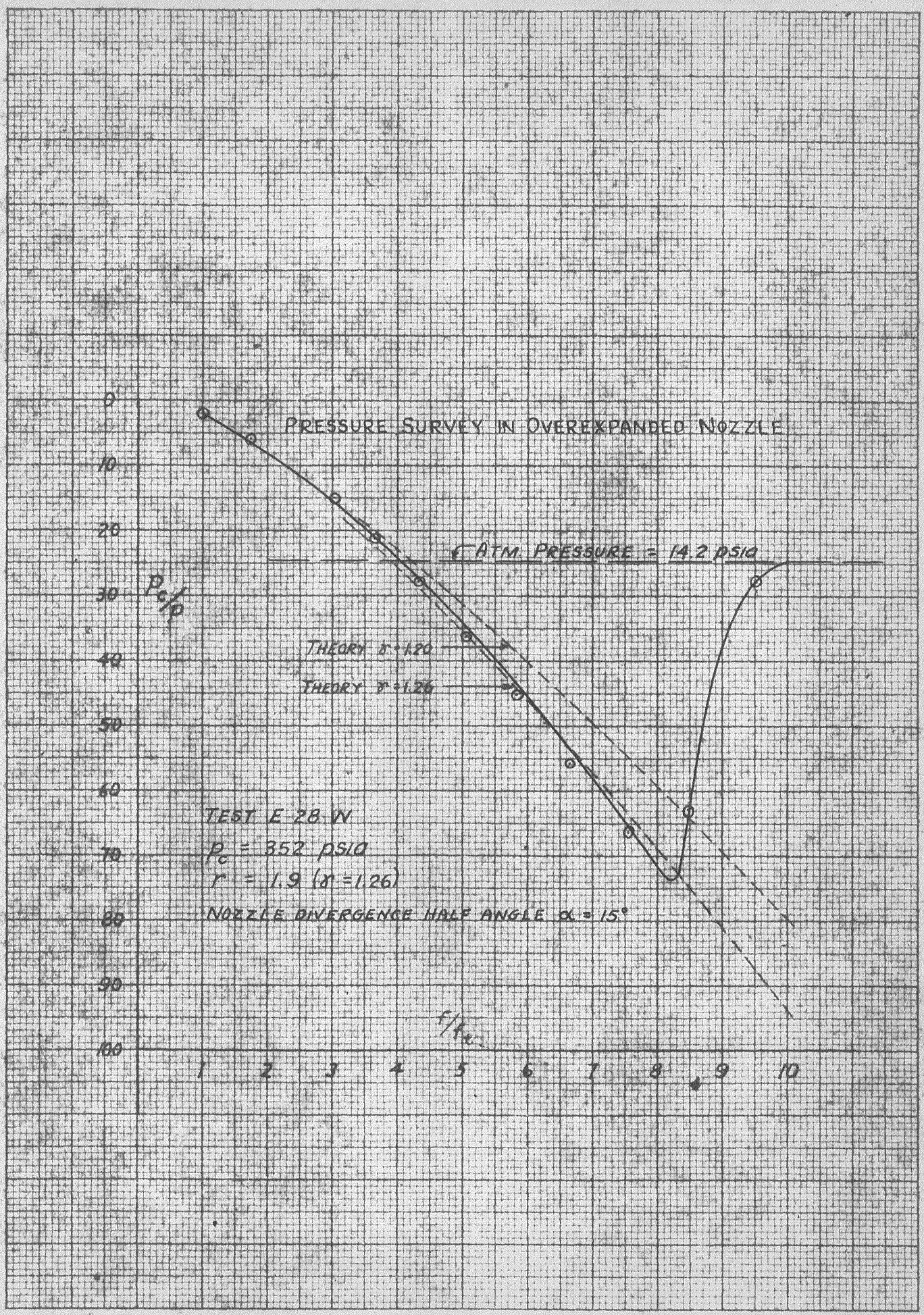
PRESSURE SURVEY IN OVEREXPANDED NOZZLE
ATM. PRESSURE = 14.2 PSIA
P_c/P
THEORY $\gamma = 1.20$
THEORY $\gamma = 1.26$
TEST E 28 W
P_c = 352 PSIA
r = 1.9 (γ = 1.26)
NOZZLE DIVERGENCE HALF ANGLE α = 15°
r/r_t
0
10
20
30
40
50
60
70
80
90
100
1
2
3
4
5
6
7
8
9
10

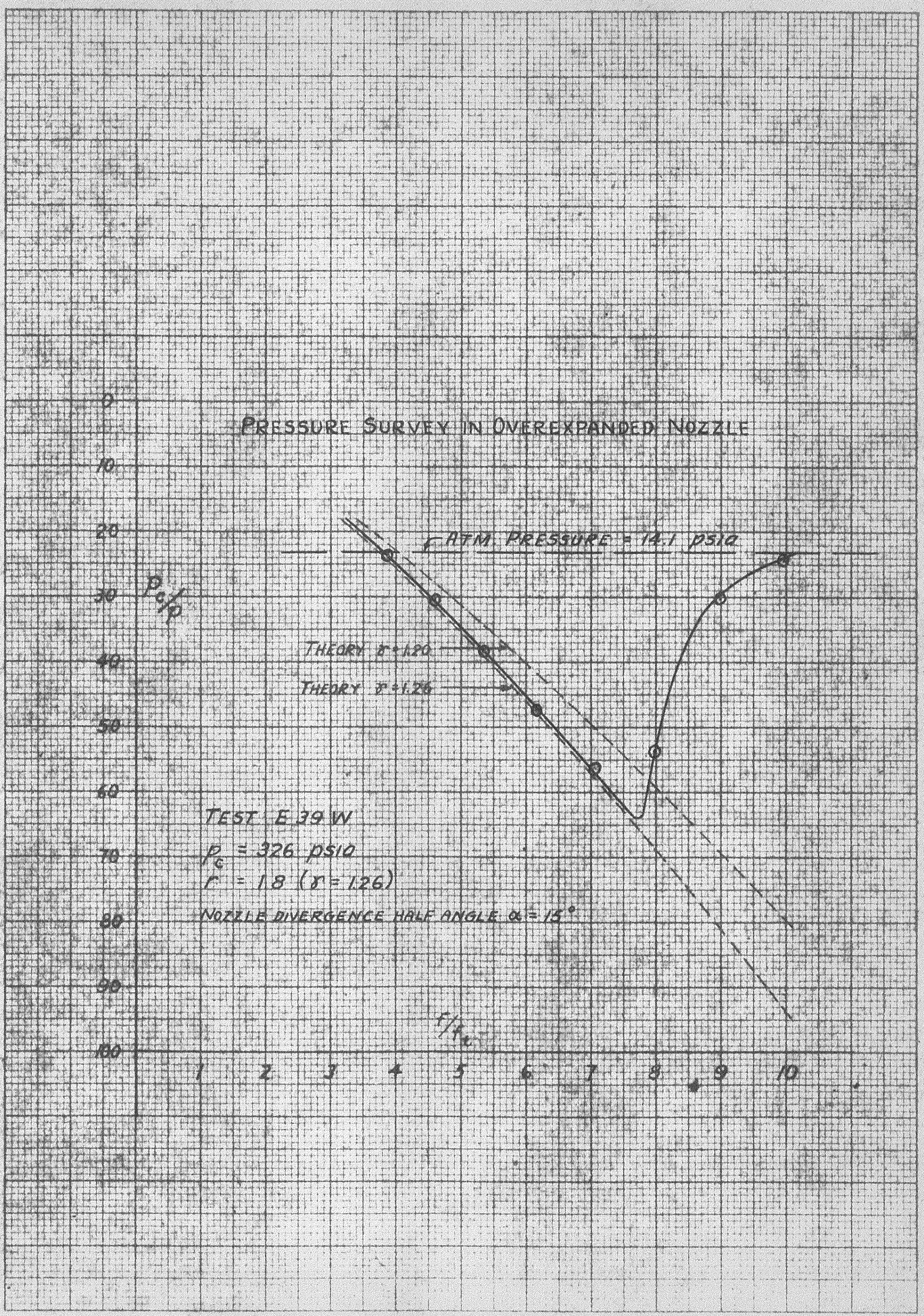
PRESSURE SURVEY IN OVEREXPANDED NOZZLE
ATM. PRESSURE = 14.1 psia
p_c/p
THEORY $\gamma = 1.20$
THEORY $\gamma = 1.26$
TEST E 39 W
p_c = 326 psia
r = 1.8 (γ = 1.26)
NOZZLE DIVERGENCE HALF ANGLE α = 13°
r/r_t
0
10
20
30
40
50
60
70
80
90
100
1
2
3
4
5
6
7
8
9
10

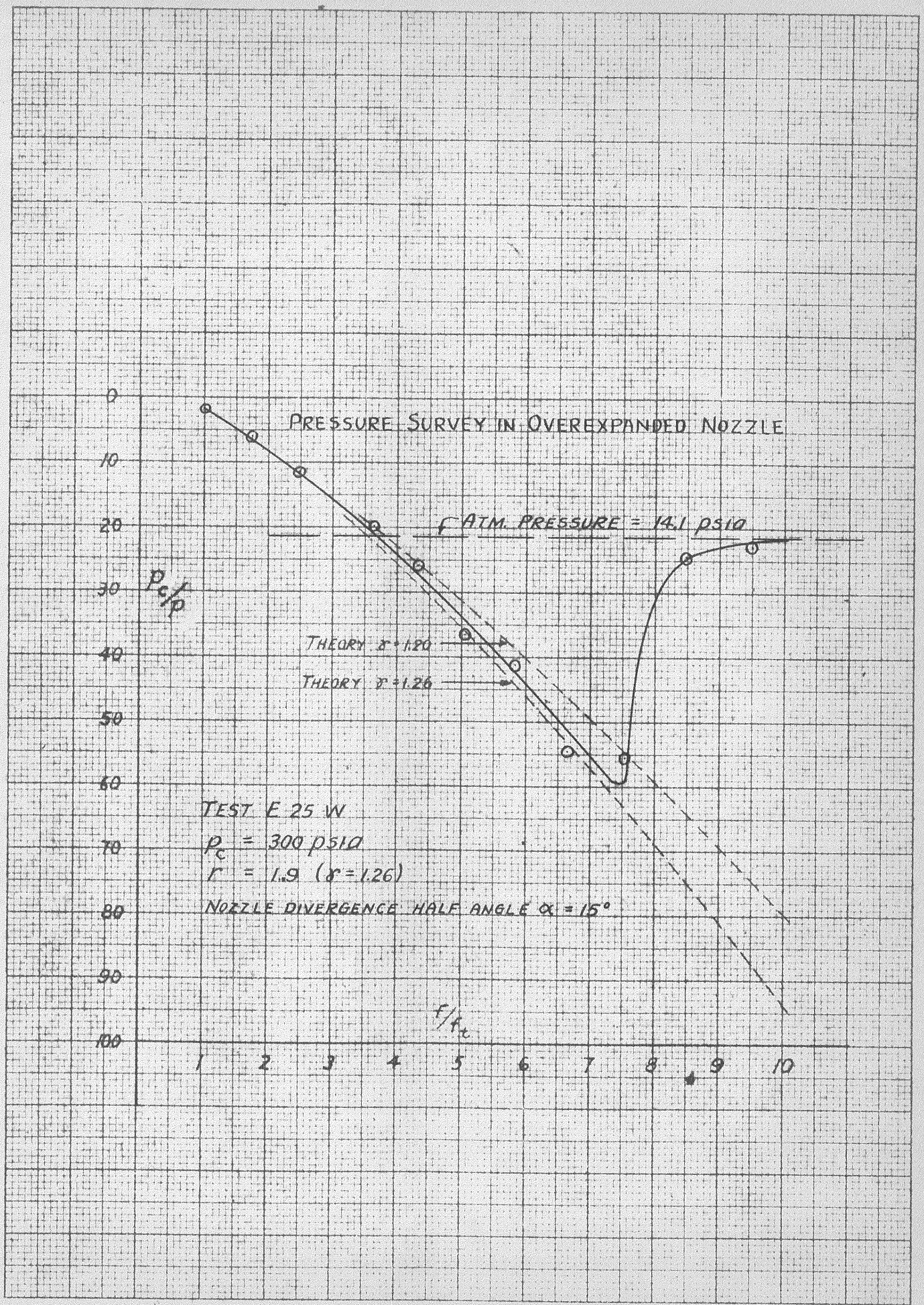
PRESSURE SURVEY IN OVEREXPANDED NOZZLE
ATM. PRESSURE = 14.1 PSIA
p_c/p
THEORY γ = 1.20
THEORY γ = 1.26
TEST E 25 W
p_c = 300 PSIA
Γ = 1.9 (γ = 1.26)
NOZZLE DIVERGENCE HALF ANGLE α = 15°
f/f_t
0
10
20
30
40
50
60
70
80
90
100
1
2
3
4
5
6
7
8
9
10

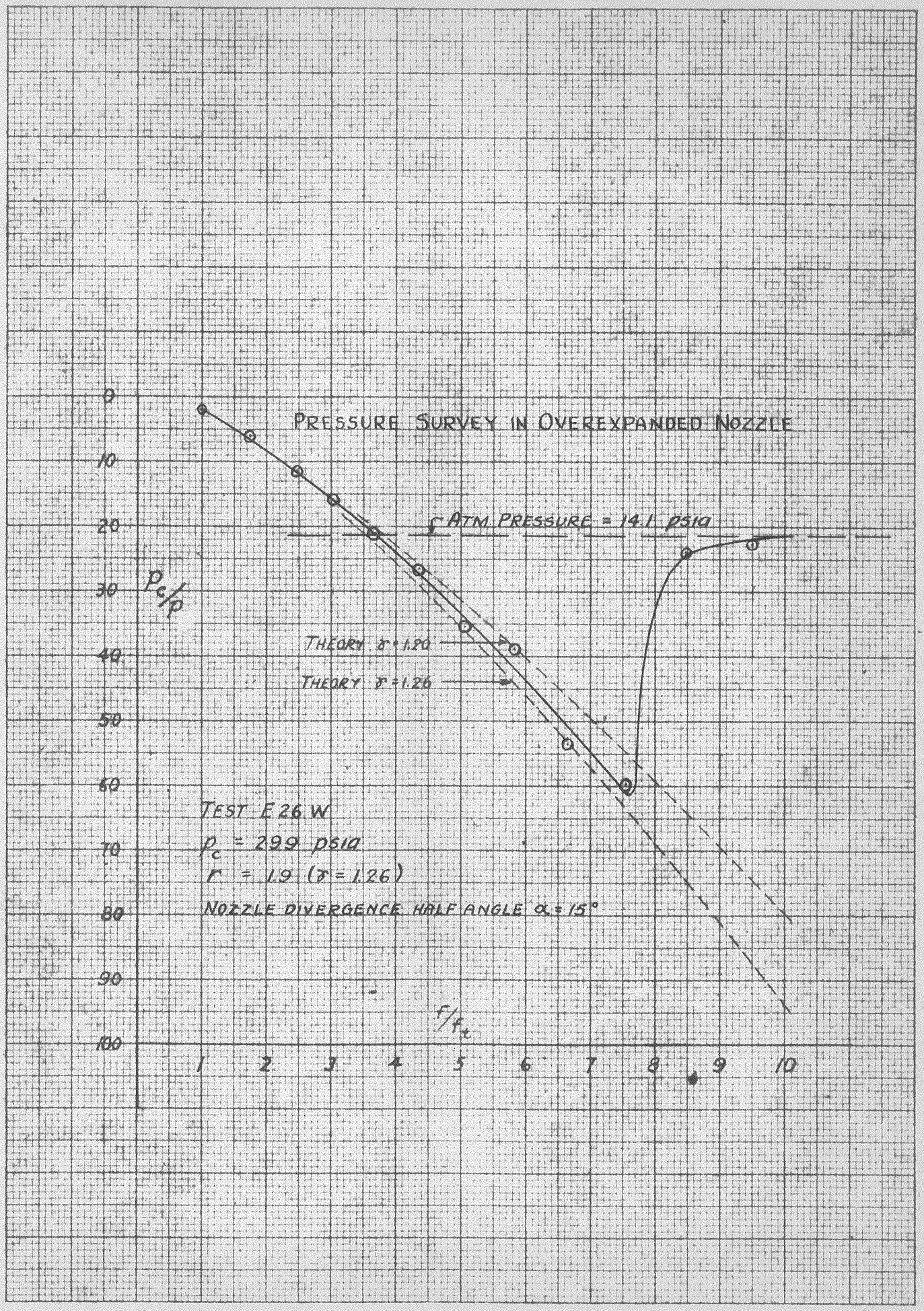
PRESSURE SURVEY IN OVEREXPANDED NOZZLE
ATM. PRESSURE = 14.1 psia
p_c/p
THEORY $\gamma = 1.20$
THEORY $\gamma = 1.26$
0
10
20
30
40
50
60
70
80
90
100
TEST E 26 W
p_c = 299 psia
r = 1.9 ($\gamma = 1.26$)
NOZZLE DIVERGENCE HALF ANGLE $\alpha = 15°$
r/r_t
1
2
3
4
5
6
7
8
9
10

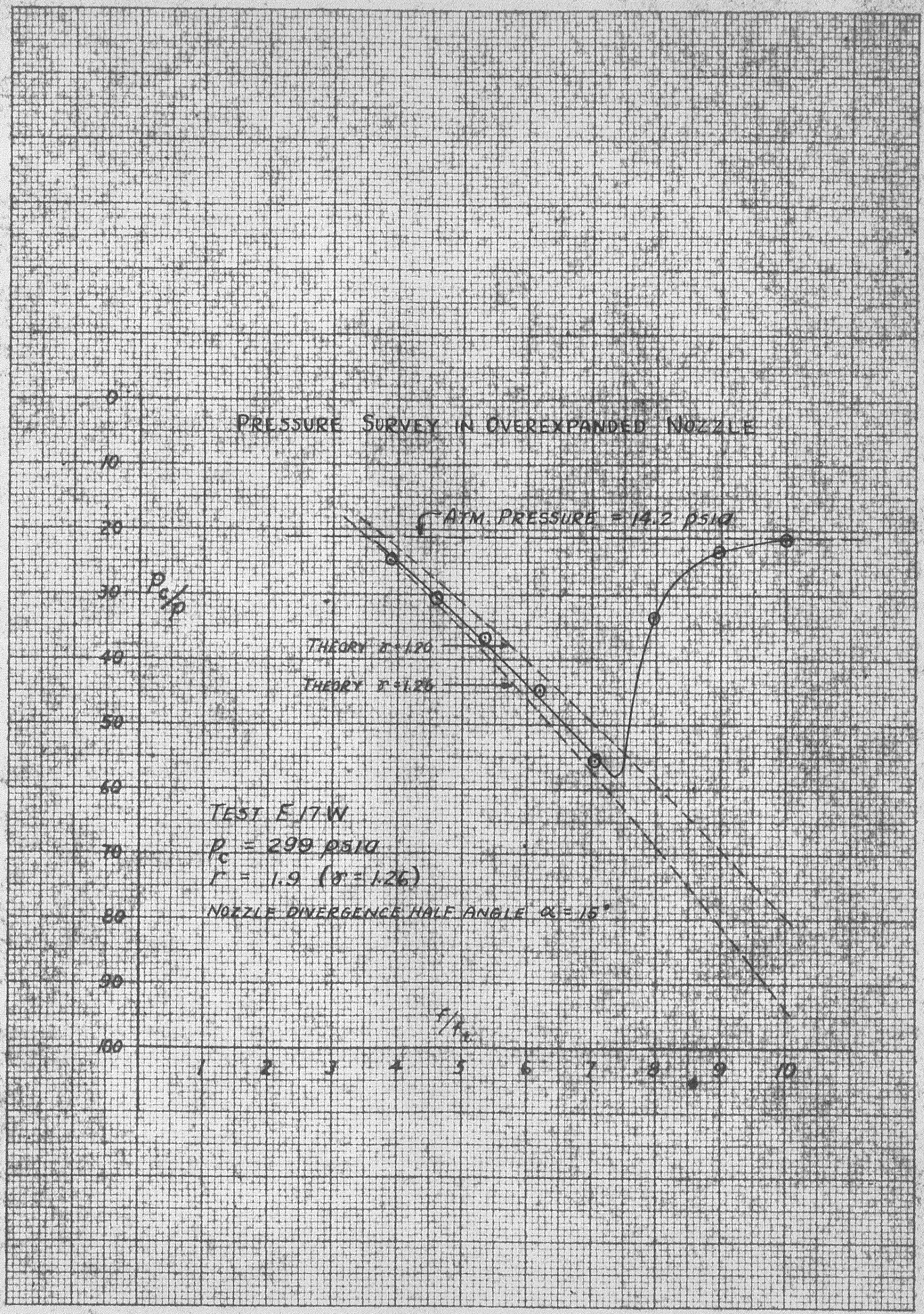
PRESSURE SURVEY IN OVEREXPANDED NOZZLE
ATM. PRESSURE = 14.2 psia
THEORY γ=1.26
THEORY γ=1.26
TEST E.17W
p_c = 299 psia
Γ = 1.9 (γ = 1.26)
NOZZLE DIVERGENCE HALF ANGLE α = 15°
p_c/p
r/r_t
0
10
20
30
40
50
60
70
80
90
100
1
2
3
4
5
6
7
8
9
10

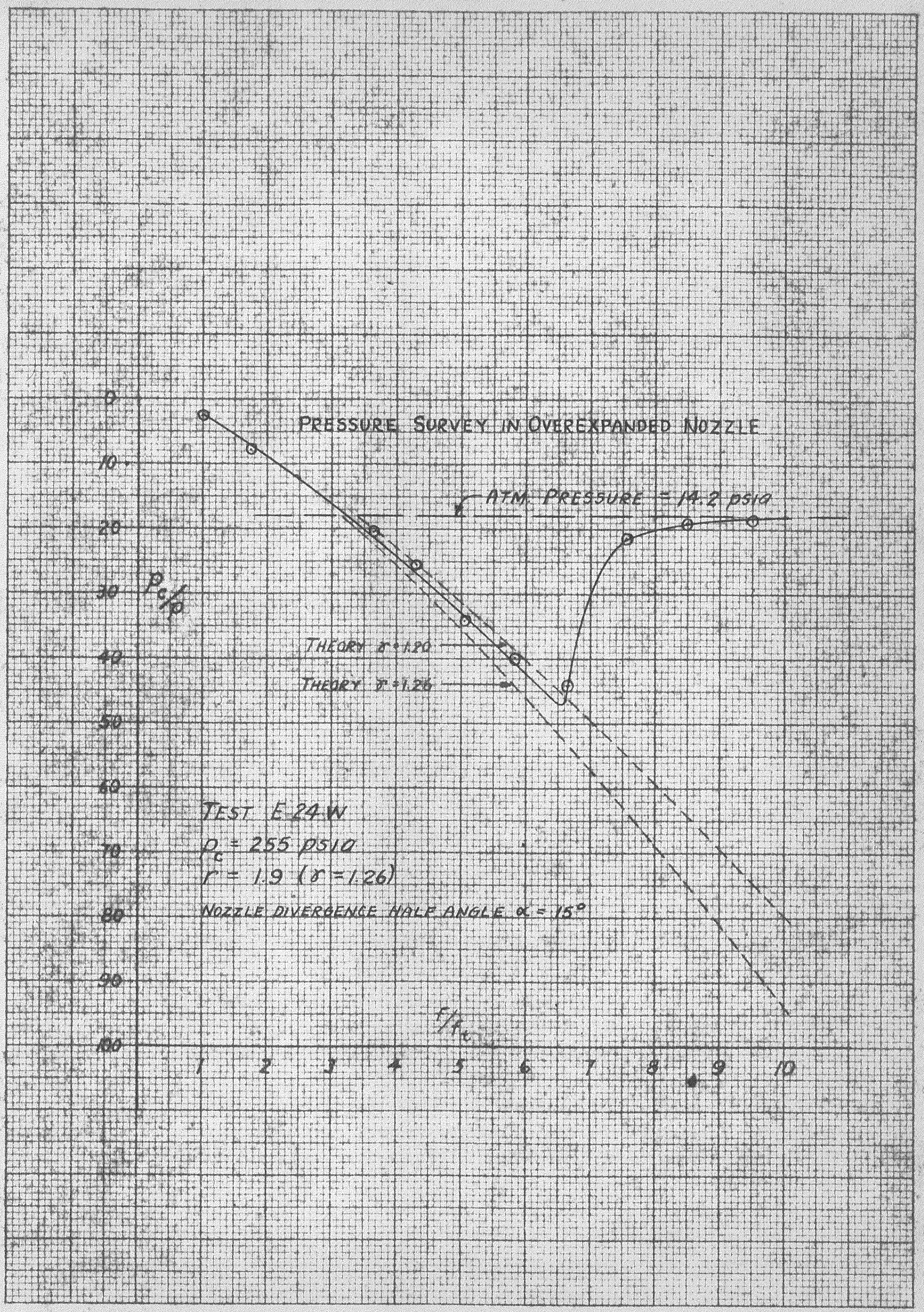
PRESSURE SURVEY IN OVEREXPANDED NOZZLE
ATM. PRESSURE = 14.2 PSIA
THEORY γ = 1.20
THEORY γ = 1.26
P_c/P_0
0
10
20
30
40
50
60
70
80
90
100
1
2
3
4
5
6
7
8
9
10
r/r_t
TEST E 24 W
P_c = 255 PSIA
r = 1.9 (γ = 1.26)
NOZZLE DIVERGENCE HALF ANGLE α = 15°

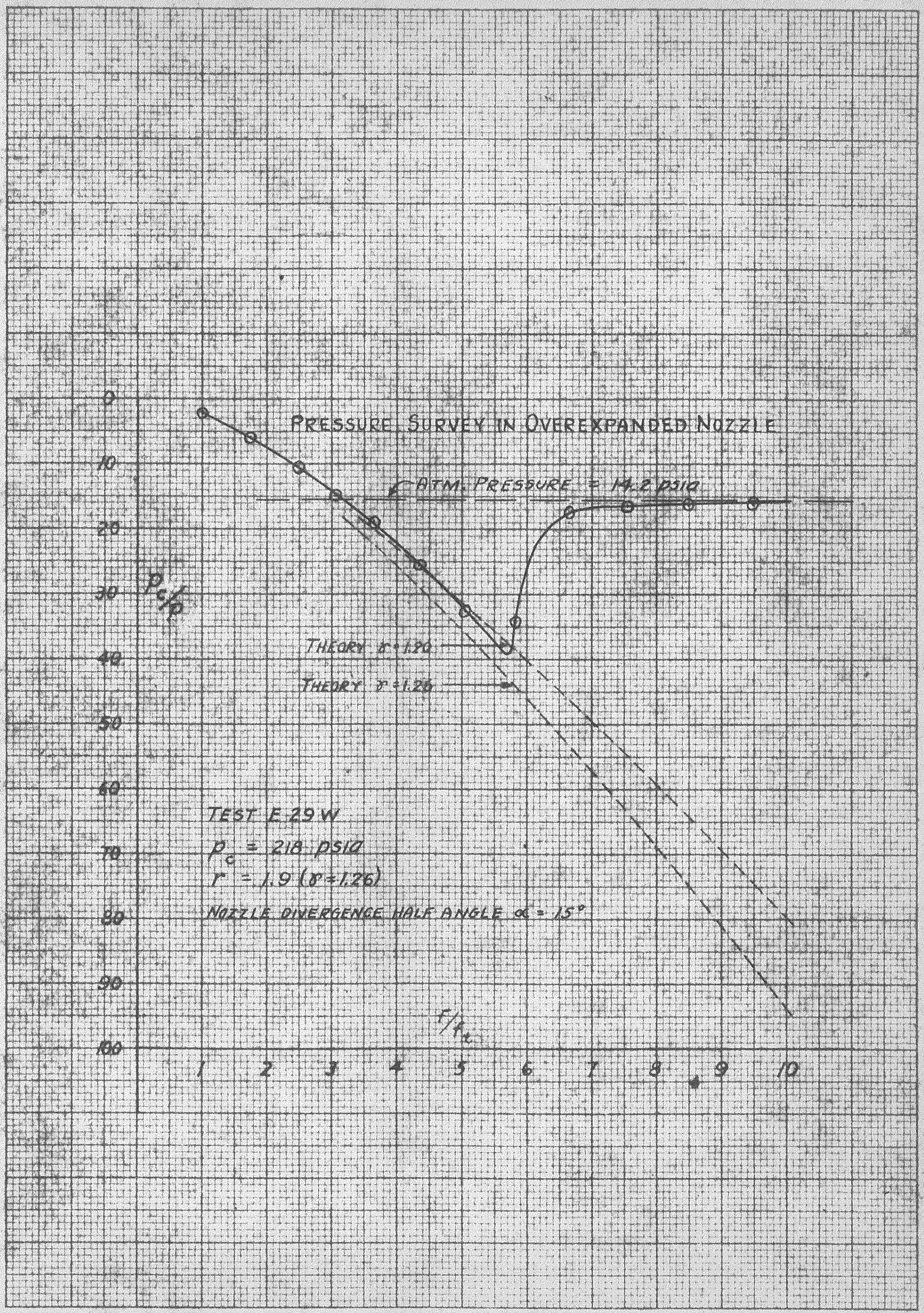
PRESSURE SURVEY IN OVEREXPANDED NOZZLE
ATM. PRESSURE = 14.2 PSIA
p_c/p
THEORY $\gamma = 1.20$
THEORY $\gamma = 1.26$
TEST E 29 W
p_c = 218 PSIA
γ = 1.9 ($\gamma = 1.26$)
NOZZLE DIVERGENCE HALF ANGLE α = 15°
r/r_t
0
10
20
30
40
50
60
70
80
90
100
1
2
3
4
5
6
7
8
9
10

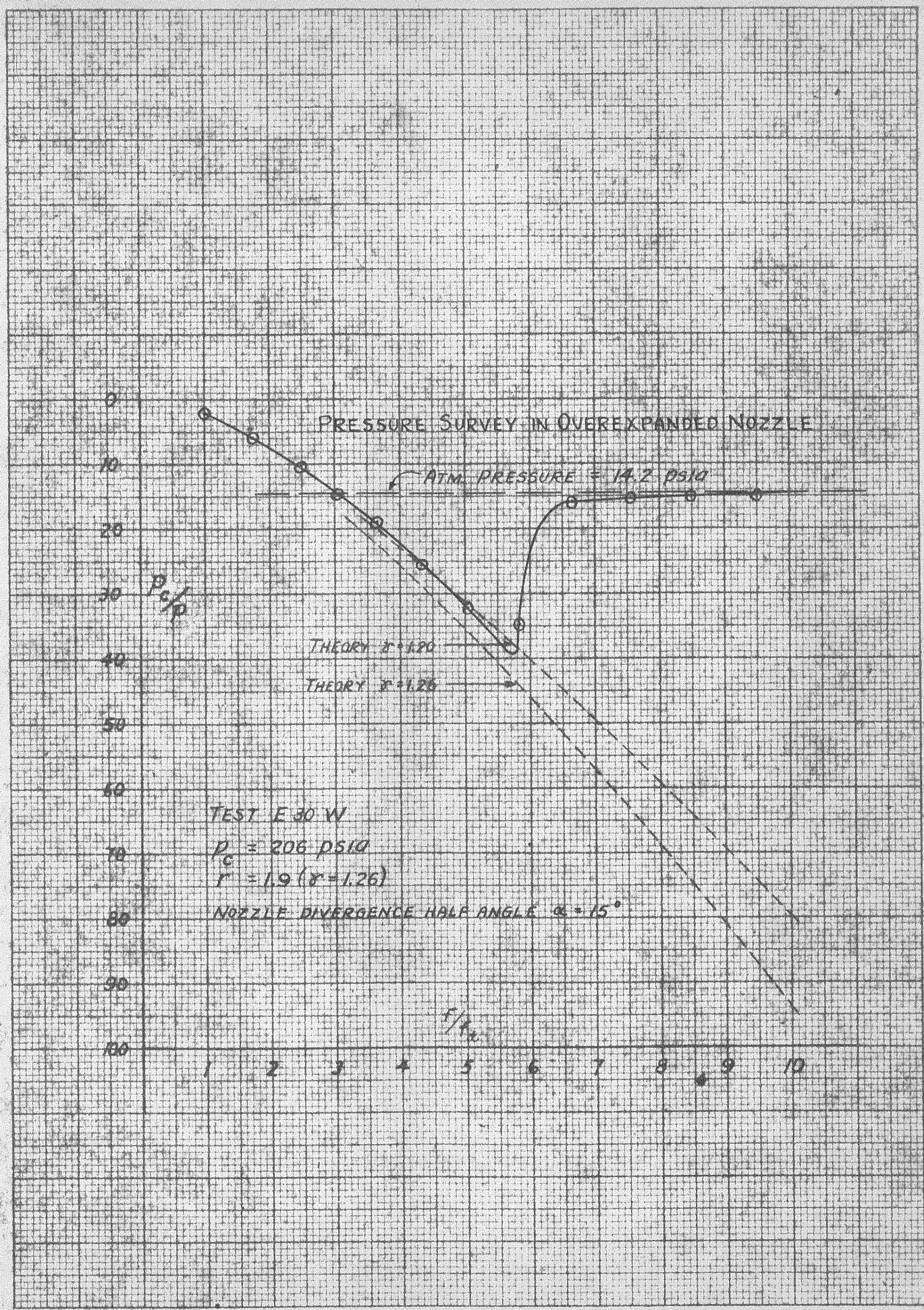
PRESSURE SURVEY IN OVEREXPANDED NOZZLE
ATM. PRESSURE = 14.2 PSIA
P_c/P_0
THEORY γ=1.20
THEORY γ=1.26
TEST E 30 W
P_c = 206 PSIA
r = 1.9 (γ=1.26)
NOZZLE DIVERGENCE HALF ANGLE α = 15°
r/r_t
0
10
20
30
40
50
60
70
80
90
100
1
2
3
4
5
6
7
8
9
10

BIBLIOGRAPHY

REFERENCES

1. The Problem of Escape of the Earth by Rocket, Malina and Summerfield, Journal Aero. Sc., Vol. 14, No. 8, Aug. 1947.

2. Jet Propulsion Reference Text, Air Technical Service Command, 1946, p. 132-147.

3. Progress Report on Experiments with Over-expanded Nozzles, C. R. Foster, GALCIT Jet Propulsion Lab., (tentative title, as work unpublished as yet).

4. Vertical Flight Performance of Rocket Missiles and an Estimation of their Horizontal Ranges, W. Z. Chien, GALCIT-JPL report 4-11, June, 1945.

5. Flow Structure and Pressure Recovery in Supersonic Tunnels, H. Eggink, ZWB Forschungsbancht, #1756, translated by Cornell Aero. Lab., May, 1947

6. Standard Atmosphere-Table and Data, Walter Diehl, NACA T.N. #218, 1940.

7. Tentative Tables for Properties of the Upper Atmosphere, Warfield, NACA T.N. 1200, Jan. 1947.

8. Characteristics of the Rocket Motor Unit Based on the Theory of Perfect Gases, Malina, Journal Franklin Inst., Vol. 230, 1940, p. 433.

9. Aerodynamics of a Compressible Fluid, Liepmann and Puckett, J. Wiley and Son, 1947, p. 23-60.

ADDITIONAL BIBLIOGRAPHY

1. On Flow of Gases at High Speeds, T. E. Stanton, R. Soc. of London Proceedings, Series A, Vol. 3, 1926, P. 306,-324.

2. Gas Dynamics, A. Buseman, Handbuch der Experimental Physik, Vo. 4, Part 1, 1931, p. 395, 399.

3. Theoretical Studies on the Flow Through Nozzles and Related Problems, AMP report 82.1R, AMG-NYU #43, OSRD 591.

4. On Supersonic Compressors and Nozzles, AMP report 82.1R (suppl.) OSRD 4416.

5. Abrupt Energy Transformation in Flowing Gases, N. P. Bailey, ASME Trans., Vol. 69, No. 7, Oct. 1947.

6. The Mechanics and Thermodynamics of Steady One-Dimensional Flow, Shapiro and Hawthorne, Journal App. Mech., Vol. 14, No. 47, Dec. 1947.

7. The Mechanics of Compressible Fluids, G. I. Taylor and J. W. MacColl, Aerodynamic Theory, W. F. Durand, Vol. 3, Sect. h, Jan. 1943.

8. Flow Through Nozzles at Supersonic Speeds, R. P. Frazer, Chemical Technology Dept., Imperial College of Science.

9. Steam and Gas Turbines, A. Stodola, (translated) McGraw-Hill, 1927.